Spring 2009

Elemental and strontium isotope constraints on coupled high- and low-temperature hydothermal fluids throughout an eruptive cycle at 9 deg 50'N East Pacific Rise

Jill Marie McDermott
University of New Hampshire, Durham

Follow this and additional works at: https://scholars.unh.edu/thesis

ELEMENTAL AND SR ISOTOPE CONSTRAINTS ON COUPLED HIGH- AND LOW-TEMPERATURE
HYDROTHERMAL FLUIDS THROUGHOUT AN ERUPTIVE CYCLE AT 9°50'N EAST PACIFIC RISE

BY

JILL MARIE MCDERMOTT
B.A., Dartmouth College, 2006

THESIS

Submitted to the University of New Hampshire
in Partial Fulfillment of
the Requirements for the Degree of

Master of Science
in
Geochemical Systems

May, 2009

UMI Number: 1466940

INFORMATION TO USERS

The quality of this reproduction is dependent upon the quality of the copy
submitted. Broken or indistinct print, colored or poor quality illustrations
and photographs, print bleed-through, substandard margins, and improper
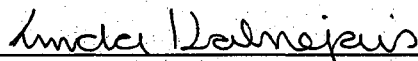alignment can adversely affect reproduction.
In the unlikely event that the author did not send a complete manuscript
and there are missing pages, these will be noted. Also, if unauthorized
copyright material had to be removed, a note will indicate the deletion.

UMI®
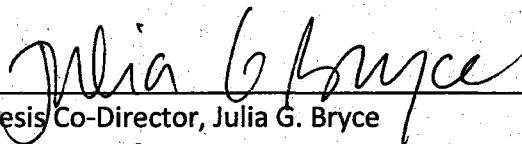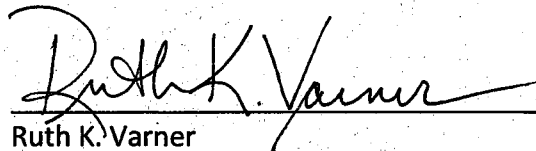
This thesis has been examined and approved.

Thesis Co-Director, Linda Kalnejais
Assistant Professor,
UNH Earth Sciences

Thesis Co-Director, Julia G. Bryce
Assistant Professor,
UNH Earth Sciences

Ruth K. Varner
Research Assistant Professor,
UNH Earth, Oceans and Space and Earth Sciences

Rachel M. Haymon
Professor,
UCSB Earth Science

5/13/2009
Date

ii

ACKNOWLEDGMENTS

TABLE OF CONTENTS

LIST OF TABLES

LIST OF FIGURES

ABSTRACT

ELEMENTAL AND SR ISOTOPE CONSTRAINTS ON COUPLED HIGH- AND LOW-TEMPERATURE HYDROTHERMAL FLUIDS THROUGHOUT AN ERUPTIVE CYCLE AT 9°50'N EAST PACIFIC RISE

by

Jill Marie McDermott
University of New Hampshire, May, 2009

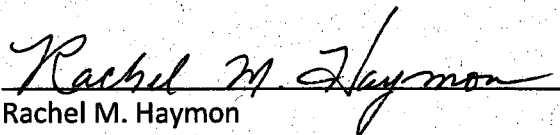Low-temperature hydrothermal fluids, long considered to be simple binary mixtures

of high-temperature fluids and seawater (Edmond et al, 1979ab), impact ocean chemistry

while providing energy to thriving ecosystems at mid-ocean ridges (MORs). This thesis

investigates whether processes other than simple mixing may influence the evolution of low

temperature hydrothermal fluids. In particular, the role of anhydrite dissolution is

addressed.

9°50'N EPR contains high-temperature vents (Ty and Io) that have been associated

with low-temperature venting (BM82) for over a decade and remained active following an

eruption in 2005-2006. The Sr isotope systematics of adjacent high- and low-temperature

fluids will support either a binary seawater-hydrothermal mixture, or will support additional

components. The Sr isotopic composition of fluids sampled in 1994 to 2007, determined via

thermal ionization mass spectrometry, is reported. $^{87}Sr/^{86}Sr$ ranges are 0.70902 to 0.70917

in BM82 fluids. Pre-eruption Ty and Io end member $^{87}Sr/^{86}Sr$ range is 0.70394 to 0.70419,

which aligns with previous EPR studies (0.7030-0.7040, (Ravizza et al., 2001)). However,

immediate post-eruption end member $^{87}Sr/^{86}Sr$ ranges from 0.70511 to 0.70654, closer to

the seawater value. These results imply that immediate post-eruption water-rock reactions do not achieve the same degree of isotopic equilibrium with basalt as reactions during more stable periods (Butterfield et al., 1997; Von Damm, 2000). Additionally, anhydrite dissolution following an eruption may contribute 2-7% of low-temperature fluid Ca. Our findings demonstrate that MOR hydrothermal anhydrite deposits may be a temporary sink for Ca, Sr, and SO_4^{2-}, and that the hydrothermal flux component of these elemental budgets must be reinterpreted. Additional findings include evidence for halite precipitation and albitization in the high-temperature fluid time series, as well as indication of seawater infiltration into the discharge zone in March 2004 and in the post-eruptive 2006-2007 sampling interval.

INTRODUCTION

Deep sea mid-ocean ridge (MOR) hydrothermal systems were first discovered approximately 30 years ago at the Galapagos Spreading Center (Corliss et. al., 1979). Prior to 1979, submarine hot springs were known to exist at the Red Sea Spreading Center and in shallow water locations. Deep sea MOR hydrothermal systems impart major chemical and physical impacts on the oceans, affecting global heat and chemical fluxes and thermohaline circulation (e.g. Edmond et al., 1979a; Staudigel and Hart, 1983; Von Damm et al., 1985; Von Damm, 1995). Furthermore, they enable the existence of biological communities independent of solar energy. In a deep sea MOR hydrothermal system, circulating seawater extracts heat from subsurface magma in fractured oceanic crust where tectonic plates are diverging. This water undergoes a variety of water-rock reactions and collects magmatic gases. The heated, chemically-altered fluids are thermally buoyant and are discharged as sulfide-rich "black smoker" vents on the seafloor (Spiess et al., 1980). High-temperature focused flows form mineral structures on the seafloor (Haymon and Kastner, 1981; Goldfarb et al., 1983), and vent fluids at temperatures equal to or greater than 250°C. These black smoker vents are often surrounded by areas of low-temperature diffuse flow, which circulate in the upper oceanic crust, vent directly from the rock substrate, and generally have temperatures less than or equal to 70°C (Von Damm, 1995; German and Von Damm,

1

2004). Coupled low-temperature and high-temperature hydrothermal systems account for an estimated 25% of Earth's internal heat loss (Stein and Stein, 1994). Hydrothermal fluids additionally provide evidence of processes occurring within young oceanic crust, which presently is difficult to drill without the presence of sediment cover.

The relative importance of high- and low-temperature flow for the heat and element fluxes to the global ocean continues to be debated. While some recent studies propose that low-temperature flow may be volumetrically more important than high-temperature flow (Schultz and Elderfield, 1997; Mottl, 2003), others conclude instead that the heat flux may be equally partitioned between the two vent types (Veirs et al., 2006). Von Damm (1995) suggests that despite the lower chemical anomalies in low-temperature fluids, if the volume of low-temperature flow is indeed much greater than that of high-temperature flow, low-temperature flow may be a more important seafloor hydrothermal chemical contributor. Due in part to more difficult sampling conditions as a result of variation in robustness of flow, low-temperature fluids have not been as extensively studied as high-temperature fluids. Prevailing assumptions state that low-temperature fluids are simple dilutions of high-temperature fluids, and therefore high-temperature fluid data have been considered sufficient for the purposes of flux calculations (e.g. Edmond et al., 1979ab; Von Damm and Lilley, 2004). However, if low-temperature fluids are not simple dilutions of high-temperature fluids, more must be known about the processes that control their compositions before flux calculations can be refined.

We now know that the relationships between high- and low-temperature fluids are affected by volcanic and seismic events on decadal timescales at the fast-spreading East Pacific Rise (EPR) mid-ocean ridge (Haymon et al, 1993; Von Damm et al., 2006) and that any individual vent has a unique chemistry that can vary on minute-to-yearly timescales (Von Damm, 1995). The short timescales of these processes necessitates a time series approach to understanding the variation in fluid chemistry as well as the controlling mechanisms, in order to fully quantify fluxes.

This thesis addresses the relationships between high- and low-temperature fluids in terms of temperature and major and minor element chemical variation over the course of an eruptive cycle at 9-10°N East Pacific Rise (EPR) bracketed by eruptions in 1991-92 and 2005-06. I also discuss Sr isotope variation over the pre- and post-eruptive periods for both fluid types. Ravizza et al. (2001) used Sr isotopes to identify the presence of an intermediate, partially-reacted fluid mixing into a high-temperature hydrothermal vent at 9-10°N EPR. Sr isotope data, therefore, coupled with elemental Ca and Sr abundances, can be used as a tracer of sub-surface processes to constrain mixing relationships between high- and low-temperature fluids. Sr isotopic data may therefore be used as a method to address the deviations from non-conservative mixing that have possible implications for anhydrite dissolution into the low- and/or high-temperature fluids during the sampling interval.

With respect to the stability of anhydrite deposits, both low- and high-temperature fluid composition controls include fluid temperature, redox state, and the relative volumes and rates of convection of seawater mixing in through fractures in the discharge zone. The

likelihood of higher volumes of seawater entrainment during and following an eruption is

high, due to higher crustal permeability and more vigorous rates of convection, and thus it

possible that anhydrite deposits may form quickly and then re-dissolve. From a high-

temperature fluid perspective, Ca, Sr, SO_4^{2-}, and Mg can all be removed from both the high-

temperature fluids and seawater into mineral deposits, in both the chimney structure and in

the stockwork (Haymon, 1983). When mineral deposits have sealed in fluid conduits,

thereby creating more reducing subsurface conditions, anhydrite becomes

thermodynamically unstable and can be re-mobilized. This study will address how an

eruption affects the stability of anhydrite deposits in both the high- and low-temperature

fluids.

CHAPTER I

BACKGROUND

Previous low-temperature fluid chemical studies

Prior to 1977 it was hypothesized that elemental abundances in the ocean were

controlled by input fluxes of elements from the continents from streams and rivers as well

as oceanic sedimentary sinks (Sillen, 1961). If it is assumed that the ocean is in steady state,

these fluxes should be equal and opposite. With the discovery of the first deep sea

hydrothermal vent sites in 1977, elemental fluxes due to hydrothermal activity were

calculated quickly by Edmond et al. (1979a,b) based on the chemistry of fluids sampled at

the Galapagos Spreading Center (GSC). These fluids were all low-temperature, less than

20°C when sampled. Edmond et al. (1979a) calculated sinks for Mg and SO_4^{2-}, sources for Li,

Rb, Ca, K, Si, Ba, and more complex additions and removals of Na and Cl. Edmond et al.

(1979b) noted that the sampled fluid chemistry indicated a dilution of high-temperature

fluids with seawater. This discussion formed the first interpretation of low-temperature

fluid formation and the consequent deposition of metal sulfide within the crust. Edmond et

al. (1979b) postulated that these metal sulfide deposits form as a result of mixing of high-

temperature fluids with seawater or near-seawater during the ascent through the crust in

5

the subsurface discharge zone. Edmond et al. (1979b) indeed found that transition metal (Cu, Ni, Cd, Cr, U) abundances were depleted with respect to their seawater concentrations due to precipitation in the subsurface. Flux questions have since become more complicated with the discovery of high-temperature vents and wide ranges in fluid composition, both spatially and temporally.

One overarching goal of hydrothermal fluid research remains the determination of heat and element fluxes to the ocean due to the global hydrothermal system, and the reactions that control low-temperature fluid chemistry have implications for both elemental and heat flux calculations. Since its discovery at the GSC, low-temperature flow has been considered to be a simple dilution of seawater and high-temperature flow. However, published data for low-temperature fluids at 9-10°N EPR prove otherwise. Von Damm and Lilley (2004) showed depletion of H_2S, CO_2, and H_2 and production of CH_4 in low-temperature fluids, relative to the values expected from conservative mixing of high-temperature fluids with seawater, providing strong support that low-temperature fluids are undergoing further reaction within the subsurface. Methane and H_2 are important species in microbial methanogenesis, and are used as an indicator by Von Damm and Lilley (2004) to identify the influence of a sub-seafloor microbial biosphere on low-temperature flow composition. Low-temperature fluids are therefore not the product of simple conservative dilutions of high-temperature fluids with seawater, but experience additional processes that include sub-seafloor biological activity.

Controls on hydrothermal fluid chemistry

Von Damm (1995) discussed the factors which determine the elemental composition

in a vent fluid. These include (1) the source for an element from seawater, rock, and/or

magma degassing, (2) whether an element will form one or more stable aqueous species

allowing for transport within the fluid, and (3) whether the element will precipitate as a

mineral phase. Von Damm (2000) identified phase separation and water-rock interaction as

the two dominant controls on hydrothermal vent fluid composition, with magmatic

degassing also playing a role. Geochemical modeling enables prediction of mineral

solubility conditions and potential precipitation.

In subsequent discussion, I will refer to the chemical constituents of hydrothermal

fluids using elemental, rather than ionic nomenclature (e.g. Cl rather than Cl⁻) for two main

reasons. First, the speciation of dissolved constituents in a hydrothermal solution is not

measured, or always known. Secondly, most methods for determining the chemical

constituents of hydrothermal fluids measure total elemental abundances. Any exception to

this nomenclature will be noted and discussed when that particular chemical constituent is

introduced.

Phase Separation

Bischoff (1991) showed that at the average mid-ocean ridge crest pressure of about

250 bars in the 9-10°N EPR region, seawater will boil subcritically at temperatures ≤ 388°C.

Subcritical boiling results in phase separation, during which the fluid will be partitioned into

two physically and chemically distinct phases: a "vapor" phase and a denser liquid "brine" phase. At subcritical conditions, the vapor phase will have a Cl content less than that of seawater, while the brine phase will have a Cl content greater than that of seawater. Phase separation is known to be ubiquitous in hydrothermal fluids, as very few high-temperature fluids contain Cl equivalent to seawater. Vapor phase fluids are more commonly sampled (Von Damm, 1995; Von Damm, 2000; Von Damm, 2004). Current belief is that the denser brines may be stored in the shallow oceanic crust for an unconstrained period of time prior to venting.

Phase separation is the most important control on Cl concentration in hydrothermal fluids, and greatly influences water-rock reaction conditions. With the precipitation of SO_4^{2-} and titration of alkalinity (see later discussion), Cl is by far the dominant anion in hydrothermal fluids. With the exception of possible halite dissolution or precipitation (Oosting and Von Damm, 1996; Von Damm, 2000), there are almost no known mineralogic sinks for Cl in these systems, and many cations maintain their element-to-Cl ratios during phase separation (German and Von Damm, 2004). Changes in Cl therefore have a strong effect on mineral solubility, as Cl affects the formation of aqueous metal ion complexes, ionic strength, and charge balance constraints in a solution (Seyfried and Ding, 1995). Within a hydrothermal fluid, element mobility is highly dependent on both temperature and pressure conditions and Cl concentration.

<u>Water-rock reaction</u>

The source of an element can be determined by knowing the composition of local ambient seawater, and of rock present in the system. As seawater passes through rock and is heated, reactive exchange with the rock begins in the downflow zone, and continues through the reaction and discharge zones as detailed for major elements in Figure 1. As seawater is progressively heated, Mg is quantitatively removed by precipitation of magnesium hydroxy silicates in the downflow zone, and protons are produced. The pH is lowered so substantially that all alkalinity is titrated away. At a temperature > 130°C, anhydrite ($CaSO_4$) precipitates. There is more SO_4^{2-} than Ca in seawater, thus additional Ca must be leached from rock if more than 33% of available seawater sulfate is precipitated via this mechanism (German and Von Damm, 2004). It is known that some Ca is leached from the rock via Na-Ca replacement in plagioclase feldspar, called albitization, to precipitate more of the SO_4^{2-} derived from seawater. Additional SO_4^{2-} may infiltrate the reaction zone and be reduced to H_2S. Some S is also leached directly from sulfides that are primary igneous phases. Shanks (2001) has found H_2S in hydrothermal fluids of nearly any temperature. Also at temperatures ~150°C, mobilization of alkalis including K, Rb, and Li occurs (Alt, 1995). In the reaction zone, the fluid reaches its greatest temperature, water-rock reactions continue, and phase separation may occur. It is conceivable that any fluid may have undergone phase separation multiple times, and the true system is undoubtedly more complex than we know or assume; however, due to a lack of better constraints and for greatest simplicity in a conceptual model, phase separation is assumed to occur once

within the reaction zone. The reaction zone is also assumed to be the site of magmatic degassing input (German and Von Damm, 2004). Gaseous species (e.g. CO_2 and He) may be affected by magmatic degassing inputs, but these processes remain poorly understood (Von Damm, 2000; Lilley et al.,2003). Additional water-rock reactions occur in the reaction and discharge zones, including large additions of leached Si, Fe, and Mn (German and Von Damm, 2004). Within the discharge zone, infiltrating seawater may add SO_4^{2-}, which will precipitate as anhydrite if temperatures are greater than 130°C. Leached constituents can also precipitate, depositing SiO_2 and Fe- and Mn-bearing minerals within the altered basalt, or "stockwork," in the discharge zone. Changes in physical conditions within the discharge zone may lead to mineral replacements (e.g. SiO_2 often replaces anhydrite in stockworks). When temperatures are less than 300°C, metal sulfides will precipitate, either sub-surface or in chimneys.

Due to the present difficulty to drill fresh, un-sedimented basalt, sub-surface rock composition is rarely known, and thus the common assumption is that the composition of rock at depth matches that of surficial rock. Altered basalt samples gathered from seafloor exposures can provide a means to better understand mineral deposition and alteration processes.
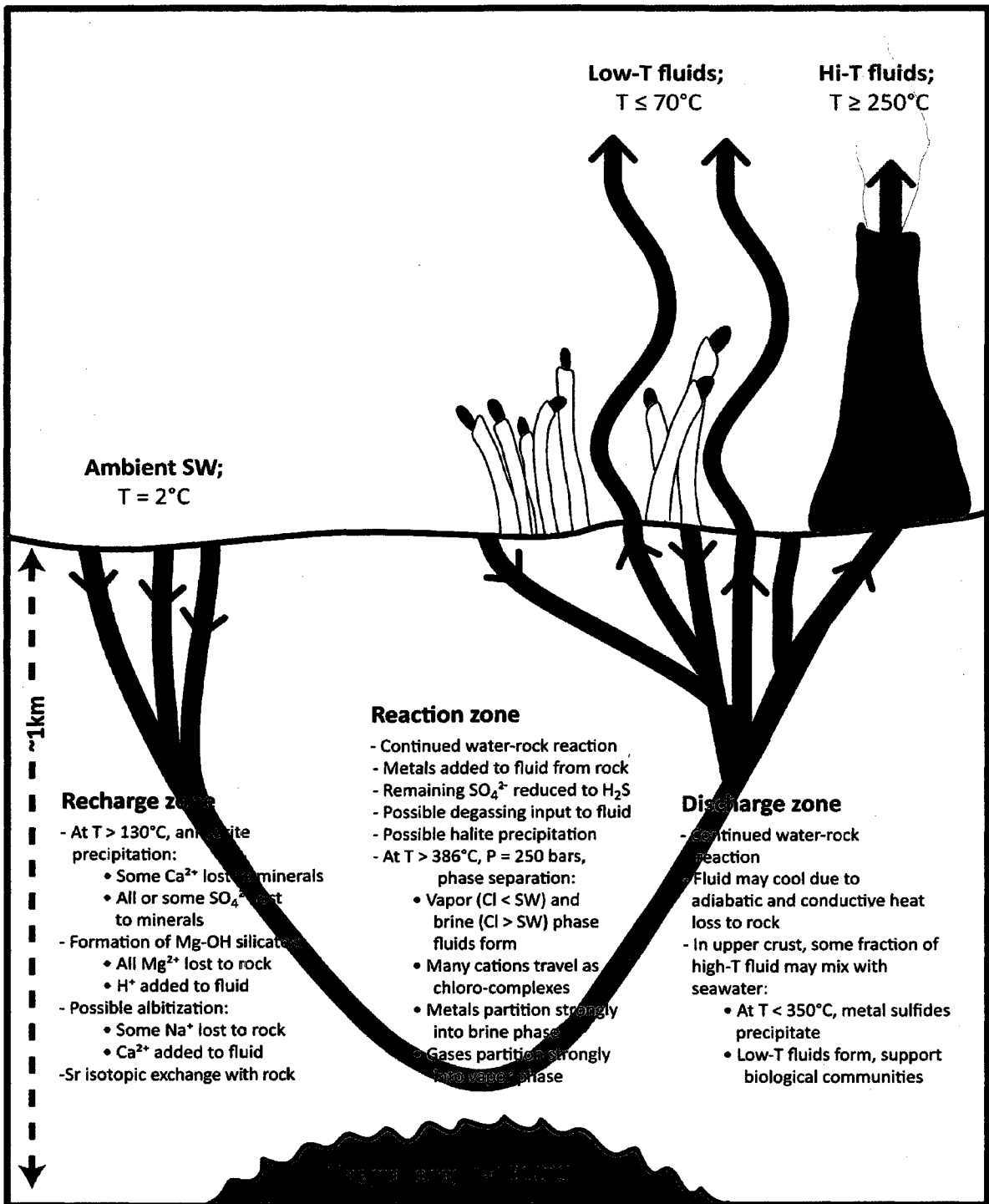
Figure 1: Schematic description of chemical processes occurring to a hydrothermal fluid as it begins as seawater and passes through the recharge, reaction, and discharge zones. After (Von Damm, 1995) and (German and Von Damm, 2004).

Controls on Ca, elemental Sr, and SO_4^{2-}

Von Damm (1995) described the sources and controlling mechanisms on element composition in hydrothermal systems, including those elements of interest to this study: Ca, SO_4^{2-}, elemental Sr, and isotopic Sr.

After normalization to Cl to correct for phase separation effects, hydrothermal Ca concentrations are generally elevated with respect to seawater concentrations, based on prior work by Von Damm (1995). Calcium is usually the second most abundant cation in hydrothermal fluids, with Na being the most abundant. Calcium is present in seawater but in hydrothermal fluids, seawater-sourced Ca is precipitated with SO_4^{2-} as anhydrite in the downflow zone. Due to the fact that there is more SO_4^{2-} than Ca in seawater, additional Ca must be leached from rock if more than 33% of available seawater sulfate is precipitated via anhydrite precipitation in the downflow zone (German and Von Damm, 2004). Therefore, Ca in hydrothermal fluids is derived mainly from a rock source (Von Damm, 1995).

Calcium is the cation released during water-rock interaction when Na is taken up during albitization reactions, and it is also exchanged via other mineral processes, including anhydrite and epidote or other Ca-Al-Si mineral phases.

The elemental Sr content of hydrothermal fluids can vary between enrichments or depletions, but is not strictly coupled with Cl (Von Damm, 1995). Due to the chemical similarity between the two alkali earth metals Sr and Ca, Sr is thought to be removed and added via the same processes as Ca.

Sulfate content of a high-temperature hydrothermal fluid, as already described, is essentially zero, due to removal by the two main processes of anhydrite precipitation in the downflow and reduction to H_2S in the reaction zones.

Controls on isotopic Sr

Strontium isotope variations within hydrothermal systems act as geochemical tracers of fluid evolution and mixing during circulation through the crust. Strontium has four naturally-occurring isotopes, including ^{88}Sr, ^{87}Sr, ^{86}Sr, and ^{84}Sr. All are stable, and have abundances of 82.53 percent, 7.04 percent, 9.87 percent, and 0.56 percent, respectively (Faure, 1977a; DePaolo and Ingram, 1985). Radioactive ^{87}Rb in rocks produces stable ^{87}Sr via beta decay:

$$^{87}Rb \rightarrow {}^{87}Sr + \beta^- + v + Q$$
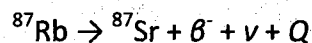
with a half-life of 4.75×10^{10} years (Kinsey et al, 1996), where β^- is a beta particle, v is an anti-neutrino, and Q is the decay energy. Thus, the amount of ^{87}Sr in a rock containing ^{87}Rb increases continuously as a function of time, and isotopic Sr composition is expressed as $^{87}Sr/^{86}Sr$. Due to the relatively long half-life, Sr isotope ratios in hydrothermal systems are best used as a means of elucidating reactions and processes occurring in the shallow oceanic crust, rather than for radiometric dating purposes. 9-10°N EPR basalt $^{87}Sr/^{86}Sr$ values fall in a very tight range between 0.70244 ± 5 to 0.70257 ± 6, and average 0.7025 (Sims et al., 2002). The present-day value of modern seawater $^{87}Sr/^{86}Sr$ is 0.70918 (Hodell et al., 1990).

To date, there have been a very limited number of published studies reporting Sr isotope systematics in hydrothermal fluids (Figure 2). Albarède et al. (1981) reported a high-temperature hydrothermal fluid end member $^{87}Sr/^{86}Sr$ of 0.7030 for a single high-temperature vent at 21°N EPR. Ravizza et al. (2000) reported end member $^{87}Sr/^{86}Sr$ at 9°46'-9°54'N EPR to range from more radiogenic values of 0.7042 (P vent and Bio9') and 0.7041 (Biovent) in more northern vents to less radiogenic values of 0.7039 and 0.7037 (A and L) in more southern vents (Ravizza et al., 2000) (Figure 2, 3). Ravizza et al. (2000) is the only published Sr isotope study of the 9°50'N EPR vents, and only includes high-temperature fluids sampled at one time point, in November 1996. My study aims to enhance our knowledge of the variability of Sr isotopes in two high-temperature vents (Ty and Io) over time, and also explores the relationship between $^{87}Sr/^{86}Sr$ values in coupled high-temperature vents (Ty and Io) and adjacent low-temperature flow (Biomarker 82). If subsurface anhydrite deposits with a unique $^{87}Sr/^{86}Sr$ signature are dissolving into low-temperature fluids, the Sr isotope systematics of adjacent high- and low-temperature vents will either record a two-component seawater-hydrothermal mixture, or will support anhydrite dissolution as an additional third component. This conceptual model for fluid evolution at low- and high-temperature vents is further described in Figure 4. An additional possibility is the presence of a possible fourth component, comprised of entrained seawater that is only partially reacted within the discharge zone. The low-temperature hydrothermal fluid mixture may therefore include four components: seawater, anhydrite, high-temperature hydrothermal fluid, and altered seawater.
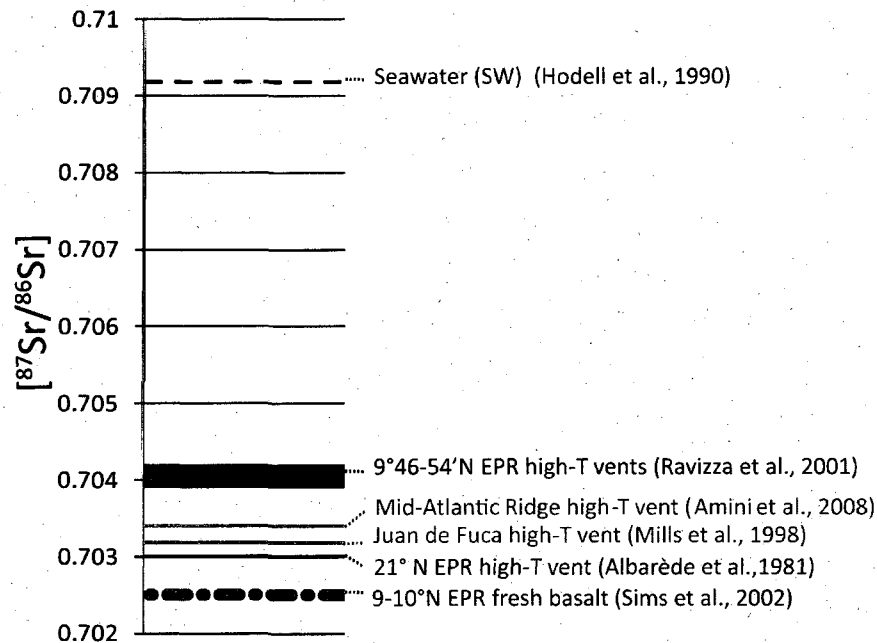
Figure 2: Summary of selected published studies reporting Sr isotope systematics in hydrothermal fluids, framed by the two end member $^{87}Sr/^{86}Sr$ values in the deep sea MOR hydrothermal system: modern seawater and 9-10°N EPR fresh basalt. The measured variability in values is represented by the thickness of the line.

Hydrothermal black smoker chimney growth

The hollow mineral formations which precipitate when high-temperature hydrothermal fluids are discharged at the seafloor are known as black smoker chimneys (Spiess et al., 1980; Haymon and Kastner, 1981). In a bare-basalt hosted deep sea MOR hydrothermal system such as the EPR, these chimneys undergo a complex growth history. Haymon (1983) analyzed chimneys from 21°N EPR, and described this growth history as occurring in two stages. Stage I occurs in the early history of the chimney, when seawater is heated to greater than 130°C, and anhydrite reaches super-saturation and precipitates to form the chimney walls. Caminite, a Mg-hydroxysulfate-hydrate mineral, can also

precipitate with the anhydrite. In stage II, continued outward precipitation of anhydrite will seal in the cracks in the chimney walls, thereby insulating the high-temperature fluid from mixing with seawater. This results in a hotter, more acidic, more reducing fluid passing through the central conduit of the chimney. Anhydrite is not stable in a reducing environment, and is progressively dissolved and replaced by Cu-Fe sulfide minerals.

It is likely that similar processes of mineral precipitation and dissolution occur in the plumbing system, or stockwork, within the discharge zone of a high-temperature vent (R. Haymon, pers. comm.). Anhydrite, and possibly caminite, may form if a large volume of seawater is suddenly entrained within the stockwork (e.g. during a cracking event brought on by a volcanic eruption). Indeed, Seyfried and Ding (1995) report that the dissolved Fe and Cu content of high-temperature fluids at 21°N EPR (HG vent, Von Damm et al., 1985) are consistent with a subsurface mineral assemblage which includes pyrite, magnetite, and anhydrite.

Calcium, Sr, SO_4^{2-}, and Mg can therefore all be removed from both the high-temperature fluids and seawater into mineral deposits, in both the chimney structure (during growth stage I) and in the stockwork (following mixing in of more oxidizing seawater in the discharge zone). Calcium, Sr, SO_4^{2-}, and Mg can also be dissolved and thus re-mobilized into the high-temperature hydrothermal fluids, whether by replacement of anhydrite or caminite in the chimneys by Cu-Fe sulfide minerals (during growth stage II), or dissolution of anhydrite in the stockwork due to a shift toward a more-reducing redox state in fluids passing through the discharge zone. It is therefore known from mineralogical

studies that Ca, Sr, SO_4^{2-}, and Mg are present in deposits during some portion of the growth history of black smoker chimneys and potentially in subsurface stockwork deposits, as anhydrite and caminite, but that this is an ephemeral sink of unknown magnitude. This study will address how the stability of anhydrite deposits in both the high- and low-temperature fluids may be affected by an eruption, and whether the re-mobilization signal may be detected in the high- and/or low-temperature fluids.
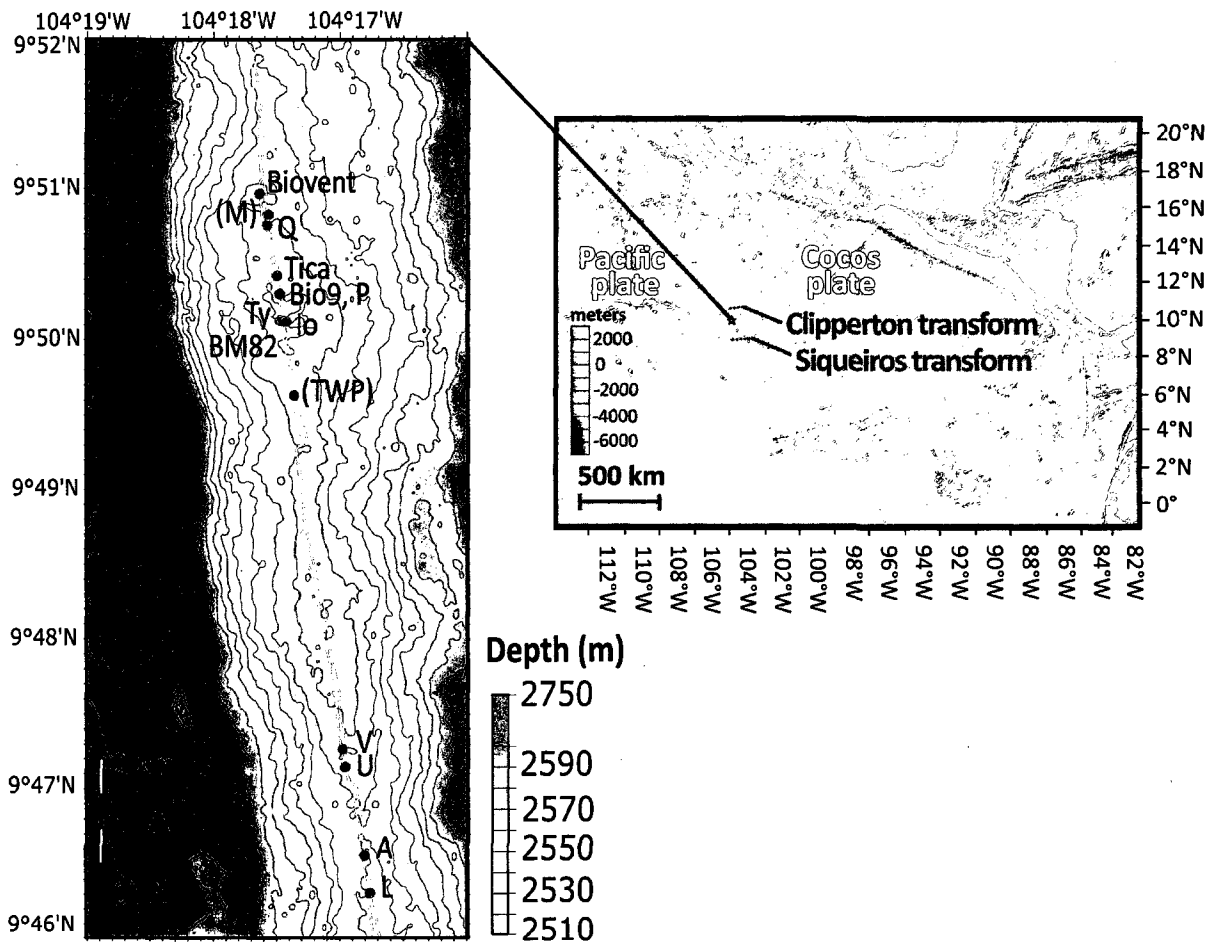
Figure 3: Location map of the 9°46-52'N section of the East Pacific Rise, bounded on the north by the Clipperton transform fault, on the south by the Siqueiros transform fault, on the west by the Pacific plate, and on the east by the Cocos plate (Image adapted from GeoMapApp, Mercator projection, http://www.geomapapp.org/). The detailed map shows pre-eruption multi-beam bathymetry and is adapted after Cochran et al. (1999). The axial summit trough (AST) is denoted by yellow lines. High-temperature vent sites are marked with red circles, and the BM82 low-temperature vent site is marked with a purple circle. Vent names in parentheses refer to vents that were observed to be extinct immediately following the eruption.
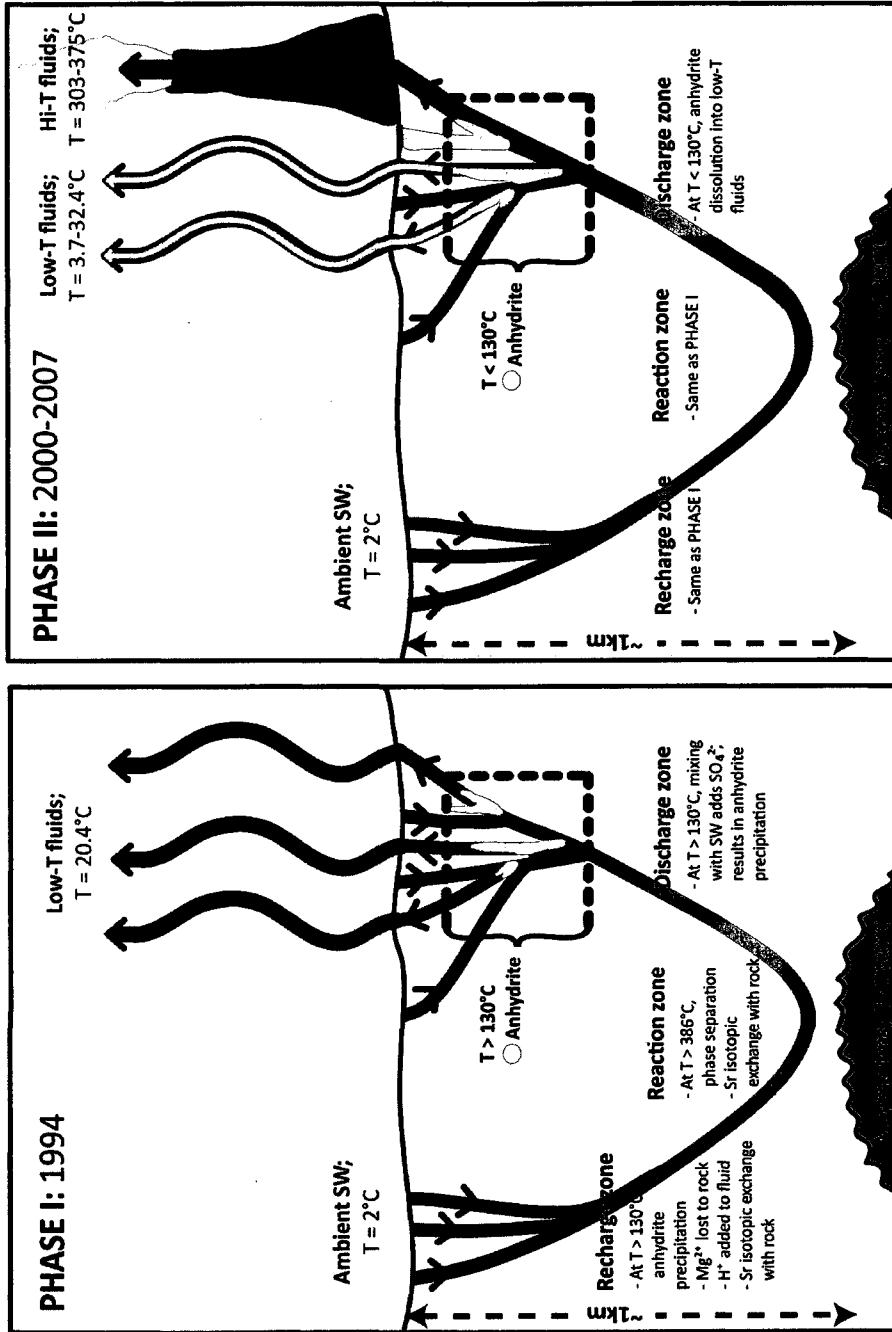
Figure 4: Conceptual model of fluid evolution. In Phase I, which corresponds with the 1994 sampling interval, only the low-temperature BM82 site was active. I hypothesize that anhydrite was precipitating sub-surface during Phase I. In Phase II, which corresponds to the 2000-2007 sampling interval, the high-temperature vents Ty and Io had formed and BM82 remained active. I hypothesize that anhydrite may be dissolving into the low-temperature fluids during Phase II, during the time period when the BM82 fluids were cooler in temperature, remobilizing Ca, Sr, and SO$_4$.

CHAPTER II

GEOLOGICAL SETTING

The 9-10°N latitude segment of the East Pacific Rise (EPR) is the site of a highly

detailed multidisciplinary study which has been ongoing since a volcanic eruption was

discovered there less than a month after its occurrence during an Ocean Drilling Project

(ODP) site survey in 1991 (Haymon et al., 1993). With a full spreading rate of 11cm yr^{-1}

(Klitgord and Mammerickx, 1982; Carbotte and Macdonald, 1992), 9-10°N EPR is classified

as a fast spreading ridge, and is bordered by the Pacific plate on the west and the Cocos

plate on the east (Figure 3). In the study area for this thesis, the water depth is 2500 ± 10m.

Multi-channel seismic surveys of the area conducted in 1985 (Detrick et al., 1987) match the

preliminary results of 3D seismic reflection imaging conducted in 2008 (Carbotte, pers.

comm.) to place the axial magma chamber at an approximate depth of 1.5 km beneath the

seafloor.

Time series studies at 9-10°N EPR

The site was chosen as a drill site by ODP with the goal of drilling zero-age oceanic crust and was the subject of a detailed photographic survey in 1989 by Argo II (Haymon et al., 1991). A 1991 dive program utilizing the *Deep Submergence Vehicle (DSV) Alvin* revealed an unexpected landscape within the Axial Summit Trough (AST), a trough-shaped feature which runs along the axis of the EPR. The dive program revealed vitreous new lava emplacement along an eruptive fissure system in the trough floor, freshly killed tubeworms, and blown-apart sulfide structures in the AST (Haymon et al., 1993). During this 25 dive series, temporal variations in the chemistry of vent fluids were observed on the time scale of days (Von Damm et al., 1995; Von Damm, 2000), in sharp contrast to prior studies, in which the observed chemistry of vent fluids had appeared temporally stable (e.g. Campbell et al., 1988). Despite the failed attempt of the ODP to drill new oceanic crust on Leg 142 in 1992, the discovery of the eruption at 9-10°N gave rise to a detailed and multi-disciplinary study of this MOR system.

Since 1991, oceanographic research cruises headed by principal investigators in the fields of chemistry, biology, and geophysics have monitored yearly changes at the 9-10°N EPR site. Among these principal investigators, Karen Von Damm of the University of New Hampshire has reported temporal variability in the temperature and chemistry of individual vents in the 9-10°N EPR study site (e.g. Von Damm et. al., 1995, 1997; Von Damm, 2000, 2004; Von Damm and Lilley, 2004). Due to the present difficulty to drill young, un-sedimented ocean crust at MORs, the chemical changes in the fluids, along with seismicity

and seismic structure, serve as one of our best indicators of processes occurring within the upper oceanic crust.

Low-temperature flow regions at 9-10°N EPR that formed post-1991-eruption, and their temporal and spatial biological colonization, have been described by Shank et al. (1998). Biological settlement took place in the most robust sites of low-temperature flow, located between 9°49-51'N and known as the 'Bio-Geotransect.' This robust flow is not continuous along the AST, rather, there are several discrete sites of low-temperature flow along this several-kilometer long stretch of ridge. Shank et al. (1998) hypothesized that while other factors (e.g. distances from larval sources, physical oceanographic processes) are certainly important during the early re-colonization of a post-eruptive vent community, geochemical conditions exerted a vital control over colonization patterns on a decadal timescale, due to the complex life strategies of different species, the pronounced chemical variability of fluids, and the transient nature of vent habitats.

Site description

The EPR 8-11°N segment is presently a Ridge 2000 Integrated Studies Site (http://www.ridge2000.org), with many advantages for long-term interdisciplinary work which include tectonic and morphologic diversity, ongoing monitoring of seismicity, and the abundance and diversity of known hydrothermal vents, plumes, and biological communities, along with the aforementioned direct observations of seafloor phenomena associated with the 1991 volcanic eruption (Haymon et al., 2002). The vent area chosen for this study

22

contains the high-temperature vents 'Ty' and 'Io' and a nearby region of vigorous low-temperature flow called 'Biomarker 82' (BM82), contained within the Bio-Geotransect and marked by one of 120 biomarkers following the 1991-92 eruption at 9°50'N (Figure 5). Prior to 1997, there was no high-temperature flow at BM82. In November 1997, part of the low-temperature flow focused into two high-temperature vents, subsequently named Ty and Io (Von Damm and Lilley, 2004). The AST near Ty, Io, and BM82 is a shallow ~2-4m trough that is ~45m wide, and is divided by a bathymetric high that is ~20m wide and ~2-3m in height.

Ty and Io are ~15m apart, and both are ~6-7m from BM82 (Figure 5). In 2005, these vents were surrounded by a new lava flow produced by a major eruption at the EPR, the timing of which is reported by Rubin et al. (2008), who used radiometric ^{210}Po-^{210}Pb to date the fresh lavas. Based on these age dates and geologic mapping, Rubin and al. (2008) report that 80% of the eruption lava volume had been emplaced by October 2005, and the eruption was 100% complete by January 2006. Although the 2005 eruption at 9-10°N EPR resulted in new lava emplacement and the loss of the physical biomarkers between the last sampling period in March 2004 and the first sampling period in June 2006, venting at the original Ty, Io and BM82 locations remained active immediately post-2005-eruption, as observed by the science party on the R/V Atlantis RESET06 (June-July 2006) and AT15-13 cruises (November 2006). During a DSV Alvin dive in December 2007, I observed that while Ty vent was still actively venting, there was no discernable fluid flow or temperature anomaly around Io vent, and it has since been considered to be inactive. In October 2008, an R/V Atlantis cruise reported that Ty vent is also now inactive.
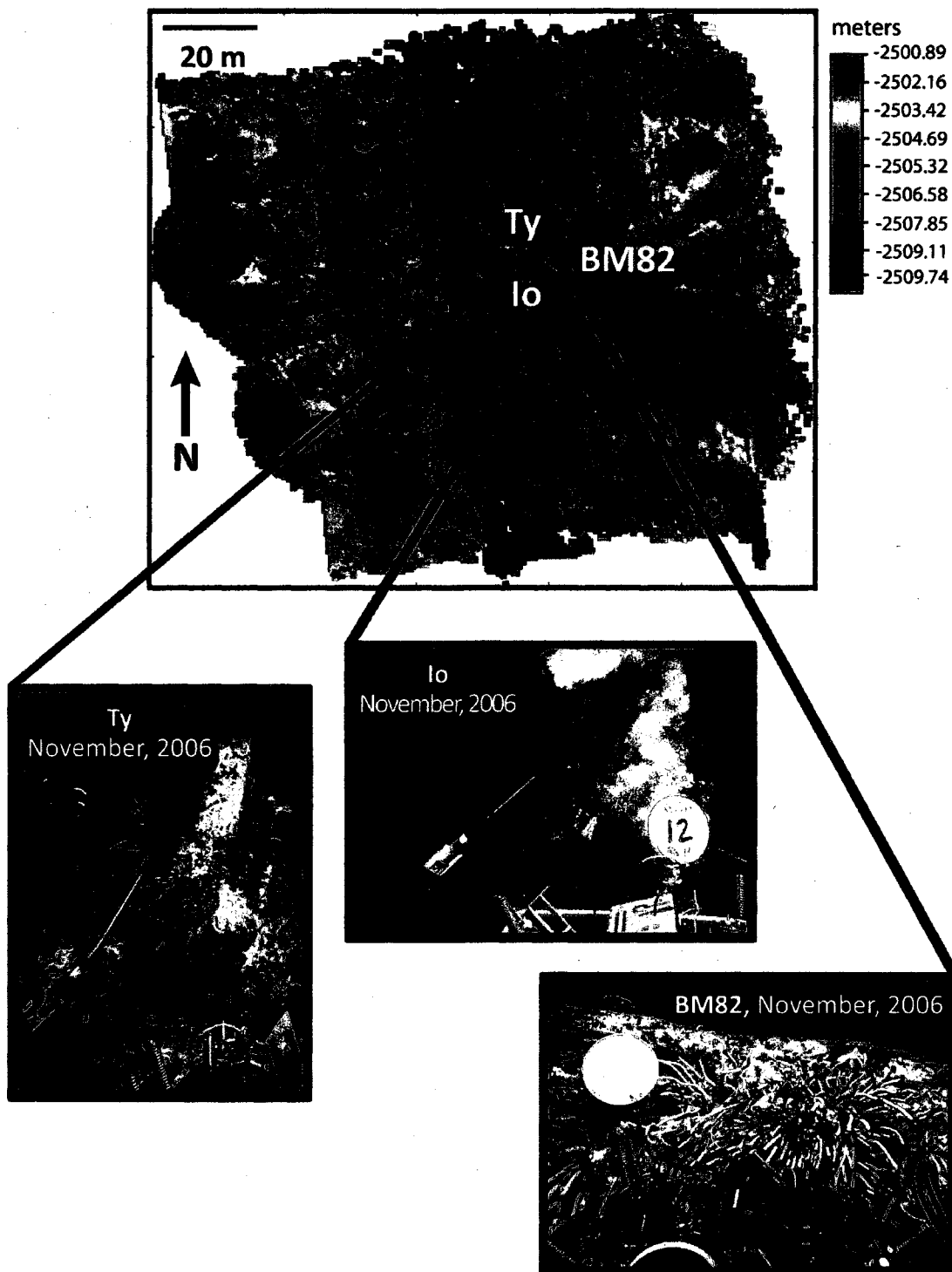
Figure 5: Top map shows detailed ABE micro-bathymetry of the Ty, Io, BM82 site, provided by D. Fornari and the R2K DMO. Ty and Io are about 15m apart, and both are about 6-7m from BM82. In vent photographs, bucket lid markers are about 30 cm in diameter, and HOBO temperature probes are about 1 m long.

CHAPTER III

METHODS

Over 15 years of time series work has been conducted at the 9-10°N site, and there exist fluid data documenting temperature, alkalinity, pH, and major, some minor, and some trace element changes in high-temperature and adjacent low-temperature flow. The extensive data set collected over this timescale includes two well-documented volcanic eruptions in 1991 and 1992 (Haymon et al., 1993; Rubin et al., 1994) and a recently discovered eruption that occurred in 2005-2006 (Cowen et al., 2007; Tolstoy et al., 2006; Rubin et al., 2008). A published subset of the low-temperature data focused only on those elements that provided evidence for chemical uptake by a subsurface biosphere (i.e. H_2, CH_4, CO_2, Fe, and Mn) (Von Damm and Lilley, 2004). This is the first consideration of these data for other element concentrations, and this study additionally incorporates new high- and low-temperature data from samples collected post-2005-eruption.

Sampling

This study utilized the Von Damm sample library at the University of New Hampshire (UNH) as well as samples collected from *R/V Atlantis* cruises in June-July 2006, November-

December 2006, and December 2007. Fluids at the Ty and Io vents and BM82 low-temperature flow area were sampled using 760mL titanium syringe bottle pairs on the *DSV Alvin* (Von Damm et al., 1985), which allows collection of uncontaminated samples for all metals except for titanium. In situ sampling temperatures were recorded using *Alvin*'s high-temperature probe as well as an inductively coupled link (ICL) temperature device on each pair of sampling bottles. Ambient local seawater samples were also collected utilizing the fluid sampling procedure. Samples were acidified with 0.5-1.0 mL of concentrated 3x distilled HCl, and stored in high-density polyethylene (HDPE) bottles on the day of sampling. Splits for shipboard chemical analysis were collected prior to acidification. A challenge in trace metal analysis is the potential for entrainment of precipitating particles within the sampling bottles, and thus the precipitates were rinsed out of the bottles during the sample draw, termed the "dregs" fraction, and saved in HDPE bottles.

Sample preparation

In the UNH lab, samples were filtered through 0.45μm Nucleopore® filters in a laminar flow bench to prevent contamination. The acidified, filtered fluid fraction samples are stored at room temperature in HDPE bottles. The filters and filtered particles as well as the dregs will be digested in Teflon microwave digestion vessels, for inclusion in the total metal concentration calculations in future work.

Major and minor element chemical analysis

Completed shipboard analyses for samples collected between 1991-2007 include pH, alkalinity by Gran Plot potentiometic titration, H_2S by iodimetric titration, silica and nutrients by colorimetric methods (Si, NH_4, PO_4), and major and minor elements and species (Na, Mg, Ca, Li, K, Sr, SO_4^{2-}, Br) by ion chromatography (IC). At UNH samples were additionally analyzed for Cl by potentiometric titration, and for metals (Fe, Mn, Cu, Zn) and major ions (Na, Mg, Ca, Li, K, Sr) by flame atomic absorption spectroscopy (FAAS). Method precisions are summarized in Table 1. UNH lab analyses were performed on filtered, acidified samples, and standardized to IAPSO Standard Seawater, a NIST-certified standard with a precisely known electrical conductivity ratio and salinity, except for H_2S and Si, which were standardized to Dilut-it® standard solutions. The major and minor elemental characterization allows for charge balancing of the samples using EQ3/6 (Wolery, 1992).

The FAAS method for Sr has been historically applied in the shore-based laboratory, but has a precision of 2%. A more precise method (1% precision) for determining elemental Sr was developed via inductively coupled plasma mass spectrometry (ICP-MS). Twenty samples were run per day on the Nu Instruments AttoM HR-ICP-MS at UNH. Samples were diluted gravimetrically 3500x to approximately 22 nmol/kg Sr with 2% 3x sub-boiling Teflon® distilled "Optima" HNO_3 Optima HNO_3, based on Sr composition determined earlier via IC and FAAS. All samples and standards were spiked with 12nmol/kg Yttrium (Assurance Spex-Certiprep standard) to correct for signal drift. Standards were run at 0, 5.8, 11.6, 17.4, 23.2, 29.0, and 34.8 nmol/kg Sr concentration (Ricca Chemical Company AA standard) in 2%

Element/Species	Method	Precision
Cl	Potentiometric titration	± 0.5 %
Li	FAAS/FAAS with standard additions	± 1 % / ± 3 %
Na	FAAS	± 2 %
K	FAAS	± 1 %
Mg	FAAS	± 1 %
Ca	FAAS	± 1 %
Sr elemental	HR-ICP-MS	± 1 %
Sr isotopes	TIMS	± 0.000018
pH (25°C, 1 atm)	Potentiometry	± 0.01
Alkalinity$_{total}$	Potentiometric titration/Gran plot	± 0.5 %
H$_2$S	Colorimetry/Starch titration	± 5 %
SO$_4^{2-}$	Ion chromatography	± 1 %
Br	Ion chromatography	± 3 %
Si	Colorimetry	± 1 %

Table 1: Summary of analytical methods and precisions. FAAS, flame atomic absorption spectroscopy; ICP-MS, inductively coupled plasma mass spectrometry; TIMS, thermal ionization mass spectrometry. With the exception of the new elemental Sr and isotopic Sr methods developed specifically for this study, precisions are after (Von Damm, 2000).

Optima HNO$_3$ after every 20 samples. A monitor consisting of 22 nmol/kg Sr in 2% Optima HNO$_3$ was run every 5 samples, along with a duplicate sample every 10 samples, to monitor signal stability and method precision. A bottom seawater sample was run several times, and all results were standardized to IAPSO seawater. For HR-ICP-MS operating conditions, see Appendix A.

In preparation for Sr isotope analysis of the hydrothermal fluids, Sr was separated from the sample matrix using EiChrom Sr Spec resin, adapting the methods employed by Ravizza et al., 2000 and Bryce et al., 2005. Sample aliquots ranging between 0.2-2.0 mL were pipeted into 7 mL HNO$_3$-clean Teflon® Savillex vials from the acidified fluid fraction

such that each sample would contain ~30 nmol of total Sr. Concentrated Optima HNO_3 was added such that the samples were in 3N HNO_3, and the samples were dried down on a hotplate under laminar flow to minimize their organic content. They were brought back up in 400 μL of 3N HNO_3, and sonicated for 20 minutes to ensure complete dissolution. The samples were then run through columns according to the method outlined in Appendix B. After completion of the column work, samples were dried down completely under laminar flow and brought back up in 2 drops of concentrated Optima HNO_3, then heated in closed vials until samples were completely dissolved and a small drop of ~20 μL volume remained.

Strontium isotope analysis

Strontium isotopes were measured on vent samples at Boston University by thermal ionization mass spectrometry (TIMS) using the Finnigan Triton. In a laminar flow bench, sample volumes of 1.0μL (~100ng) were loaded on single Re filaments and dried, and 2.0μL TaO in 5% phosphoric acid activator was added and dried prior to loading in the turret. To ionize Sr, manual runs resulted in the best result when the sample was ramped to 2400mA (200mA/min) and then ramped slowly (100-50mA/min) to 3500mA, which corresponded with a pyrometer temperature of ~1400°C and 2-4 volts of signal intensity in ^{88}Sr. During the course of sample analysis repeat runs of NIST SRM 987 (100ng loads) yielded an external $^{87}Sr/^{86}Sr$ reproducibility of 0.710247 ± 19 2σ (n=6). Repeat 100ng load runs of an in-house standard gave a long term external $^{87}Sr/^{86}Sr$ reproducibility of .707507 ± 18 2σ

(n=16). Two analyses on IAPSO seawater yielded $^{87}Sr/^{86}Sr$ of 0.709169 ± 4 2σ and 0.709179

± 7 2σ, in agreement with the accepted modern seawater value (Hodell et al., 1990).

Due to slight differences in their atomic masses, the ionization potential of ^{86}Sr and

^{87}Sr differs, and results in mass dependent fractionation within the TIMS. A correction, or

fractionation, factor is calculated by normalizing the measured $^{86}Sr/^{88}Sr$ to the accepted

$^{86}Sr/^{88}Sr$ value. This same fractionation factor is then applied linearly to correct the

measured $^{87}Sr/^{86}Sr$.

Recent advances in high precision isotope ratio instruments, such as the multi-

collector inductively coupled plasma mass spectrometer (MC-ICP-MS) and the TIMS, have

resulted in a small number of studies reporting $^{88}Sr/^{86}Sr$ fractionation in marine

environments, specifically corals (Fietze and Eisenhauer, 2006; Halicz et al., 2008;

Ruggeberg et al., 2008). It is not known how the higher temperature and pressure

conditions in a hydrothermal MOR setting may affect potential fractionation of $^{86}Sr/^{88}Sr$ in

hydrothermal fluids. If this process is occurring, however, I am assuming that it affects all

the fluids to a similar degree. Hence, the changes in fluid isotopic composition over time

may still be compared on a relative basis. See Table 2a and Table 2b for temperature, major

and minor elements, Sr isotope, pH, and alkalinity raw data.

High-temperature end member calculation

Seawater always comprises some volume of a hydrothermal fluid sample, due to (1)

seawater used to fill the dead volume in the titanium bottles prior to sampling and (2)

seawater entrainment during sample collection. Based on studies that show Mg ≈ 0

mmol/kg in pure vent fluids (e.g. Bischoff and Dickson, 1975), elemental end members were

calculated for a high-temperature fluid by performing a least-squares regression of an

individual chemical species versus Mg, assuming passage through the ambient bottom

seawater composition, and extrapolating to 0 mmol/kg Mg. In the case of a Sr isotope end

member calculation, sample and seawater isotopic values were plotted against Mg/Sr to

account for the variation in Sr between seawater and the samples. Chemical data for all

majors samples collected for a vent at one time (one dive), plus 15 inputs for the seawater

value are used for each high-temperature fluid end member regression, an example of

which is shown in Figure 6. Generally speaking, the standard error of the intercept is equal

to or less than the method precision, so method precisions were applied to determine end

member as well as discrete sample uncertainties, unless specifically noted. See Table 3 for

calculated end member data.

Mixing hyperbola equation and uncertainty analysis

One method used to examine the relationship between high- and low-temperature

fluids at a particular sampling interval was the application of Sr isotopes to draw mixing

hyperbolae for the high-temperature fluid-seawater mixtures. The Sr isotope composition

of a mixture was calculated according to the equation:

$$[^{87}Sr/^{86}Sr]_{mix} = \frac{(f)[Sr]_{SW}[^{87}Sr/^{86}Sr]_{SW} + (1-f)[Sr]_{Hi\text{-}T}[^{87}Sr/^{86}Sr]_{Hi\text{-}T}}{(f)[Sr]_{SW}+(1-f)[Sr]_{Hi\text{-}T}}$$

Where f is the mole fraction of seawater in the mixture, $[Sr]_{SW}$ is the elemental Sr

concentration of seawater, $[^{87}Sr/^{86}Sr]_{SW}$ is the isotopic Sr composition of seawater, $[Sr]_{Hi-T}$ is

the calculated end member elemental Sr concentration of the high-temperature fluid

(Figure 6 shows example end member calculation) , and $[^{87}Sr/^{86}Sr]_{Hi-T}$ is the calculated end

member isotopic Sr composition of the high-temperature fluid (Faure, 1977b). This

equation expresses the mixture as a mass balance that assumes constant ^{86}Sr abundances in

both end members. The Sr isotope mixture hyperbolae were plotted versus elemental Sr,

elemental Ca/Sr, and elemental Mg/Sr by applying the same mole fraction of seawater as

for the mixture.

In order to determine the uncertainty in these hyperbolae, a Monte Carlo statistical

analysis was performed (Bevington and Robinson, 2003). The mean and twice the standard

error of each of the four input values as described above were input into a spreadsheet

which generated 10,000 randomly-generated inverse normal distributed values. The values

used are described as follows:

Mean $[Sr]_{SW}$ = 89.53 µmol/kg; 2x standard error $[Sr]_{SW}$ = 0.8953

Mean $[^{87}Sr/^{86}Sr]_{SW}$ = 0.7091702; 2x standard error $[^{87}Sr/^{86}Sr]_{SW}$ = 0.0000541 (based on 600+ runs of bottom seawater)

Mean $[Sr]_{Hi-T}$ = Calculated end member value (Table 3); 2x standard error $[Sr]_{Hi-T}$ = Uncertainty on end member value (Table 3)

$[^{87}Sr/^{86}Sr]_{Hi-T}$ = Calculated end member value (Table 3); 2x standard error $[Sr]_{Hi-T}$ = 0.0000541

These 10,000 x 4 values were then input into the mixing equation (above) for f values

ranging from 0-1 (pure seawater to pure high-temperature hydrothermal mixture)

(increment 0.025) to generate 10,000 result values for each f value. The mean and standard

deviation of these 10,000 results for each f represent the uncertainty in the mixture. For

the mixing hyperbolae plots (presented in the Results and Discussion Chapter) the

uncertainty in the y-axis (the isotopic mixture uncertainty, as calculated above) was

compared with that of the x-axis (the elemental concentration or elemental ratio

uncertainty, based on method precisions) and the greater error is plotted.
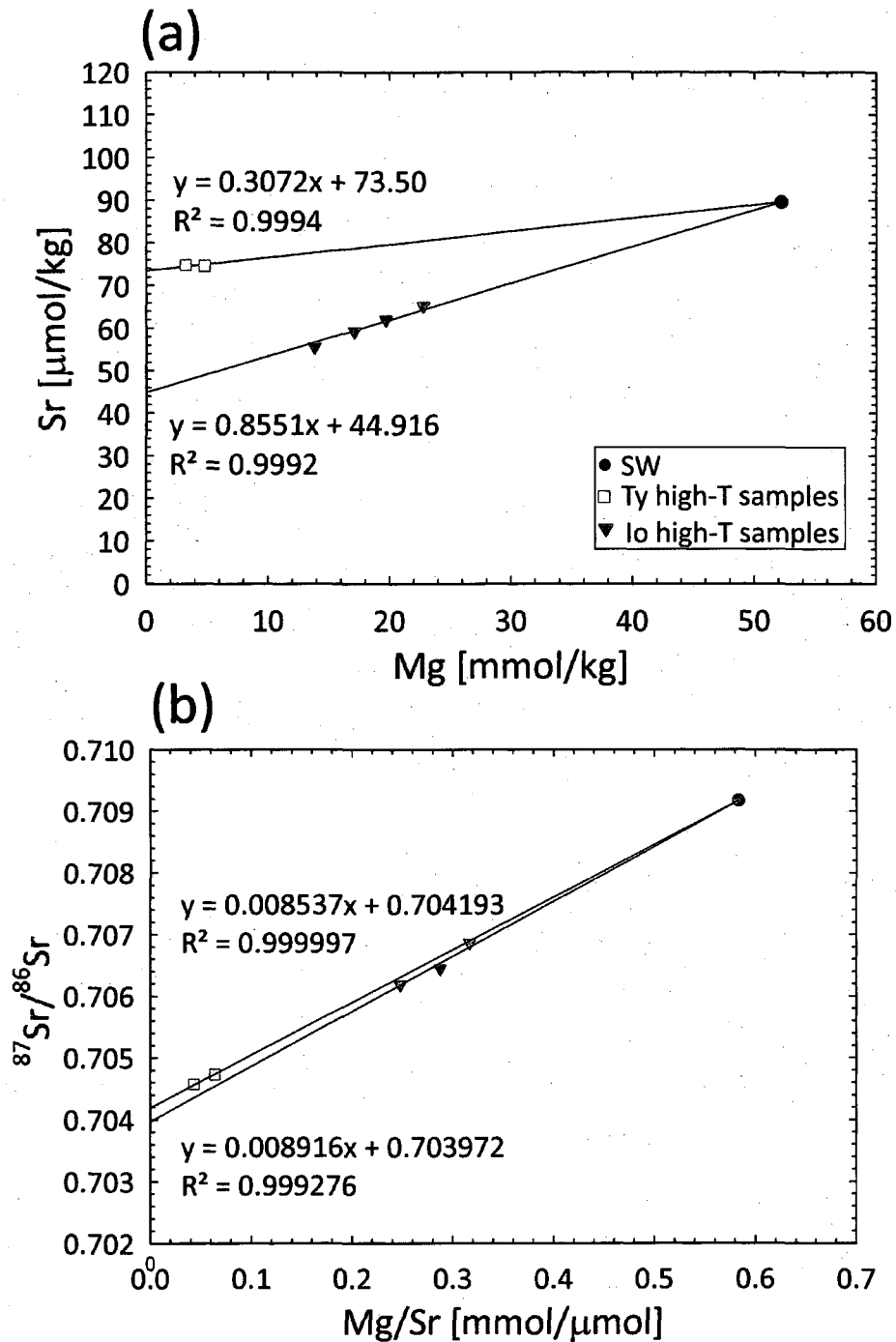
Figure 6: Examples of end member plots and regressions, shown for (a) elemental Sr and (b) isotopic Sr, for discrete Ty (orange squares) and Io (red triangles) samples collected in April 2000. The seawater value is indicated with a blue circle. The 0.0 Mg (for Sr) and 0.0 Mg/Sr (for ^{87}Sr/^{86}Sr) intercept is taken to represent the end member value for that vent.

Vent	Date	Max Meas T [°C]	Mg [mmol/l]	Cl [mmol]	Si [mmol]	H₂S [mmol]	Na-Meas [mmol]	Na-CB [mmol]	K [mmol]	Li [μmol/l]	Ca [mmol]	Sr [μmol]	SO₄²⁻ [mmol]	Br [μmol]	⁸⁷Sr/⁸⁶Sr	pH	Alk [meq/l]
BM82	10/27/1994	20.4	48.5 ± 0.5	534 ± 3	0.767 ± 0.008	0.163 ± 0.008	469 ± 9	460 ± 9	10.3 ± 0.1	43.7 ± 0.4	11.0 ± 0.1	91.2 ± 0.9	26.5 ± 0.3	n.m.	0.709063 ± 5	5.82	2.27
BM82	10/27/1994	20.4	49.7 ± 0.5	536 ± 3	0.753 ± 0.007	0.106 ± 0.005	465 ± 9	458 ± 9	11.3 ± 0.1	5.00 ± 0.05	11.2 ± 0.1	89.5 ± 0.9	26.3 ± 0.3	n.m.	0.709073 ± 7	5.84	2.24
BM82	10/27/1994	20.4	49.8 ± 0.5	546 ± 3	0.727 ± 0.007	0.356 ± 0.018	465 ± 9	467 ± 9	11.7 ± 0.1	5.7 ± 0.06	11.1 ± 0.1	83.0 ± 0.8	26.3 ± 0.3	n.m.	0.709078 ± 7	5.86	2.29
BM82	4/16/2000	10.5	51.4 ± 0.5	535 ± 3	0.294 ± 0.003	0.0291 ± 0.0015	449 ± 9	460 ± 9	10.1 ± 0.1	21.2 ± 0.2	10.3 ± 0.1	91.3 ± 0.9	27.6 ± 0.3	801 ± 24	0.709107 ± 6	6.14	2.29
BM82	4/16/2000	10.5	51.8 ± 0.5	535 ± 3	0.295 ± 0.003	0.0291 ± 0.0031	451 ± 9	459 ± 9	10.2 ± 0.1	21.3 ± 0.2	10.4 ± 0.1	90.5 ± 0.9	27.6 ± 0.3	808 ± 24	0.709112 ± 6	6.20	2.26
BM82	4/16/2000	10.5	52.1 ± 0.5	537 ± 3	0.284 ± 0.003	0.0610 ± 0.0031	470 ± 9	459 ± 9	10.1 ± 0.1	19.9 ± 0.2	10.4 ± 0.1	89.1 ± 0.9	27.5 ± 0.3	850 ± 26	n.m.	6.54	2.32
BM82	1/19/2002	3.7	51.7 ± 0.5	547 ± 3	0.182 ± 0.002	n.m.²	463 ± 9	472 ± 9	10.3 ± 0.1	23.2 ± 0.2	10.3 ± 0.1	89.5 ± 0.9	28.2 ± 0.3	813 ± 24	0.709165 ± 7	n.m.	1.51
BM82	1/19/2002	3.7	51.4 ± 0.5	540 ± 3	0.228 ± 0.002	n.m.	459 ± 9	466 ± 9	10.1 ± 0.1	24.0 ± 0.2	10.1 ± 0.1	88.6 ± 0.9	28.2 ± 0.3	819 ± 25	0.709154 ± 7	6.19	2.35
BM82	1/19/2002	3.7	50.7 ± 0.5	539 ± 3	0.217 ± 0.002	n.m.	461 ± 9	465 ± 9	10.6 ± 0.1	24.3 ± 0.3	10.4 ± 0.1	89.9 ± 0.9	27.9 ± 0.3	816 ± 24	0.709148 ± 6	5.87	2.47
BM82	3/21/2004	13.7	51.6 ± 0.5	540 ± 3	0.200 ± 0.002	n.m.	453 ± 9	461 ± 9	10.1 ± 0.1	22.3 ± 0.2	10.2 ± 0.1	94.8 ± 0.9	25.9 ± 0.3	963 ± 29	0.709166 ± 3	7.23	2.39
BM82	3/21/2004	13.7	50.6 ± 0.5	542 ± 3	0.665 ± 0.007	0.0581 ± 0.0029	454 ± 9	462 ± 9	10.4 ± 0.1	36.2 ± 0.4	10.7 ± 0.1	91.5 ± 0.9	25 ± 0.3	979 ± 29	0.709019 ± 3	6.18	2.44
BM82	3/21/2004	13.7	51.5 ± 0.5	539 ± 3	0.591 ± 0.006	0.0920 ± 0.0046	457 ± 9	457 ± 9	10.1 ± 0.1	27.2 ± 0.3	10.9 ± 0.1	90.5 ± 0.9	24.8 ± 0.3	964 ± 29	0.709127 ± 5	6.82	2.55
BM82	6/27/2006	20.8	51.7 ± 0.5	537 ± 3	0.375 ± 0.004	n.m.	452 ± 9	n.m.	9.93 ± 0.10	33.1 ± 0.3	10.6 ± 0.1	78.8 ± 0.8	27.0 ± 0.3	891 ± 27	0.709154 ± 4	6.49	2.54
BM82	6/27/2006	20.8	52.9 ± 0.5	534 ± 3	0.282 ± 0.003	n.m.	457 ± 9	n.m.	10.9 ± 0.1	17.9 ± 0.2	11.1 ± 0.1	88.9 ± 0.9	27.5 ± 0.3	908 ± 27	0.709160 ± 5	6.72	2.68
BM82	6/27/2006	20.8	52.1 ± 0.5	535 ± 3	0.233 ± 0.002	n.m.	452 ± 9	n.m.	10.1 ± 0.1	22.8 ± 0.2	10.5 ± 0.1	88.8 ± 0.9	27.6 ± 0.3	899 ± 27	0.709171 ± 5	6.81	2.46
BM82	6/27/2006	20.8	52.1 ± 0.5	532 ± 3	0.290 ± 0.003	n.m.	451 ± 9	n.m.	9.93 ± 0.10	24.0 ± 0.2	10.5 ± 0.1	87.7 ± 0.9	27.5 ± 0.3	905 ± 27	0.709159 ± 4	6.66	2.49
BM82	11/29/2006	30.6	50.5 ± 0.5	524 ± 3	0.723 ± 0.007	0.856 ± 0.043	437 ± 9	451 ± 9	9.60 ± 0.10	28.7 ± 0.3	10.4 ± 0.1	85.1 ± 0.9	27.7 ± 0.3	918 ± 28	0.709157 ± 7	5.26	2.31
BM82	11/29/2006	30.6	50.8 ± 0.5	528 ± 3	0.600 ± 0.006	0.368 ± 0.035	434 ± 9	454 ± 9	9.56 ± 0.1	27.6 ± 0.3	10.7 ± 0.1	85.7 ± 0.9	27.9 ± 0.3	910 ± 27	0.709151 ± 6	4.92	2.35
BM82	11/29/2006	30.6	50.8 ± 0.5	528 ± 3	0.668 ± 0.007	0.692 ± 0.035	435 ± 9	455 ± 9	9.65 ± 0.1	24.9 ± 0.2	10.6 ± 0.1	87.2 ± 0.9	28.5 ± 0.3	932 ± 28	0.709151 ± 7	5.36	2.35
BM82	12/16/2007	32.4	49.4 ± 0.5	520 ± 3	0.680 ± 0.007	5.86 ± 0.29	447 ± 9	n.m.	10.1 ± 0.1	n.m.	9.75 ± 0.10	84.9 ± 0.8	n.m.	n.m.	0.709165 ± 8	0.94	2.30
BM82	12/16/2007	32.4	49.0 ± 0.5	522 ± 3	0.629 ± 0.006	5.96 ± 0.30	449 ± 9	n.m.	10.5 ± 0.1	n.m.	9.73 ± 0.10	83.8 ± 0.8	n.m.	n.m.	0.709166 ± 11	0.50	2.38
BM82	12/16/2007	32.4	49.7 ± 0.5	518 ± 3	0.681 ± 0.007	5.98 ± 0.30	452 ± 9	n.m.	10.3 ± 0.1	n.m.	9.45 ± 0.09	86.8 ± 0.9	n.m.	n.m.	0.709152 ± 7	0.51	2.49
Seawater	6/28/2006	2.0	52.4 ± 0.5	537 ± 3	0.126 ± 0.001	0.0000	453 ± 9	n.m.	10.1 ± 0.1	25.6 ± 0.3	10.3 ± 0.1	89.5 ± 0.9	25.8 ± 0.3	938 ± 28	0.709171 ± 7	7.58	2.40

¹all are per kilogram
²n.m. = not measured

Table 2a: Summary of raw data for low-temperature BM82 filtered fluid sample fractions. Bottom seawater data also reported. Na-CB are charge-balanced values, while Na-Meas are measured values. Errors are 2x standard error.

35

Table 2b: Summary of raw data for high-temperature Ty and Io fluid sample fractions. Bottom seawater data also reported. Na-CB are charge-balanced values, while Na-Meas are measured values. Errors are 2x standard error.

Vent	Date	Max Meas T [°C]	Mg [mmol][1]	Cl [mmol]	Si [mmol]	H_2S [mmol]	Na-Meas [mmol]	Na-CB [mmol]	K [mmol]	Li [μmol][1]	Ca [mmol]	Sr [μmol]	SO_4^{2-} [mmol]	Br [μmol]	$^{87}Sr/^{86}Sr$	pH	Alk [meq][1]
Io.1	4/23/2000	347	19.7±0.2	383±2	6.28±0.06	5.45±0.27	327±7	330±7	10.2±0.1	203±2	10.2±0.1	62.1±0.6	10.7±0.1	603±18	0.70687±6	3.50	-0.338
Io.1	4/23/2000	347	22.8±0.2	396±2	5.82±0.06	4.98±0.25	338±7	340±7	10.1±0.1	191±2	10.3±0.1	65.4±0.7	11.7±0.1	618±19	n.m.	3.61	-0.225
Io.1	4/23/2000	347	13.8±0.1	360±2	8.14±0.08	6.18±0.31	302±6	311±6	10.2±0.1	251±3	10.1±0.1	55.7±0.6	7.18±0.07	556±17	0.706192±7	3.33	-0.507
Io.1	4/23/2000	347	17.1±0.2	364±2	7.36±0.07	5.52±0.28	314±6	311±6	10.3±0.1	228±2	10.0±0.1	59.4±0.6	8.51±0.09	567±17	0.706452±6	3.41	-0.409
Io.2	1/19/2002	350	17.0±0.2	493±2	8.46±0.08	6.82±0.34	422±8	423±8	14.7±0.1	350±4	15.1±0.2	85.4±0.9	9.53±0.10	766±23	0.705770±6	3.12	-0.622
Io.2	1/19/2002	350	10.6±0.1	484±2	10.3±0.1	5.67±0.28	414±8	415±8	15.4±0.2	400±4	15.8±0.2	83.6±0.8	6.00±0.06	761±23	n.m.	3.05	-0.739
Io.2	1/19/2002	350	2.99±0.03	474±2	11.7±0.1	6.39±0.32	406±8	406±8	16.2±0.2	474±5	17.7±0.2	83.5±0.8	2.12±0.02	754±23	n.m.	2.96	-0.710
Io.2	1/19/2002	350	6.65±0.07	480±2	10.9±0.1	6.39±0.32	408±8	411±8	16.4±0.2	434±4	16.6±0.2	83.2±0.8	3.71±0.04	743±22	0.704798±8	3.06	-0.680
Io.5	3/21/2004	353	2.23±0.02	535±3	12.8±0.1	6.31±0.32	453±9	460±9	18.6±0.2	625±6	20.3±0.2	101±1	0.968±0.010	975±29	0.704140±6	3.17	-0.683
Io.5	3/21/2004	353	4.76±0.05	541±3	12.1±0.1	6.09±0.30	456±9	464±9	18.0±0.2	591±6	20.1±0.2	98.6±1.0	2.90±0.03	974±29	0.704370±3	3.25	-0.571
Io.8	6/30/2006	375	29.5±0.3	343±2	2.44±0.02	12.8±0.6	278±6	n.m.	6.42±0.06	23.5±0.2	9.41±0.09	64.6±0.6	16.8±0.2	588±18	0.708923±7	3.76	0.174
Io.8	6/30/2006	375	34.2±0.3	383±2	1.76±0.02	11.5±0.6	322±6	n.m.	7.18±0.07	20.7±0.2	12.8±0.1	82.7±0.8	19.5±0.2	624±19	0.708925±10	4.63	0.753
Io.8	6/30/2006	375	29.8±0.3	343±2	2.04±0.02	11.3±0.6	280±6	n.m.	6.29±0.06	20.8±0.2	10.6±0.1	64.8±0.6	18.0±0.2	562±17	0.708877±6	4.47	0.686
Io.8	6/30/2006	375	28.7±0.3	370±2	1.85±0.02	11.3±0.6	281±6	n.m.	6.30±0.06	22.7±0.2	11.0±0.1	68.5±0.7	20.6±0.2	634±19	0.708887±13	4.70	0.872
Io.9	7/1/2006	374	27.7±0.3	326±2	2.80±0.03	15.2±0.8	273±5	n.m.	6.09±0.06	21.4±0.2	6.47±0.06	48.3±0.5	14.2±0.1	556±17	0.709037±18	3.67	-0.140
Io.9	7/1/2006	374	26.4±0.3	314±2	3.07±0.03	15.5±0.8	265±5	n.m.	5.66±0.06	22.2±0.2	6.35±0.06	45.4±0.5	14.0±0.1	536±16	0.708982±4	3.63	-0.229
Io.9	7/1/2006	374	20.8±0.2	289±1	3.39±0.03	16.6±0.8	231±5	n.m.	4.76±0.05	22.9±0.2	5.16±0.05	36.8±0.4	13.0±0.1	506±15	n.m.	3.38	-0.471
Io.9	7/1/2006	374	25.3±0.3	361±2	2.28±0.02	11.9±0.6	257±5	n.m.	5.58±0.06	20.0±0.2	6.15±0.06	42.5±0.4	17.7±0.2	605±18	0.708955±5	4.54	0.481
Io.10	11/28/2006	303	32.4±0.3	414±2	4.81±0.05	6.02±0.30	350±7	355±7	7.80±0.08	44.9±0.4	10.0±0.1	64.3±0.6	17.1±0.2	717±22	0.708612±7	4.69	0.581
Io.10	11/28/2006	303	36.5±0.4	444±2	3.72±0.04	4.89±0.24	376±8	382±8	8.55±0.09	43.4±0.4	10.3±0.1	69.3±0.7	19.9±0.2	768±23	0.708782±5	4.92	0.984
Ty.4	4/22/2000	352	3.24±0.03	416±2	12.5±0.1	6.78±0.34	354±7	357±7	13.9±0.1	407±4	15.6±0.2	74.8±0.7	1.54±0.02	672±20	0.704570±7	3.18	-0.670
Ty.4	4/22/2000	352	4.79±0.03	419±2	12.8±0.1	6.84±0.34	365±7	359±7	14.1±0.1	395±4	15.4±0.2	74.6±0.7	2.41±0.02	675±20	0.704733±7	3.13	-0.758
Ty.5	1/19/2002	349	3.48±0.03	547±3	14.2±0.1	6.89±0.34	463±9	467±9	19.0±0.2	524±5	21.7±0.2	103±1	1.75±0.02	871±26	0.704361±7	3.85	-0.077
Ty.5	1/19/2002	349	3.41±0.03	548±3	14.1±0.1	7.98±0.40	464±9	468±9	18.3±0.2	523±5	21.6±0.2	97.8±1.0	1.66±0.02	865±26	0.704377±6	3.22	-1.31
Ty.5	1/19/2002	349	3.10±0.03	546±3	14.0±0.1	7.23±0.36	468±9	466±9	19.0±0.2	526±5	21.5±0.2	101±1	1.35±0.01	870±26	0.704343±6	3.97	-0.736
Ty.8	3/21/2004	323	3.74±0.04	579±3	15.0±0.2	5.14±0.26	496±10	494±10	19.2±0.2	629±6	23.3±0.2	111±1	1.39±0.01	1058±32	0.704281±15	3.15	-0.776
Ty.8	3/21/2004	323	4.30±0.04	582±3	14.3±0.1	5.35±0.27	499±10	494±10	19.4±0.2	612±6	23.7±0.2	110±1	0.994±0.010	1044±31	n.m.	3.16	-0.760
Ty.8	3/21/2004	323	3.16±0.03	582±3	15.1±0.2	5.40±0.27	503±10	495±10	20.2±0.2	619±6	23.8±0.2	115±1	1.14±0.01	1056±32	0.704288±7	3.11	-0.802
Ty.8	3/21/2004	323	3.81±0.04	581±3	14.3±0.1	5.17±0.26	499±10	494±10	19.7±0.2	627±6	23.2±0.2	111±1	0.877±0.009	1063±32	0.704309±7	3.14	-0.738
Ty.10	11/29/2006	359	22.7±0.02	313±2	4.86±0.05	16.4±0.82	257±5	258±5	5.67±0.06	35.3±0.4	11.3±0.1	57.9±0.6	12.5±0.1	552±17	0.708305±6	2.80	-1.51
Ty.10	11/29/2006	359	40.9±0.4	454±2	1.94±0.02	7.20±0.36	393±8	385±8	8.29±0.08	30.1±0.3	11.2±0.1	74.1±0.7	22.4±0.2	789±24	0.708918±9	4.57	0.349
Ty.10	11/29/2006	359	14.5±0.1	254±1	6.01±0.06	20.1±1.1	209±4	207±4	4.55±0.05	35.2±0.4	11.3±0.1	48.1±0.5	9.05±0.09	447±13	0.707901±6	2.78	-1.99
Ty.10	11/29/2006	359	37.2±0.4	254±1	2.43±0.02	8.85±0.44	363±7	365±7	7.75±0.08	30.5±0.3	11.1±0.1	74.1±0.7	19.9±0.2	741±22	0.708844±7	3.92	0.133
Ty.12	12/16/2007	319	2.68±0.03	178±1	14.8±0.2	12.4±0.6	153±3	n.m.	3.41±0.03	n.m.	6.75±0.07	20.5±0.2	n.m.	n.m.	0.706679±6	3.59	-0.315
Ty.12	12/16/2007	319	3.96±0.04	179±1	14.4±0.1	11.7±0.6	156±3	n.m.	3.54±0.04	n.m.	6.63±0.07	20.9±0.2	n.m.	n.m.	0.706735±7	3.66	-0.278
Ty.12	12/16/2007	319	2.78±0.03	179±1	14.6±0.2	11.6±0.6	150±3	n.m.	3.55±0.04	n.m.	6.82±0.07	20.8±0.2	n.m.	n.m.	0.706706±13	3.66	-0.220
Ty.12	12/16/2007	319	2.64±0.03	179±1	14.7±0.2	12.3±0.6	150±3	n.m.	3.43±0.03	n.m.	6.57±0.07	20.5±0.2	n.m.	n.m.	0.706715±12	3.61	-0.280
Seawater	6/28/2006	2.0	52.4±0.5	537±3	0.126±0.001	0.0000	453±9	n.m.	10.1±0.1	25.6±0.3	10.3±0.1	89.5±0.9	25.8±0.3	938±28	0.709171±7	7.58	2.40

[1] all are per kilogram
[2] n.m. = not measured

Vent	Date	Max Meas T [°C]	Min Mg [mmol]	Cl [mmol]	Si [mmol]	H₂S-LR [mmol]	Na-Meas [mmol]	Na-CB [mmol]	K [mmol]	Li [µmol]	Ca [mmol]	Sr [µmol]	SO₄²⁻ [mmol]	Br [µmol]	⁸⁷Sr/⁸⁶Sr	pH	Alk [meq]
Ty.4	4/22/2000	352	2.25 ± 0.0?	406 ± 2	13.8 ± 0.1	7.38 ± 0.37	350 ± 7	351 ± 7	14.3 ± 0.1	429 ± 4	15.9 ± 0.2	73.5	-0.215 ± 0.002	653 ± 20	0.704193 ± 5	3.97	-0.74
Ty.5	1/19/2002	349	2.71 ± 0.03	547 ± 3	15.1 ± 0.2	7.87 ± 0.39	465 ± 9	467 ± 9	19.3 ± 0.2	562 ± 6	22.4 ± 0.2	101	-0.223 ± 0.002	870 ± 26	0.704071 ± 6	n.m.	n.m.
Ty.8	3/21/2004	323	3.16 ± 0.03	584 ± 3	16.0 ± 0.2	5.67 ± 0.28	502 ± 10	497 ± 10	20.5 ± 0.2	672 ± 7	24.6 ± 0.2	114	-0.996 ± 0.010	1071 ± 32	0.704011 ± 15	3.11	-0.80
Ty.10	11/29/2006	359	14.5 ± 0.1	143 ± 1	8.33 ± 0.08	28.7 ± 1.4	100 ± 2	105 ± 2	2.29 ± 0.02	40.5 ± 0.4	12.1 ± 0.1	32.3	1.03 ± 0.01	335 ± 10	0.706539 ± 101	≤ 2.78	≤ -1.99
Ty.12	12/16/2007	319	2.64 ± 0.03	157 ± 1	15.5 ± 0.2	12.7 ± 0.64	133 ± 3	n.m.²	3.08 ± 0.03	n.m.	6.47 ± 0.06	16.5	n.m.	n.m.	0.705901 ± 9	3.59	-0.22
Io.1	4/23/2000	347	8.55 ± 0.09	286 ± 1	10.6 ± 0.1	8.51 ± 0.43	244 ± 5	247 ± 5	10.2 ± 0.1	323 ± 3	10.3 ± 0.1	44.9	-0.566 ± 0.006	448 ± 13	0.703972 ± 81	n.m.	n.m.
Io.2	1/19/2002	349	2.99 ± 0.03	470 ± 2	12.6 ± 0.1	7.55 ± 0.38	401 ± 8	403 ± 8	16.9 ± 0.17	498 ± 5	17.6 ± 0.2	82.7	0.377 ± 0.004	738 ± 22	0.704069 ± 8	2.96	-0.71
In.5	3/21/2004	353	1.97 ± 0.02	529 ± 23	14.1 ± 0.1	6.64 ± 0.33	454 ± 9	462 ± 9	18.9 ± 0.19	651 ± 7	20.9 ± 0.2	101	1.0381 ± 0.000	984 ± 30	0.703939 ± 7	3.17	-0.68
Io.9	7/1/2006	374	20.8 ± 0.2	101 ± 1	5.74 ± 0.06	28.3 ± 1.4	65.7 ± 1.3	n.m.	1.28 ± 0.1	17.8 ± 0.2	2.09 ± 0.02	0.584	2.46 ± 0.025	286 ± 9	n.m.	≤ 3.38	≤ -0.471
Io.10	11/28/2006	303	32.4 ± 0.3	212 ± 1	12.2 ± 0.1	16.0 ± 0.8	181 ± 4	182 ± 4	4.39 ± 0.04	78.7 ± 0.8	9.91 ± 0.10	22.8	0.469 ± 0.005	548 ± 16	0.705107 ± 47	≤ 4.69	≤ 0.581
Seawater		2.0	52.2	540	0.2	0.00	464	464	10.10	26	10.28	89.5	28.2	840	0.709171 ± 7	7.8	2.4

¹all are per kilogram
²n.m. = not measured

Table 3: Summary of calculated end members for high-temperature Ty and Io filtered fluid sample fractions. Seawater values are from Von Damm (1995, 2000, 2004) and were used to calculate high-temperature end members.

CHAPTER IV

RESULTS AND DISCUSSION

In the following discussion, I frame my analysis of high- and low-temperature fluid

chemical variation in terms of a comparison of the pre-eruptive (2000-2004) and post-

eruptive (2006-2007) trends. The data I present include temperature, pH, and alkalinity

measurements as well as Cl, Si, and other major and minor element data, including Br, Na,

Ca, Li, K, Sr, H_2S and SO_4^{2-}. I also discuss Sr isotope variation over the pre- and post-eruptive

periods for both fluid types and use these data, coupled with elemental Ca and Sr

abundances, to constrain mixing relationships between the high- and low-temperature

fluids to assess the deviations from non-conservative mixing, and consider possible

implications of anhydrite dissolution into the low-temperature fluids during the sampling

interval.

Temperature, Chloride, and Silica

The sampling temperature, along with the chloride and silica content, of a

hydrothermal vent exiting from the seafloor provides an "integrated record" of the pressure

(P) and temperature (T) reaction conditions that the fluid underwent during its passage

through the crust (Von Damm, 1995; German and Von Damm, 2004). This information can be translated into an approximate depth of fluid circulation, which in turn provides a constraint on the proximity to the heat source. Figure 7 shows the measured temperature, chloride, and silica composition of end member Ty and Io fluids and discrete BM82 samples over the 1994 to 2007 sampling period.

Temperature

The temperature reported for all vents is the maximum exit temperature recorded by the ICL on the majors bottle during sampling with the DSV Alvin. This temperature is not corrected to an end member value, and is thus considered to be a minimum temperature. Many factors contribute to lower the sampled temperature relative to the reaction zone temperature, including conductive cooling in the upflow zone, the difficulty of maneuvering a probe fully into a vent orifice, and possible sampling artifacts, including seawater entrainment into a chimney (Von Damm, 2004). For these reasons, temperature is the most uncertain of the three indicators for P-T reaction conditions, and tends to be more uncertain with lower-quality (high-Mg) samples. Despite these caveats, time series high-temperature vent temperatures, considered together with Cl and Si contents, can provide minimum temperatures for fluid-rock equilibration and be used semi-quantitatively to constrain the proximity of the fluid-mineral equilibration to the heat source.

At depths of 2500 meters (pressures ~250 bars), temperatures in excess of 389°C are required for seawater phase separation. Given the measured exit temperatures for Ty
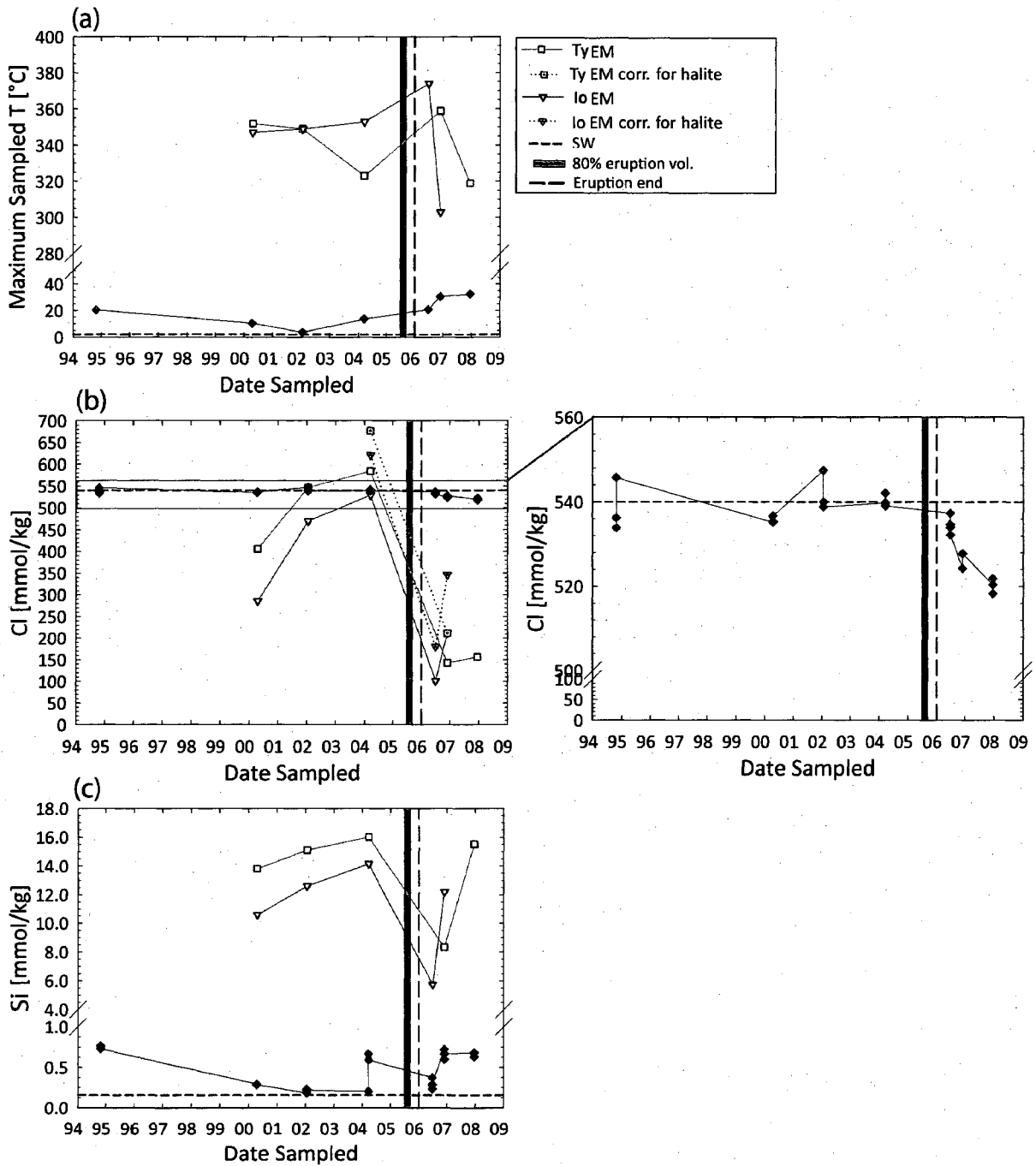
Figure 7: Caption on following page.

Figure 7: Time series summary of high-temperature Ty and Io and low-temperature BM82 vent (a) maximum sampled temperature, (b) Cl content, and (c) Si content. For these plots as well as the following time series elemental and isotopic plots (unless otherwise noted), open symbols represent high-temperature end member values (derived values), with orange squares representing Ty and red triangles representing Io. The three best (lowest Mg) discrete BM82 samples (out of 3-4 samples total) are plotted for the entire sampling interval. The blue short dashed line represents the seawater value. The vertical green bar represents emplacement of 80% of the eruption volume, while the green long dashed line marks the end of the eruption (Rubin et al., 2008). In the Cl plot, as well as in following plots for Br/Cl, Na/Cl, Ca/Cl, and Sr/Cl, additional "halite corrected" points are shown. These points were adjusted for the possibility of halite precipitation in March 2004 through the post-eruptive fluids, based on elevations in the Br/Cl. See discussion in text for more detail.

(range 319-359°C) and Io (range 303-374°C), venting Ty and Io fluids are in the single phase region, and are therefore not actively phase separating at the seafloor, throughout the sampling period (Figure 7a). Prior to the eruption, Io sampled temperature remains approximately constant around 350°C, while Ty sampled temperature drops by 29°C from 352 to 323°C. As noted in Von Damm (2004), it has been observed previously that hydrothermal fluids which travel a longer distance along the discharge zone have greater time to undergo conductive cooling. Cooler temperatures may also be a signal of seawater entrainment into the discharge zone, resulting in mixing and cooling of the fluids prior to sampling. The temperature drop in Ty vent prior to the eruption could then be interpreted as either a deepening of the heat source in the Ty reaction zone, and/or entrainment of seawater in the discharge zone.

Immediate post-eruption measured temperatures peak at both vents and then decrease over time, with temperatures of 359 to 319°C at Ty and 374 to 303°C at Io, suggesting a shallow heat source immediate post-eruption. The higher maximum exit temperatures of these fluids may also be a manifestation of enhanced vigor of convection through the more porous subsurface rock immediately following the eruption (Rosenburg et al., 1993). The cooler temperatures in 2007 suggest either a deepening heat source or entrainment of seawater into the discharge zones of both vents, as described above for Ty based on observations by Von Damm (1995). Interpretations based on maximum sampled temperature measurements, which have high uncertainty, should not be considered conclusions within themselves. However, these observations may be considered together

42

with interpretations based on Cl and Si contents, to be used semi-quantitatively to constrain

the proximity of the fluid-mineral equilibration to the heat source.

It can also be observed that BM82 is a robust area of low-temperature flow

throughout the sampling period, varying between 3.7-32.4°C and averaging 19.0°C (Figure

7a). These temperatures of less than 120°C can support biological communities, and BM82

indeed hosted profuse microbial and macrofaunal communities, including vestimentiferan

tubeworms, bracyuran crabs, zoarcid fish, amphipods, and limpets, throughout the pre-

eruption time series (Shank et al., 1998) and I have personally observed new micro- and

macro-faunal colonization post-eruption in November 2006 and December 2007.

Chloride

Throughout the sampling period, Ty and Io consistently have Cl contents distinct

from that of bottom seawater at 9°N EPR (540 mmol/kg) (e.g. Von Damm, 2000; Von Damm,

2004) (Figure 7b), demonstrating that, although their sampled exit temperatures indicate

that they are not actively phase separating at the seafloor, the fluids have unequivocally

undergone phase separation at least once during their paths through the oceanic crust. In

the pre-eruption period, Ty Cl contents increase from 406.0 mmol/kg (vapor phase) to 583.4

mmol/kg (brine phase), while Io Cl contents also increase, from 286.0 mmol/kg to 529.5

mmol/kg (vapor phase). Based on experimental studies (Bischoff and Rosenbauer, 1988;

Bischoff, 1991), Von Damm (2004) proposed that higher Cl contents indicate higher P and

higher T conditions in the reaction zone, in the case of vapor phase fluids. Once a fluid

exceeds the seawater value of 540 mmol/kg Cl, it is now tapping a brine phase fluid, or at least some fraction of the sampled fluid is sourced from a brine phase.

In an effort to more quantitatively model the P and T conditions of the deep sea MOR hydrothermal system reaction zone, Foustoukos and Seyfried (2007) have recently updated the quartz solubility model by Von Damm et al. (1991), by performing quartz solubility experiments at various chlorinities. Their empirically-derived Si-Cl solubility curves are shown in Figure 8 for the P and T conditions considered in their study. The end member Cl and Si contents of Ty and Io over the time series considered in this thesis are superimposed on Figure 8, with arrows indicating the direction of evolution of the fluids over time. If one assumes that (1) the fluids are at equilibrium with quartz and (2) no significant amount of Si or Cl is lost during the transit through the discharge zone, two observations may be drawn from the Ty and Io Cl and Si contents, considered within the framework of the Foustoukos and Seyfried model. First, the increasing Cl and Si content in the vapor phase fluids in both Ty and Io between 2000 and 2004 supports an increase in reaction zone pressure (deepening of the heat source) and hotter temperatures of phase separation in the immediate region. Additionally, the consistently higher Cl and Si contents of vapor phase Ty fluids relative to concurrent vapor phase Io fluids suggests that 2000-2004 Ty fluids may have originated from a deeper, hotter source fluid. The lower maximum sampled exit temperature of Ty, which really constitutes a minimum temperature for the fluid, may be a consequence of a longer discharge zone path, and therefore more adiabatic cooling and conductive heat loss (Figure 7a). Additionally, in 2002 and 2004, Ty was tapping

brines stored in the crust (Figure 7b). Brine phase fluids are denser than vapor phase fluids and are thought to have a longer residence time within the crust, and thus more time to cool conductively. The incorporation of these brine phase fluids is therefore likely to have contributed to the cooling of Ty vent prior to the eruption.

In the immediate post-eruption sampling interval, Cl contents reach their lowest at both vents and then increase over time, with Ty experiencing 142.9 to 156.7 mmol/kg Cl and Io experiencing 101.3 to 211.7 mmol/kg Cl (Figure 7b). These fluids also reach their lowest Si contents immediately post eruption and then increase over time (Figure 7c). Taken together, the Cl and Si contents indicate a shallower heat source immediate post-eruption followed by a deepening (Figure 8), which is consistent with the measured temperature-based interpretation. An alternative explanation for the very low Cl contents of the fluids post-eruption may be the precipitation of halite, and I will discuss evidence for this process in the following section, when the Br contents and Br/Cl ratios of the vents are considered.

During the sampling period, the Cl compositions of the BM82 fluids are much closer to that of seawater (Figure 7b), than the high-temperature fluids. It is clear, however, that these low-temperature fluids experience both depletions and enrichments in Cl, and must thus have a high-temperature component, rather than merely representing heated seawater.
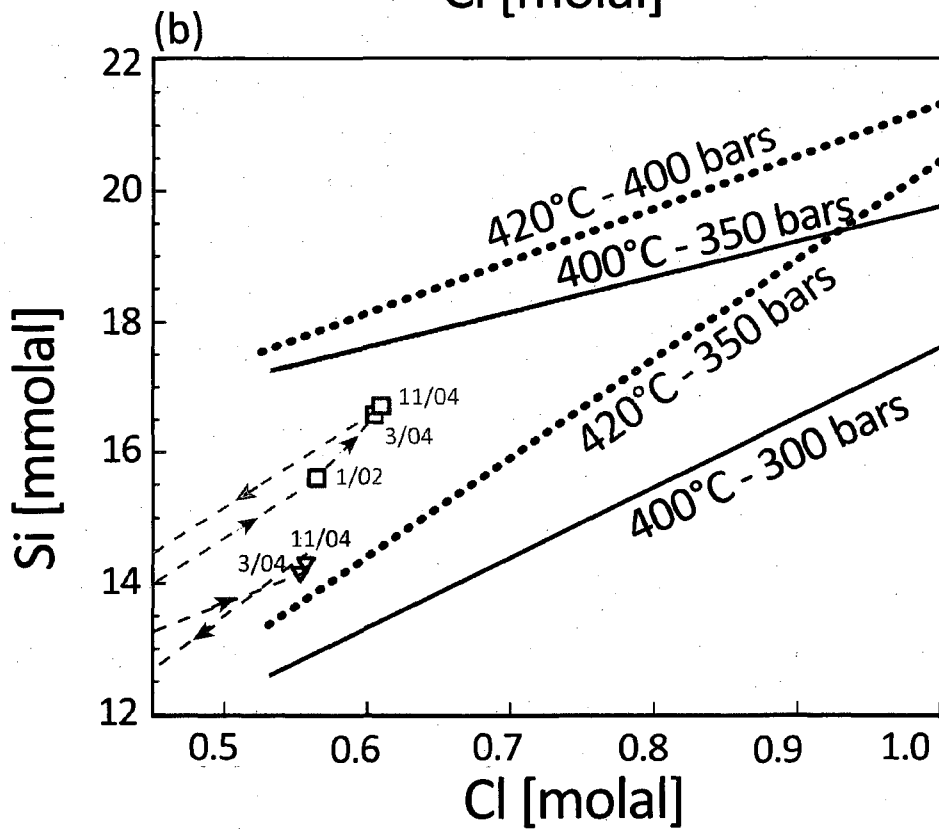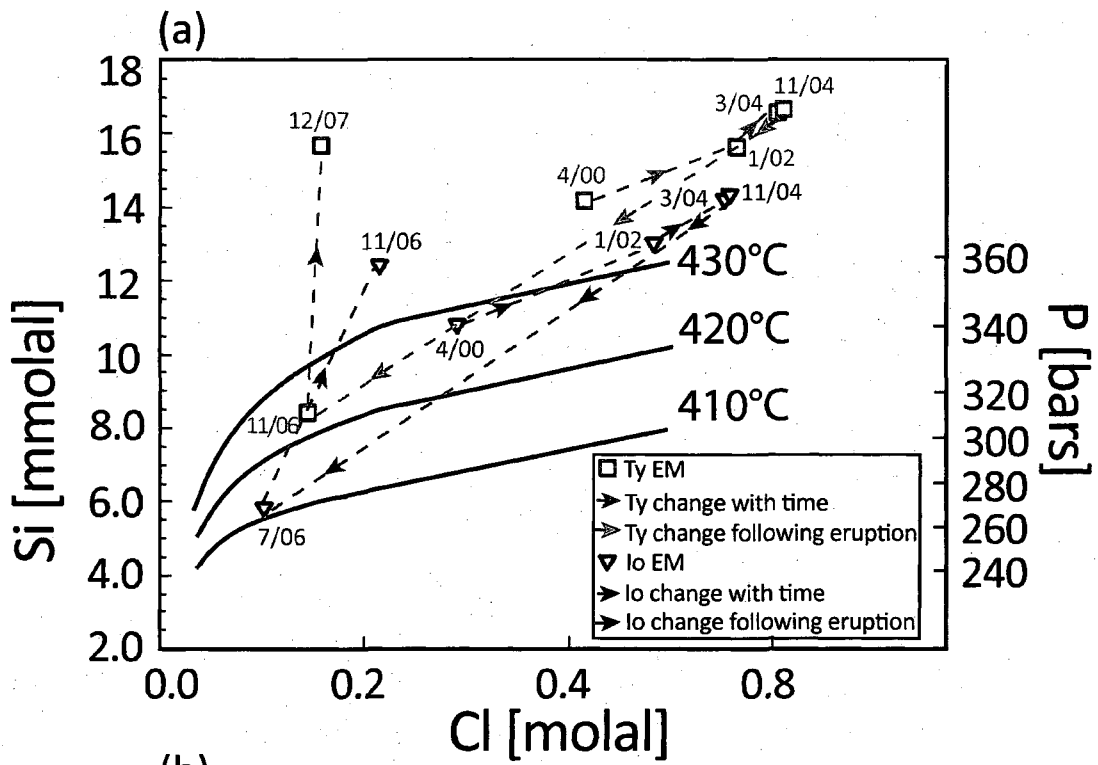
Figure 8: Caption on following page.

Figure 8: Solid black and blue dotted lines depict a Si-Cl-P-T dependent quartz solubility model developed by Foustoukos and Seyfried (2007). The model is shown for (a) vapor phase and (b) brine phase fluids. The Cl and Si contents of Ty and Io vent fluids are plotted, with all fluids plotted in (a) and just brine phase fluids plotted in (b). Fluid compositions have been converted to molal units to conform to experimental data. The evolution of a fluid in a particular vent is indicated with arrows. Arrows outlined in green highlight the change over the 2 year interval, between March 2004 and June 2006, during which the eruption occurred.

Silica

Hydrothermal fluid Si contents can be used as a third constraint on the P-T conditions of the reaction zone. Inherent in this application is the key assumption that hydrothermal fluids are at equilibrium with quartz and that no significant amount of Si is lost during the transit through the discharge zone (Von Damm 2000; Von Damm, 2004). Silica in hydrothermal fluids exists predominately as silicic acid, H_4SiO_4. In this thesis, I refer to measured silica as "Si," to maintain consistency with previously published studies by Von Damm (e.g. 1995, 2000, 2004), and because it is equimolar to SiO_2 (pure quartz) and can therefore be directly compared with experimental studies (Figure 8, 9). Figure 9 describes the solubility of quartz in pure water and seawater with changes in P and T, as calculated by the equation derived in Von Damm et al (1991), and the Si contents of Ty and Io over the sampling interval are plotted versus their maximum sampled temperatures. As stated previously, the consistently distinct Cl content of Ty and Io relative to bottom seawater at 9°N EPR demonstrates that the fluids have unequivocally undergone phase separation at least once during their paths through the oceanic crust, and therefore it can be safely assumed that they have been as hot as 386°C at pressures at least as high as 250 bars. Considering the data plotted on Figure 9, in light of the previously stated assumptions about Si, one can thus estimate that the reaction zone of Ty and Io has reached a maximum pressure of 300-350 bars.

At conditions relevant to a deep sea hydrothermal system, Si content increases with increasing T and P until temperatures exceed or are equal to 375°C, after which Si exhibits

retrograde solubility (as temperatures continue to increase, silica content decreases) (Figure

9). The increasing Si content of both Ty and Io pre-eruption, with Ty increasing from 13.8 to

16.0 mmol/kg Si and Io increasing from 10.6 to 14.1 mmol/kg fluid Si contents (Figure 7c),

when considered at and above the measured exit temperatures, is likely to represent

increasing P conditions in each particular vent with time, and therefore increasing depth to

the magma chamber (Figure 9). Immediate post-eruption Si contents reach their lowest at

both vents and then increase over time, with Ty having 8.3 to 15.5 mmol/kg Si and Io having

5.7 to 12.2 mmol/kg Si. These lower but increasing Si contents may indicate reaction

conditions of lower P (shallower heat source) and/or lower T immediately following the

eruption, followed by higher P conditions. Again these interpretations are consistent with

the measured temperature and Cl-based post-eruption interpretation. It should also be

noted that if halite is precipitating and re-dissolving in the upper oceanic crust, Si content

may be a better indicator of reaction zone depth than Cl content.
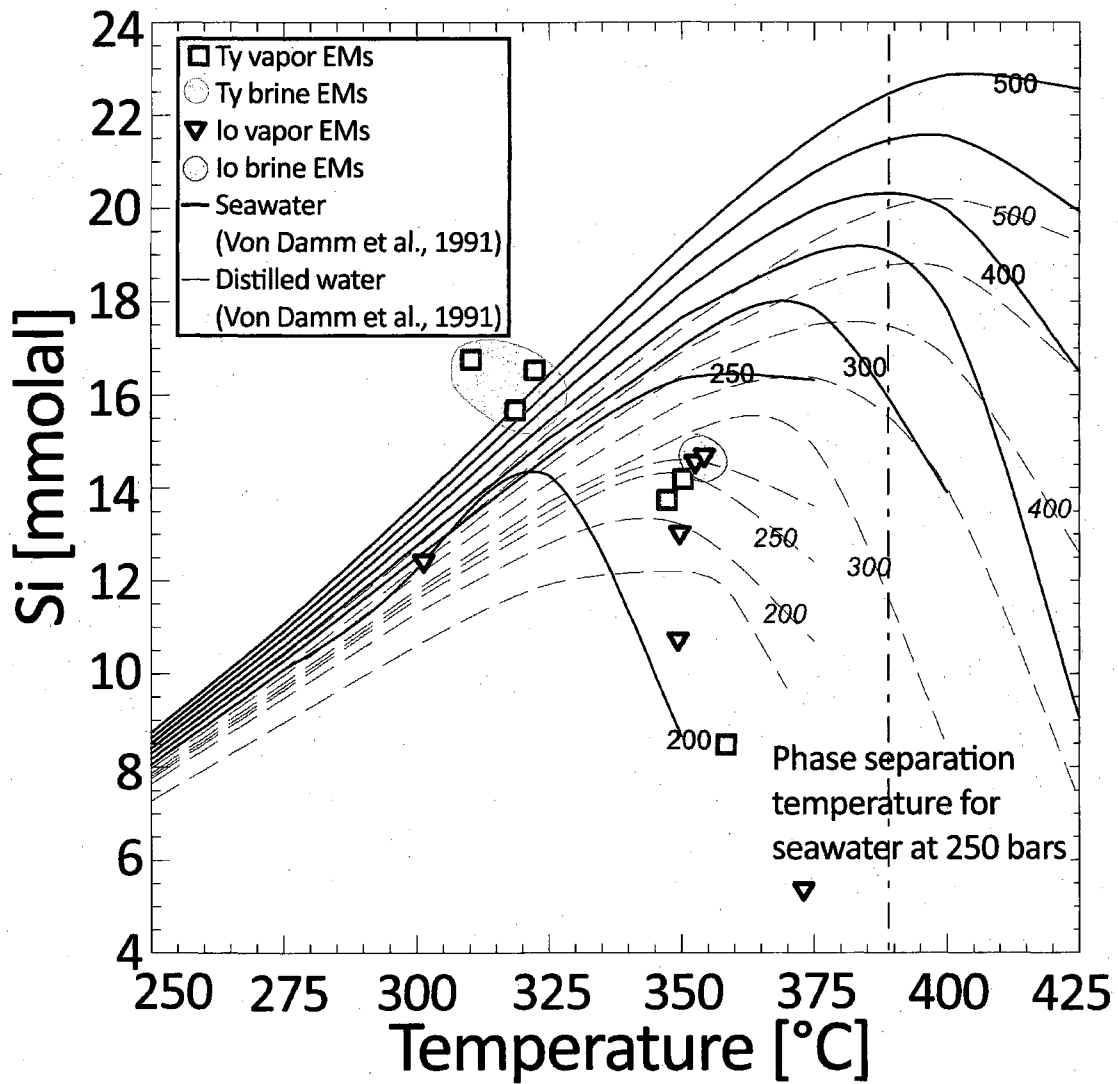
Figure 9: Temperature and pressure dependence on quartz solubility in pure water (solid lines) and seawater (dashed lines). Figure modified after (Von Damm, 2004), using an empirically-derived quartz solubility equation published by Von Damm et al. (1991). The end member Si contents of Ty and Io over the sampling interval are plotted versus their maximum sampled temperatures. Si content is a function of Cl content, so vapor phase samples should be considered according to the quartz solubility models for seawater and distilled water, while brine phase samples should be considered according to the quartz solubility model for seawater. It is known from Cl data that the Ty and Io fluids have undergone phase separation at least once during their paths through the oceanic crust, and therefore it can be inferred that they have been as hot as 386°C.

Major and minor elements, pH, alkalinity

The major and minor elemental composition, pH and alkalinity of a high-temperature hydrothermal vent exiting from the seafloor provides information about the degree of water-rock interaction, fluid residence time, and other mineralogical processes that may occur in the subsurface (e.g. Von Damm, 1985, 1995, 2000, 2004; German and Von Damm, 2004). Figures 10, 11, and 12 show the end member Br, Na, Ca, Li, K, Sr, H_2S, SO_4^{2-}, pH, and alkalinity composition of end member Ty and Io fluids over the 1994 to 2007 sampling period, as well as element-to-Cl ratios for Br, Na, Ca, Li, K, and Sr.

Bromide

Bromide has been shown to exhibit conservative behavior with Cl during phase separation (Von Damm et al., 2003). In Ty and Io, the absolute concentrations of Br vary from greater than to less than the seawater value in the pre-eruption period (Figure 10a). They then drop to less than seawater post-eruption, as would be expected based on the Cl behavior. After the eruption, Br/Cl ratios are elevated in both Ty and Io (Figure 10b). This observation, coupled with a Na/Cl value greatly exceeding the seawater value (Figure 10d), may be an indicator of halite precipitation, as described by Oosting and Von Damm (1996) and Von Damm (2000). Elevation of the Na/Cl ratio may also occur as a result of albitization, and I will describe this process in the following discussion. Oosting and Von Damm (1996) discuss the fractionation of Br from Cl that occurs when halite precipitates, due to the exclusion of the larger Br ion from the halite crystal structure. If halite precipitation were

occurring, the Br/Cl ratio would therefore increase. Sodium is less abundant in seawater than Cl (Na/Cl = 0.86), and thus if halite were precipitating at a 1:1 molar ratio of Na to Cl, the Na/Cl ratio would be lowered in the vent fluid. Von Damm (2000) further discusses the possibility that halite precipitation may occur immediately following an eruption, and be a transient event: "We infer that a small amount halite is formed at the time of eruption, perhaps by the flashing of seawater in contact with a hot lava flow, and that it is quickly re-dissolved (p. 11,217)." Indeed, Ty and Io vents in the immediate post-eruptive June and November 2006 sampling intervals show an elevated Br/Cl ratio and concurrent depletion in Na/Cl, suggesting that halite precipitation may indeed occur in deep sea MOR hydrothermal vents periodically over the course of a volcanic cycle, and is associated closely with major eruptions.

If one assumes that Br remains conservative with Cl during phase separation throughout the time period, a simple mass balance calculation based on the difference between the steady state Br/Cl ratio (2000-2002) and the elevated Br/Cl ratio (2004-2006) allows a rough estimation of the Cl possibly lost to halite precipitation (Figure 13). An example calculation is shown for Ty in March 2004:

$$\text{Measured } \frac{Br}{Cl} = \frac{1071 \text{ } \mu mol/kg}{584.3 \text{ mmol/kg}} = 1.8337 \text{ } \mu mol/mmol$$

$$\text{Average steady state } \frac{Br}{Cl} = 1.5555 \text{ } \mu mol/mmol$$

Additional Cl needed for steady state Br/Cl, x:

$$\frac{Br}{Cl} = \frac{1071\ \mu mol/kg}{584.3 + x\ mmol/kg} = 1.5555\ \mu mol/mmol$$

$$x = 104.2\ mmol/kg\ Cl$$

Therefore, in Ty in March 2004, an estimated 104.2 mmol/kg Cl was lost to Cl, which is amount equivalent to approximately 18% of the measured Cl end member. Other losses of Cl to halite precipitation were calculated similarly, and are shown in Figure 13a and 13b. As shown in Figure 10b, this mass balance calculation adjusts the Br/Cl ratio back to the steady state value. The amount of Cl lost to halite precipitation may then be added back into the total Cl budget. I have also shown adjustments to the Na/Cl, Ca/Cl, and Sr/Cl ratios (Figures 10d, 10f, 11f) in order to determine whether albitization and anhydrite precipitation or dissolution may also be a factor in determining the high-temperature fluid chemistries throughout the time series. These adjustments will be detailed further in the following discussion.

Alkali and Alkaline Earth Metals

As the dominant cation, Na also behaves conservatively with Cl during phase separation. Sodium abundance clearly tracks the Cl pattern, as seen in Figure 10c. Pre-eruption Io Na/Cl ratios are near that of seawater, but Ty shows some depletion in 2002 and 2004, but these decreases are not significantly different than the seawater ratio, when the method error is considered (Figure 10d). Io shows an Na/Cl ratio greater than seawater in 2004, but again, this increase is not significantly different than the seawater ratio, when the

method error is considered. The post-eruptive Na/Cl ratios may therefore be interpreted as stead-state values.

Post-eruption fluid Na/Cl for both vents in 2006 is significantly less than the seawater value. These low Na/Cl ratios may be due to disequilibrium of fluid-mineral processes, albitization, and halite dissolution, or some combination of these three processes. While the sampling time for the Na/Cl ratio of Ty in November 2006 coincides with the peak in the Ca/Cl ratio as well as elevated Br/Cl ratio for this vent, suggesting albitization as a potential process as well as halite precipitation, the Na/Cl ratio of Io does not coincide with a concurrent peak in Ca/Cl for this vent. Halite dissolution is therefore a possible explanation for the Io Br/Cl and Na/Cl ratios in the immediate post-eruption period of June 2006. In order to determine whether Na/Cl ratios would still be depleted after accounting for halite precipitation, I added the Cl lost to halite precipitation back into the total Cl budget and an equimolar amount of Na back into the total Na budget, and recalculated the Na/Cl ratios, as shown in Figure 10d for the 2004-2006 sampling interval. Ty vent in November 2006 still shows a depletion in the Na/Cl, and so this vent may have also been affected by albitization at this time. In order to account for possible albitization in the Ca/Cl ratio, a simple mass balance was performed as follows:

$$\text{Measured Na/Cl} = \frac{105 \text{ mmol/kg Na}}{143 \text{ mmol/kg Cl}} = 0.734 \text{ mmol/mmol}$$
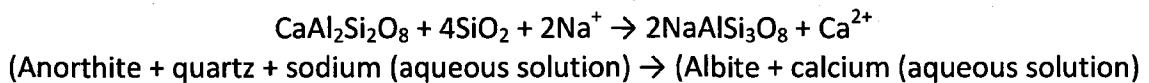
$$\text{Halite corrected } \frac{\text{Na}}{\text{Cl}} = \frac{105 + 68.5 \text{ mmol/kg Na}}{143 + 68.5 \text{ mmol/kg Cl}} = 0.8218 \text{ mmol/mmol}$$

Additional Na needed for steady state Na/Cl, y:

$$\frac{Na}{Cl} = \frac{173.8 + y \text{ mmol/kg}}{211.5 \text{ mmol/kg}} = 0.8592 \ \mu mol/mmol$$

$$y = 8.050 \text{ mmol/kg Na}$$

Albitization reaction:

$$CaAl_2Si_2O_8 + 4SiO_2 + 2Na^+ \rightarrow 2NaAlSi_3O_8 + Ca^{2+}$$
(Anorthite + quartz + sodium (aqueous solution) → (Albite + calcium (aqueous solution)

Amount of Ca added to fluid from albitization if 8.050 mmol/kg Na was lost, z:

$$z = \text{Measured Ca content of fluid} + y/2$$
$$z = 12.1 \text{ mmol/kg} + 8.050/2 \text{ mmol/kg} = 16.1 \text{ mmol/kg}$$

The Ca/Cl ratio for Ty in November 2006 can thus be recalculated to account for potential halite precipitation and albitization, as shown in Figure 10f.

Like Na, the other alkalis (Li, K) and alkaline earths (Ca, Sr) are thought to behave conservatively with Cl in hydrothermal fluids. Equilibrium or disequilibrium between fluid-mineral reactions is another important control on these elements. The elemental abundances for Ca, Li, K, and Sr throughout the time series are plotted (Figure 10e, Figure 11a, Figure 11c, Figure 11e), as are the element ratios to Cl (Figure 10f, Figure 11b, Figure 11d, Figure 11f). The pre-eruption element ratios to Cl for Li, K, Ca, and Sr are all greater than that of seawater (with the single exception of Sr in Io in 2000, which is slightly depleted) (Figure 10f, Figure 11b, Figure 11d, Figure 11f), and thus it is clear that these metals are being added by water-rock alteration. Despite changes in their absolute abundances, the consistency of the ratios during this four year period suggests that fluid-

mineral processes are at equilibrium, or steady-state. This observation of constant alkali and alkali earth to Cl ratios was also noted by Von Damm (2000) for the 1994-2002 time period for the high-temperature vents Bio9, Bio9', and P (Figure 3).

Fluid Li/Cl ratios for both vents in the post-eruptive period in 2006 and 2007 are lower that the steady-state value, but still greater than the seawater value. Similarly, post-eruption fluid K/Cl ratios for both vents drop to lower than the seawater value, then increase to just above the seawater value, but still much lower than the steady-state value. Several processes may be driving the drop in the Li/Cl and K/Cl ratios, including fluid-mineral disequilibrium and formation of clay mineral alteration products. It is likely that this drop in the ratios is again evidence for enhanced vigor of convection through the more porous subsurface rock immediately following the eruption. The resulting kinetic effect on fluid-mineral reaction is that the fluids do not have sufficient time to equilibrate with the rock. An additional process which may be affecting K and Li in the post-eruptive fluids may be the formation of illite in the discharge zone. The clay illite, which is an alteration product of basalt, incorporates the K^+ and Li^+ ions into its structure. An eruption is likely to result in fracturing subsurface, and new fluid flow paths would likely encounter fresh, relatively unaltered basalt. If illite is forming in the potentially newly-fractured, fresh basalt discharge zones beneath Ty and Io post-eruption, the result would be a lowering of these elements relative to Cl in the fluids.

Fluid Ca/Cl and Sr/Cl ratios for both vents in the post-eruptive period in 2006 and 2007 are clearly in disequilibrium with fluid-mineral processes. Io Ca/Cl and Sr/Cl values

drop very low in the immediate post-eruptive sampling interval in June 2006 for Io vent (Ty not sampled), which again may be explained by enhanced vigor of convection leading to insufficient time to allow the fluids to equilibrate with the rock. Io vent in November 2006 shows Ca/Cl values that have increased since the June 2006 sample interval, but are still lower than both the seawater and the pre-eruptive steady state range, suggesting that the fluids are still convecting too quickly to allow equilibration with the rock. Ty vent in November 2006 shows a Ca enrichment relative to the seawater and the pre-eruptive steady state range, even after correction for both halite precipitation and albitization. This suggests that there may be an additional input of Ca not accounted for by water-rock interaction and albitization. Anhydrite dissolution from either the stockwork and/or the chimney is one possible source for this excess Ca. Post-eruptive Sr/Cl ratios for both Ty and Io vents, even when corrected for halite precipitation, show values that are depleted relative to seawater and the steady-state value. Two conclusions may therefore be drawn, the first being that, in agreement with observations for Ca, the fluids are still convecting too quickly to allow equilibration with the rock post-eruption, and the second that if anhydrite is re-dissolving into Ty fluids in November 2006, the addition of Sr from anhydrite is a negligible part of the entire Sr budget, at least on the basis of mass.

Alkalinity and pH

Alkalinity was negative and pH was acid throughout the sampling period (Figures 12a, 12b). Reported pH values were measured shipboard at 25°C and 1 atmosphere under

nitrogen. The low pH of hydrothermal fluids is due to the gain in H^+ in Mg-OH precipitation reactions within the recharge and reaction zones, and is responsible for titrating the alkalinity in the original seawater source fluid, as previously discussed. When hydrothermal fluids are sampled, and some amount of seawater is incorporated, this low pH titrates some of the alkalinity of the hydrothermal-seawater mixture. When sample pH or alkalinity is plotted versus Mg, therefore, the mixture results in a titration curve, rather than a linear mixing line as generated for other elements and species (Von Damm, 2000). Von Damm (2000) examined various means of estimating logistic fits to this curve, and determined that for high-quality samples (lowest Mg less than 10 mmol/kg), the measured pH and alkalinity are close to the end member value and introduce less error than applying a logistic fit. This study follows that example, and reports the pH and alkalinity end members as the measured value for the best sample (lowest Mg). As described by Von Damm (2000), when the sample quality was too poor (lowest Mg sample greater than 20 mmol/kg) to report an end member pH or alkalinity value, the lowest measured value is reported as the maximum end member value, and a "down" arrow is displayed on the corresponding data point in Figures 12a and 12b. There is no discernable temporal trend in the pH or alkalinity data, as apparently higher values post-eruption may be artificially elevated due to sample quality issues.

<u>Sulfur species</u>

The high acidity of high-temperature vent fluids causes S to occur predominately in its reduced form as H_2S, rather than as the aqueous species HS^- or S^{2-} (German and Von Damm, 2004), and therefore H_2S and SO_4^{2-} are the S species routinely analyzed in vent fluids (e.g. Von Damm, 1995; Von Damm, 2000; Von Damm, 2004). Hydrogen sulfide is a gas, and is therefore strongly partitioned into vapor phase fluids. The end member H_2S values reported in this thesis are described as "H_2S-LR", which stands for end member H_2S calculated from a linear regression. This convention is consistent with other data sets published by Von Damm (e.g. 1995, 2000, 2004). Near-constant H_2S in the pre-eruption fluids in both vents represents fluid-mineral equilibrium, or steady-state, while higher H_2S abundances post-eruption are potentially due to input by non-equilibrium, increased water-rock reaction, as well as the production of very low-Cl vapor phase fluids (Figure 12c) (Lilley et al., 2003).

Fluid SO_4^{2-} contents are close to zero at all times in both vents (Figure 12d). Sulfate is a species which is particularly subject to sampling artifacts. For example, SO_4^{2-} will be artificially elevated if a majors bottle cores a chimney structure and anhydrite particles are incorporated into a sample. This phenomenon is easier to identify in Ca and Sr end member calculations, and is less obvious when small amounts of SO_4^{2-} are added. The incorporation of anhydrite particles during sampling could explain for the slightly elevated SO_4^{2-} in both Ty and Io following the eruption (Von Damm, 2004). All results for Ty and Io over the time series represent quantitative SO_4^{2-} removal, as supported by a similar range in result values

reported by Von Damm (2004). An additional possibility may be that some of the SO_4^{2-} in the November 2006 fluids may be sourced from re-dissolving anhydrite, as identified from the Ca/Cl results.

A final unique observation in the SO_4^{2-} data is the occurrence of an occasional negative end member value (Figure 12d). Very high negative end member values (less than -1.0 mmol/kg, as discussed by Von Damm (2000)) could indicate entrainment of seawater into a chimney prior to fluid exit, which would result in anhydrite precipitation within the chimney, in which fluid temperatures are greater than 130°C. Anhydrite is indeed found in the sulfide structures of high-temperature vents at 9-10°N EPR (R. Haymon, pers. comm.). The end member for Ty in 2004 is -0.996 mmol/kg SO_4^{2-}, which approaches but does not go lower than this -1.0 mmol/kg cut-off. This is important to note, because if seawater entrainment occurs, a small amount of Mg will be introduced into the fluid prior to sampling and a "true" end member value is therefore difficult to calculate. This is most obvious for the SO_4^{2-} calculation, where a small Mg addition will result in a negative end member value. The other important implication is that Ca and Sr will precipitate out along with the SO_4^{2-}, and thus the calculated end member Ca and Sr could be artificially lowered. It may be possible, however, that Mg introduced via seawater entrainment could be precipitated as caminite, a Mg-hydroxysulfate-hydrate mineral. Thus, while there are no SO_4^{2-} values less than -1.0 mmol/kg, entrainment of seawater may still be a significant process within Ty and Io fluids throughout this time period.

Figure 10: Time series summary of high-temperature Ty and Io vent (a) Br content, (b) Br/Cl ratio, (c) Na content, (d) Na/Cl ratio, (e) Ca content, and (f) Ca/Cl ratio. Note: Plotted Na values are charge balanced, except for Io in July 2006 and Ty in December 2007, where the measured Na value is plotted (see Table 3).
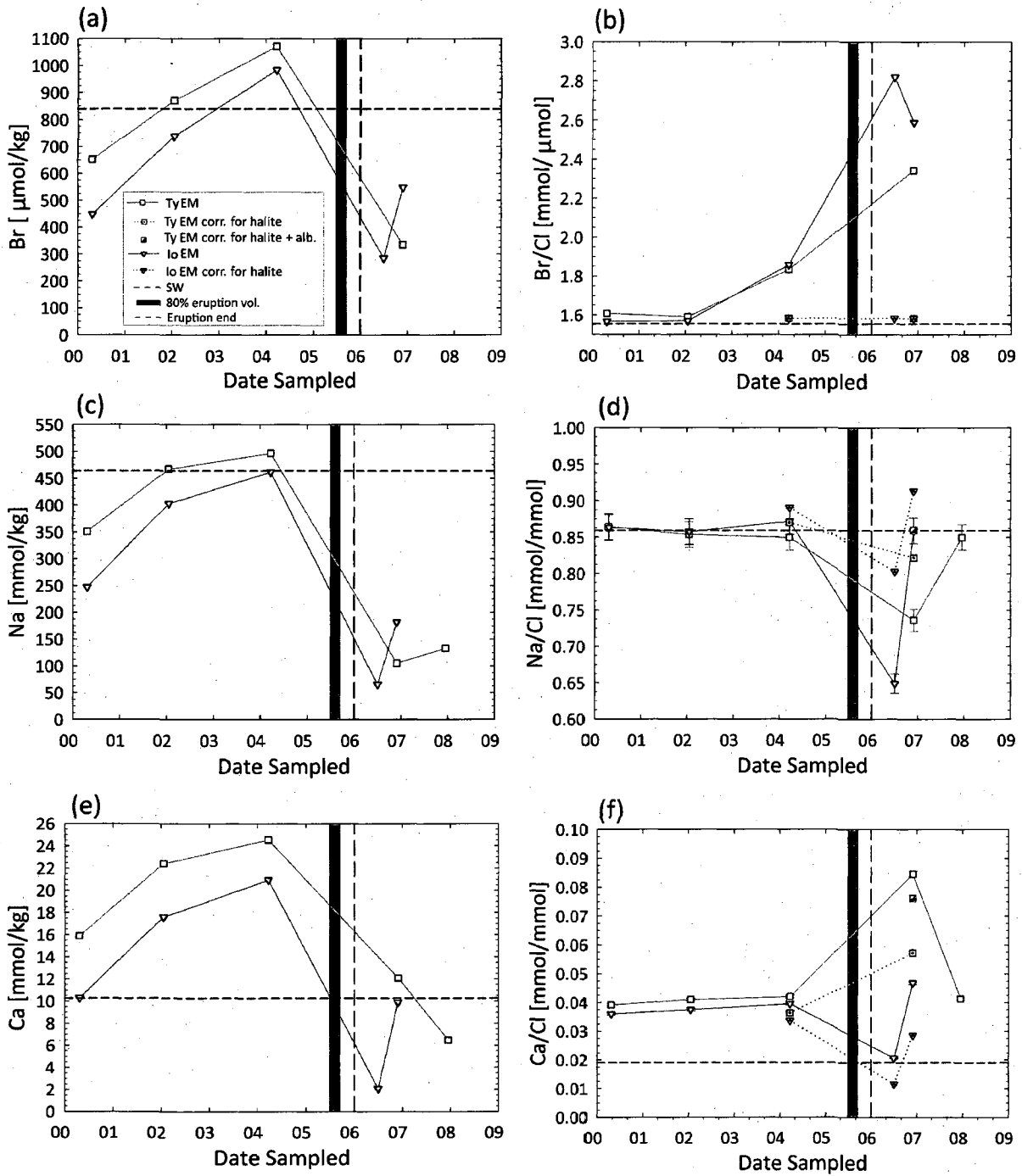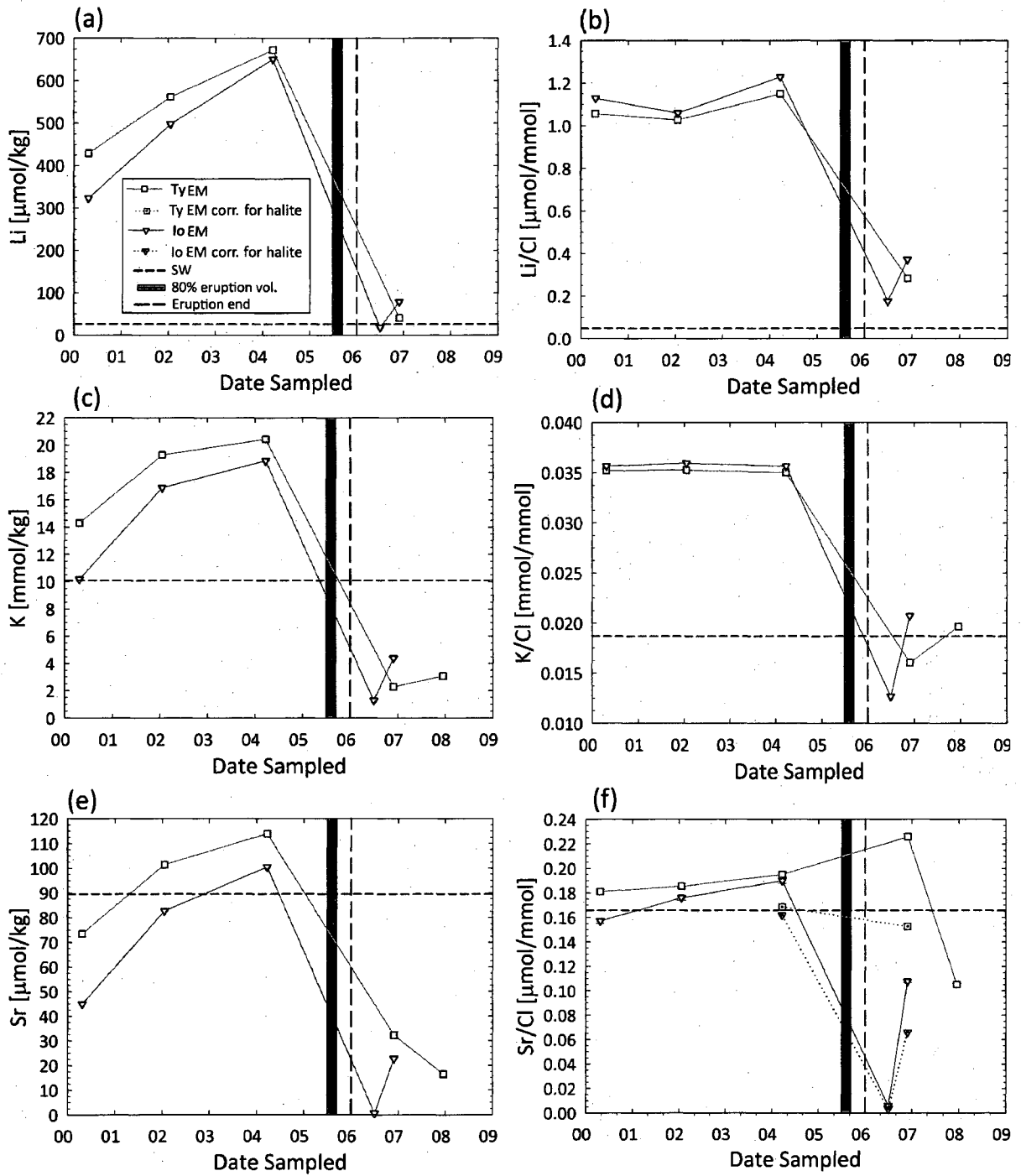
Figure 11: Time series summary of high-temperature Ty and Io vent (a) Li content, (b) Li/Cl ratio, (c) K content, (d) K/Cl ratio, (e) Sr content, and (f) Sr/Cl ratio.
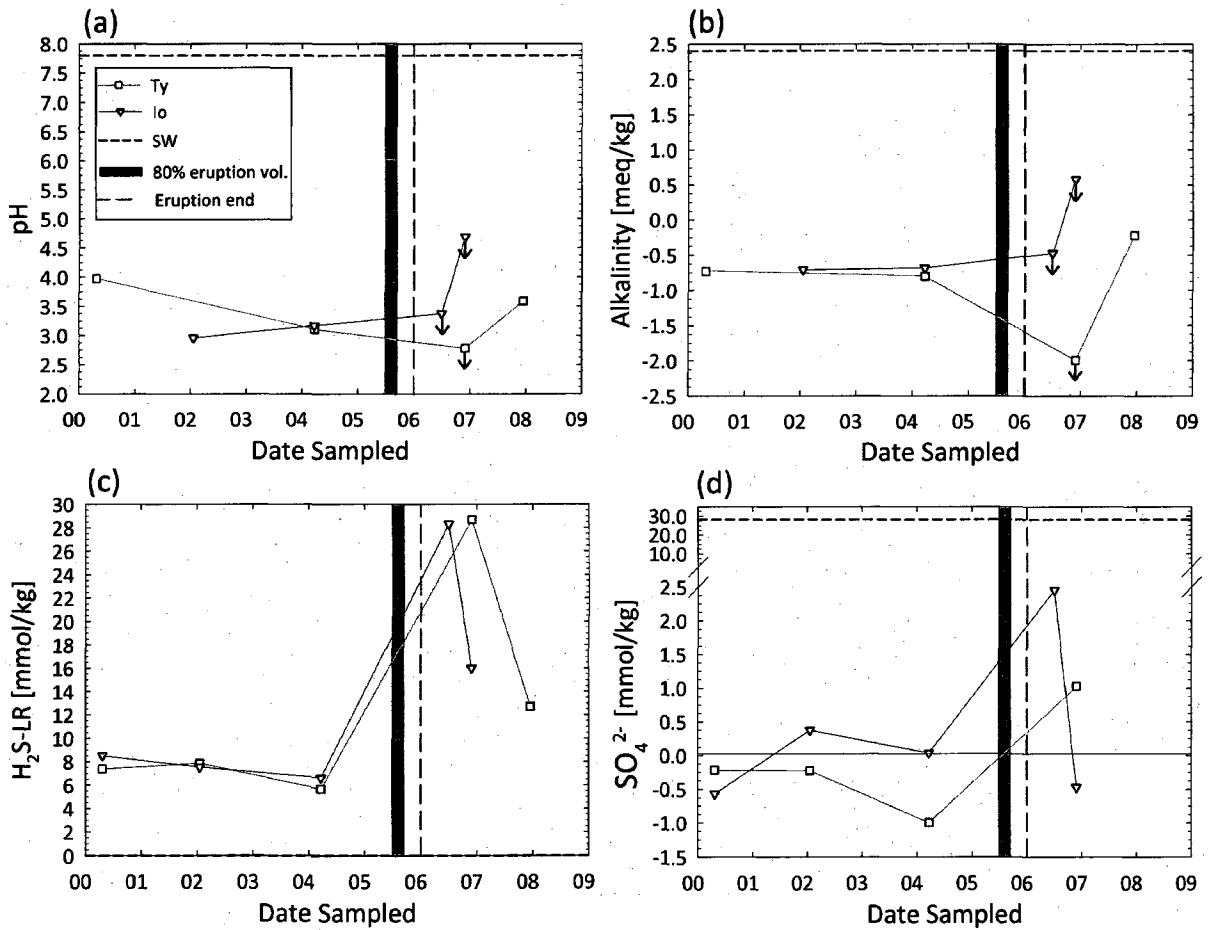
Figure 12: Time series summary of high-temperature Ty and Io vent (a) pH, (b) alkalinity, (c) H_2S, and (d) SO_4^{2-} content. Down arrows in pH and alkalinity plots denote sampling intervals when sample quality was too poor (best sample with greater than 20 mmol/kg Mg) to precisely calculate an end member. These values are therefore maxima, and the true value is likely lower.
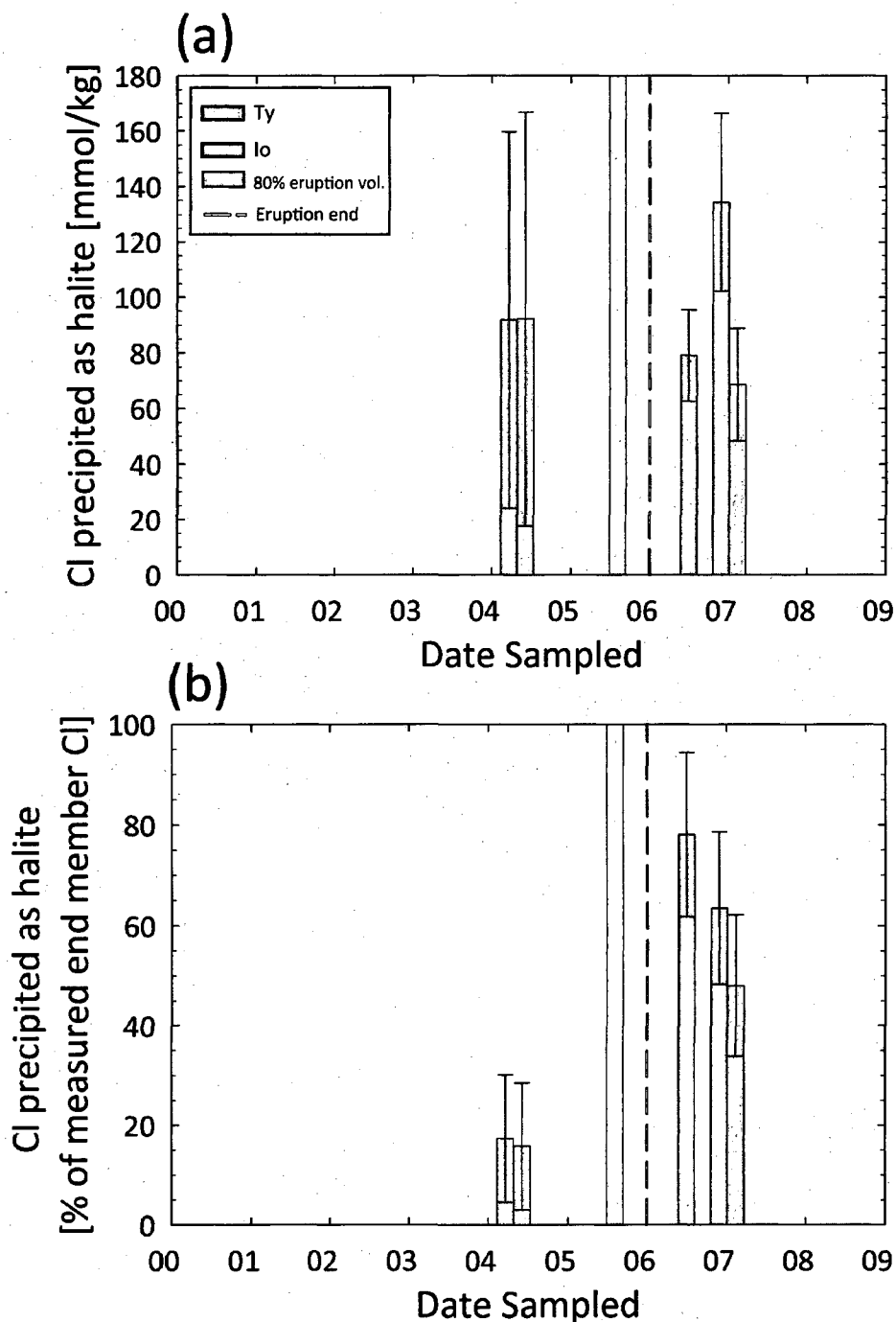
Figure 13: Summary of the amount of Cl) that may have been precipitated as halite immediately before and after the eruption, shown in (a) as moles per kilogram of solution, and in (b) as the percentage of the measured end member Cl. These values were calculated by a simple mass balance using the Br/Cl ratio, as described in the discussion under the Chloride sub-heading. Errors shown are based on method error for Cl and Br, and were propagated through the calculation, based on error calculation rules derived from the Gaussian equation for normally-distributed errors (Bevington and Robinson, 2003).

Strontium isotope time series

The $^{87}Sr/^{86}Sr$ end member results for Ty and Io and discrete sample results for BM82 are shown for the entire 1994-2007 time period in Figure 14. Pre-eruption $^{87}Sr/^{86}Sr$ values for Ty and Io are approximately constant, and range from 0.70401-0.70419 for Ty and 0.70394-0.70407 for Io. This suggests that, like elemental Sr, isotopic Sr was at fluid-mineral equilibrium, or steady-state, with the isotopic Sr basalt value prior to the eruption. This result is consistent with those reported for other high-temperature vents at 9°46'-9°54'N EPR by Ravizza et al. (2000), who reported $^{87}Sr/^{86}Sr$ in vents sampled in 1996 to range from more radiogenic values of 0.7042 (P vent and Bio9') and 0.7041 (Biovent) in more northern vents to less radiogenic values of 0.7039 and 0.7037 (A and L) in more southern vents (Figure 3). The $^{87}Sr/^{86}Sr$ values identified in Ty and Io prior to the eruption fall in between these two ranges in reported values, and are consistent with increasingly more radiogenic values in vents found at increasing distance north along the transect.

Post-eruption $^{87}Sr/^{86}Sr$ values for Ty and Io are closer to the seawater ratio than pre-eruption values, and are also the most radiogenic values reported in high-temperature end member deep sea MOR fluids (Figure 15). The $^{87}Sr/^{86}Sr$ values in Ty range from 0.70654 in November 2006 to 0.70590 in 2007, while the $^{87}Sr/^{86}Sr$ value for Io was 0.70511 in June 2006. Although isotope measurements were collected for discrete high-temperature Io samples, an end member $^{87}Sr/^{86}Sr$ ratio cannot be calculated due to the extremely low end member Sr concentration of 0.58 μmol/kg in the immediate post-eruption time. The Mg/Sr ratio of the Io fluids during June 2006 are therefore so close to the seawater value that a

regression through the fluid samples and seawater cannot be performed. These results indicate that the $^{87}Sr/^{86}Sr$ values in these high-temperature vents are not at steady state post-eruption, and the two data points in Ty may suggest a rate of return to steady state. Although there are only 2 sampling intervals post-eruption on which to base this observation, the beginnings of a return to equilibrium may be observed in the other chemical data as previously discussed, including Ca, Li, K and Sr. The post-eruption Sr isotope results also suggest the possibility that seawater may infiltrate down into the more-permeable discharge zone following an eruption. If the seawater reacts partially at high temperature, Mg may be precipitated as caminite, and the fluids would therefore still regress to a 0 Mg end member. Sr isotopes may therefore provide valuable evidence for the entrainment and partial reaction of seawater following an eruptive event.

Ravizza et al. (2001) used Sr isotopes to identify the presence of an intermediate fluid component in the composition of one of the high-temperature vents at 9-10°N EPR, Biovent, which is located north of Ty and Io (Figure 3). This intermediate fluid was shown to contain only about 50% Mg depletion, and had undergone very little Sr exchange with the basalt. The main method employed by Ravizza et al. (2001) was a comparison between the slope of a linear regression through the samples and the seawater value versus the slope of a linear regression through just the samples. Their study considered vents with 3-6 samples, and with a range in Mg/Sr of at least 0.05 mmol/μmol. The Sr isotopic results from this study as presented rely upon 2-4 samples/vent/sampling interval, and many of the Mg/Sr ranges are smaller than 0.05 mmol/μmol. The sample library at UNH does contain more

high-temperature samples for Ty and Io for some of these sampling intervals, and future work could include running more of the samples which are most likely to contain some proportion of partially-reacted Mg (e.g. March 2004, and the 2006-2007 Ty and Io samples). With a greater number of samples/vent/sampling interval, which will span a wider range in Mg/Sr, the slopes of a linear regression containing seawater versus on containing just vent fluid may be more accurately compared.

Low-temperature BM82 fluid $^{87}Sr/^{86}Sr$ values do not deviate greatly from the seawater value (Figure 14), ranging from the seawater value up to 0.70902 during the time series. Most samples do show a deviation from seawater within the error, and thus include some high-temperature fluid component within the mixture.
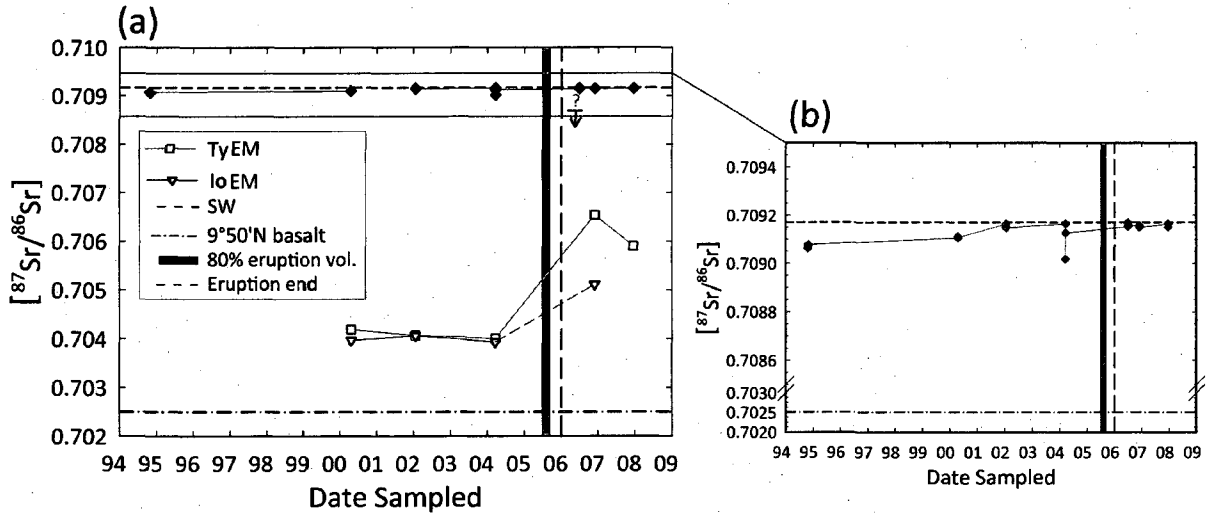
Figure 14 (above): (a) Time series summary of high-temperature Ty and Io and low-temperature BM82 vent $^{87}Sr/^{86}Sr$ values, and (b) magnification of the $^{87}Sr/^{86}Sr$ scale in order to show details in the BM82 data more clearly. Symbols are as described in Figure 7, with the addition of the brown dash dotted line, which represents the $^{87}Sr/^{86}Sr$ value in fresh basalt (Sims et al., 2002). The red question mark identifies the interval when Io was sampled, however the end member Sr of the vent was too low to calculate an end member $^{87}Sr/^{86}Sr$ value.
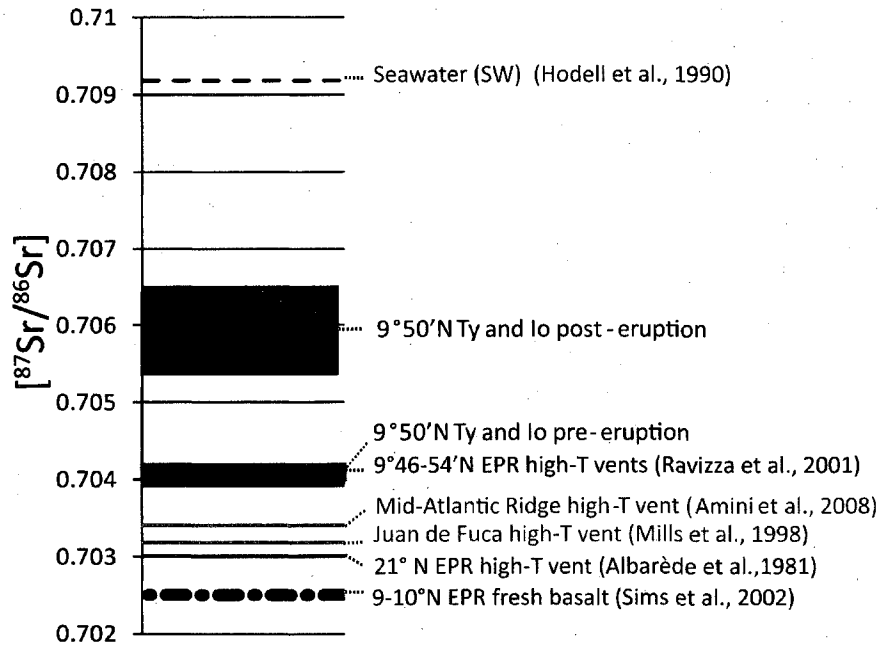
Figure 15 (above): Summary of selected published studies reporting Sr isotope systematics in hydrothermal fluids, as in Figure 2. Ranges in Ty and Io end member $^{87}Sr/^{86}Sr$ values from this study are also shown, and represent an increase in the known variability of $^{87}Sr/^{86}Sr$ values in deep sea MOR hydrothermal systems.

Mixing relationships between high- and low-temperature fluids

According to the hypothesis of this study, the Sr isotope systematics of adjacent high- and low-temperature vents will either record a binary two-component seawater-hydrothermal mixture, or will support anhydrite dissolution as an additional third component. Partially-reacted seawater may be an additional component, particularly in the post-eruptive fluids. Binary mixing hyperbolae were calculated using the elemental and isotopic Sr compositions of seawater and high-temperature Ty and Io vent end members, as described in Methods. These hyperbolae were then plotted versus elemental Sr, Ca/Sr and Mg/Sr for all sampling time points, and values for discrete low-temperature samples were superimposed to determine whether or not their compositions could be accounted for by the binary mixture. These three plots are shown for all sampling time points (with the exception of June 2006, for which an end member $^{87}Sr/^{86}Sr$ could not be calculated), including April 2000 (Figures 16a, 16b, 16c), January 2002 (Figures 17a, 17b, 17c), March 2004 (Figures 18a, 18b, 18c), November 2006 (Figures 19a, 19b, 19c), and December 2007 (Figures 20a, 20b, 20c),

Two general observations can be made about the low-temperature fluid compositions in relation to the high-temperature fluid-seawater mixtures. It is clear from the mixture plots that variations in isotopic composition of the low-temperature fluids are on small scales relative to the seawater value. These small deviations from the seawater value may preclude the detection of additional contributions of Sr from anhydrite

dissolution. In the instances when the BM82 fluids deviate from the mixing lines, the deviation is due to variation in elemental and elemental ratio compositions.

The pre-eruption April 2000 and January 2002 that the low-temperature fluids may be explained as binary mixtures, within the error. In April 2000, the three low-temperature samples show slightly elevated Sr (Figure 16a), while one sample in January 2002 shows slightly depleted Sr from the binary mixture. (Figure 17a), but otherwise these plots support previous theories that the low-temperature fluids are indeed binary mixtures with seawater, with respect to their Sr, isotopic Sr, Ca, and Mg contents.

In the immediately-pre eruption March 2004 mixing hyperbolae demonstrate, there are two plots in which the BM82 fluids deviate significantly from the binary mixing hyperbolae. The first is Figure 18a, in which two BM82 samples display higher elemental Sr concentrations. The second is Figure 18c, in which two BM82 samples display lower Mg/Sr ratios than predicted by the binary mixture. Anhydrite dissolution into the low-temperature fluids could be a potential mechanism of introducing excess Sr with negligible input of Mg (resulting in a lower Mg/Sr ratio), however, this lower Mg/Sr ratio may additionally indicate Mg depletion in the low-temperature fluids, perhaps by removal of caminite in the discharge zone stockwork. It is interesting that the $^{87}Sr/^{86}Sr$ versus Ca/Sr plot (Figure 18b) does not show a significant deviation in the Ca/Sr ratio of the BM82 fluids. A study of hydrothermal anhydrite deposits at TAG demonstrated that the Ca/Sr ratio of anhydrite varies widely, and ranges from 0.0730-0.225 mmol/µmol in 13 samples drilled from various depths in the hydrothermal mound (Mills et al., 1998). It is conceivable

therefore, that potential subsurface anhydrite deposits at 9°50'N EPR could exhibit a Ca/Sr ratio around the 0.115 mmol/μmol seawater value. Mills et al. (1998) additionally analyzed anhydrite samples for Sr isotopes, and the $^{87}Sr/^{86}Sr$ range they report for 21 samples is 0.706866-0.709128. These ranges are interpreted to represent seawater-dominated circulation through the mound, with subsequent incorporation of a high percent of seawater-derived Sr into the anhydrite. This may also be the case for subsurface anhydrite potentially dissolving in BM82 fluids, as anhydrite containing high percentages of seawater-derived Sr could account for the lack of significant deviations in the low-temperature isotopic ratios.

In the post-eruption November 2006 and December 2007 sampling intervals, the BM82 fluids do not appear to deviate significantly from the binary mixing hyperbolae (Figures 19a, 19b, 19c, 20a, 20b, 20c). To determine whether or not these, and other fluids in the pre- and post-eruptive time series, are conclusively explained by a binary high-temperature fluid-seawater mixture, a closer look was taken at the elemental abundances of Ca and Sr in the low-temperature hydrothermal fluids.

To determine whether or not the elemental abundances of Ca and Sr in the BM82 fluids can be explained by a binary high-temperature fluid-seawater mixture, the measured BM82 Ca and Sr contents were compared with the Ca and Sr contents to be expected from a binary mixture, by solving the high-temperature end member regression equation for the measured Mg of the BM82 fluids. These calculations were performed for the three highest quality (lowest Mg) BM82 samples at every sampling point in the entire time series. These

calculations assume that Mg is conservative between the high- and low-temperature fluids, an assumption that may not be true for March 2004, as previously discussed. At any particular sampling time and for any discrete BM82 sample, the calculation was performed using the Ca and Sr regression equations for both Ty and Io vents, as it is not possible to determine from these data whether the high-temperature component of the BM82 fluids is derived from just Ty or just Io, or is a mixture of both high-temperature fluids. Figure 21a and 20b, respectively, show the results of Ca and Sr molar calculations for the BM82 fluids sampled throughout the entire time series. The result of a particular BM82 sample in the Ca deviation plots is plotted in the same relative position on the time series in the Sr deviation plots in order to compare trends between Ca and Sr. The reported errors are standard errors, based on method precision, and a significant deviation is one in which the total error does not overlap the 0.0 mmol/kg value for Ca or the 0.0 μmol/kg value for Sr. For those points that are thus deemed to represent a significant deviation, the error bars are colored black, and for those that represent an insignificant deviation, the error bars are colored gray. Due to the variability of BM82 sample composition over the time series as well as at any given sampling point, these results will be considered for Ca and Sr in detail for the six individual sampling periods, and a general interpretation can then be made considering pre- versus post-eruption results.

In 2000, two BM82 fluid samples show no Ca deviation and a slight Sr excess, and one sample shows a slight Ca excess and no significant Sr deviation (Figure 21a, 21b). In 2002, one BM82 fluid sample shows no Ca deviation (when the Io regression results are

considered) and no significant Sr deviation, while the other two samples show Ca depletions and no significant Sr deviation. The 2004 BM82 samples show the highest variability of a single sampling point, with one sample showing a Ca depletion and high Sr excess, one showing no significant Ca deviation and slight Sr excess, and one showing high Ca excess and no significant Sr deviation. Sampling conditions at this time could potentially create a situation in which one sample is collected which records a different process than the others, as each majors bottle has a separate snorkel. The 2004 BM82 samples may represent fluids in which Mg is not conservative, so these results are not necessarily accurate. In general, however, the pre-eruptive BM82 fluids do not show strong evidence for anhydrite dissolution, as only two samples show Ca contents in excess of that predicted by a binary mixture mechanism. If in fact these two discrete fluid samples do represent anhydrite dissolution, the Sr deviation results suggest that no significant anhydrite-derived Sr from is incorporated into these particular fluids.

In June-July 2006, all three BM82 fluid samples show Ca excesses (Figure 21a). Two of these samples show Sr depletion and one shows no significant Sr deviation (Figure 21b). In November 2006, two BM82 fluid samples show Ca excesses, with one sample showing Sr depletion and the other showing no significant Sr deviation. One November 2006 BM82 sample shows no significant Ca deviation, as well as Sr depletion. In 2007 Io vent was observed to be extinct, only Ty vent was sampled, and thus the BM82 deviations were calculated from only this end member regression. In 2007, all three BM82 fluids show Ca depletion, with two of these samples showing no significant Sr deviation and one showing a

slight Sr depletion. The Ca deviation results of the immediate pre-eruptive BM82 fluids, sampled in June-July and November 2006, are consistent with anhydrite dissolution, as five of the six fluids show a Ca excess. These excesses represent a significant fraction of the Ca in these fluids, as these deviations make up approximately 2-7% of the total Ca in the low-temperature fluids (Figure 22a, 23a). Interestingly, four of these six samples show concurrent Sr depletion, ranging from approximately 1-6% of the total Sr in the low-temperature fluids (Figure 22b, 23b). There may be two explanations for the Sr depletions which occur in tandem with the Ca excesses. First, if anhydrite dissolution is indeed occurring, it is adding negligible amounts of Sr to the fluids. Second, an otherwise un-accounted for Sr sink may exist, such as low-temperature basalt alteration. These alteration processes may be more robust during the immediate post-eruption period, when BM82 fluids are at relatively higher temperatures than at other times during the time series (Figure 7a).

Figure 16: April 2000 high-temperature fluid-seawater binary mixture hyperbolae. Black lines are the mean [^{87}Sr/^{86}Sr], calculated as described in Methods, plotted versus (a) Sr, (b) Ca/Sr, and (c) Mg/Sr of the mixture. Dotted lines show the greatest 2σ error, which for the Sr and Ca/Sr plots is based on method precisions, and for the Mg/Sr plot is twice the standard deviation generated by the mixture hyperbola equation uncertainty analysis.

Figure 17: January 2002 high-temperature fluid-seawater binary mixture hyperbolae. Black lines are the mean [^{87}Sr/^{86}Sr], calculated as described in Methods, plotted versus (a) Sr, (b) Ca/Sr, and (c) Mg/Sr of the mixture. Dotted lines show the greatest 2σ error, as described for Figure 16.
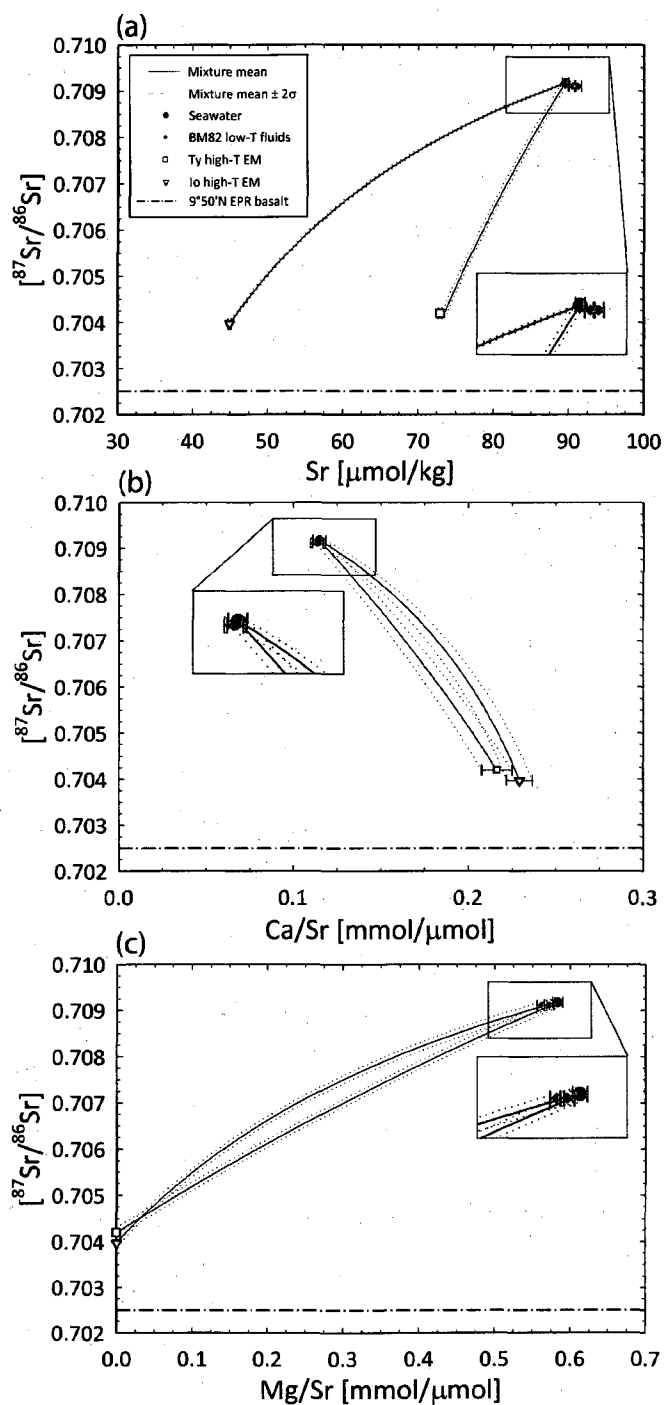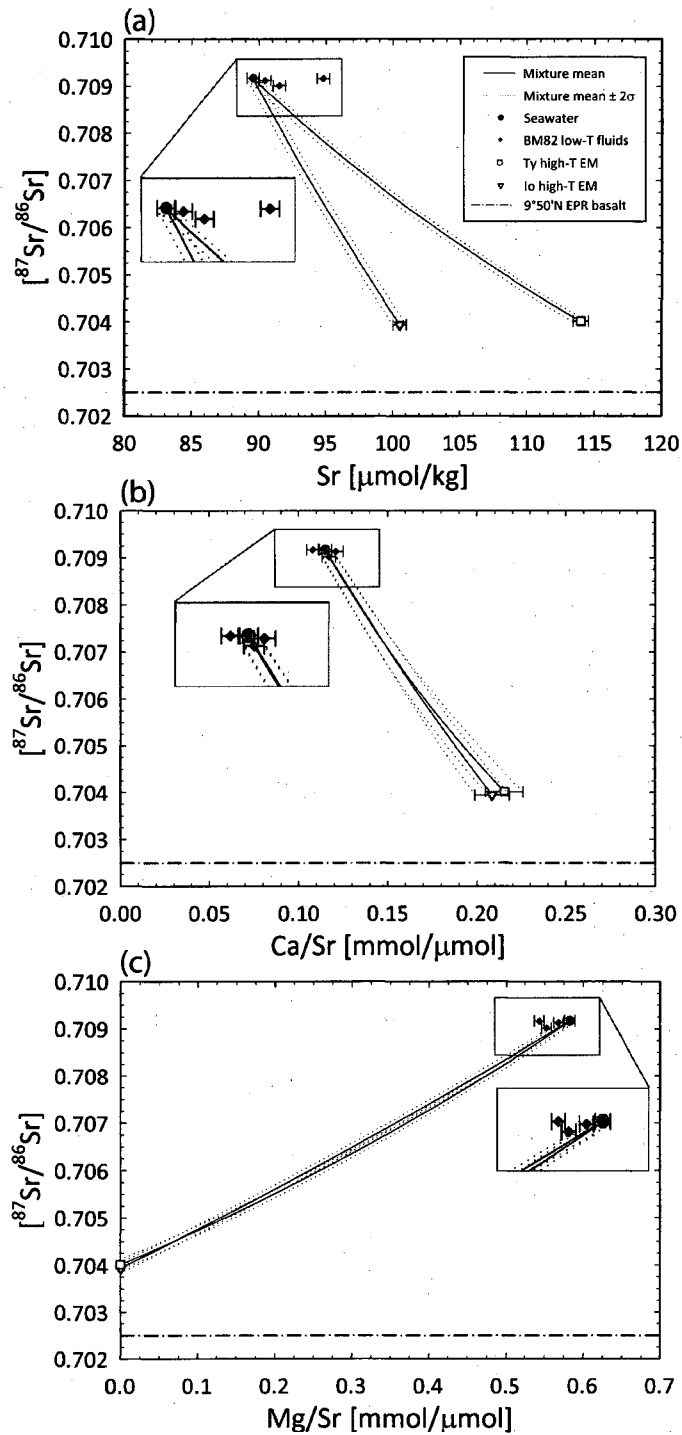
Figure 18: March 2004 high-temperature fluid-seawater binary mixture hyperbolae. Black lines are the mean [^{87}Sr/^{86}Sr], calculated as described in Methods, plotted versus (a) Sr, (b) Ca/Sr, and (c) Mg/Sr of the mixture. Dotted lines show the greatest 2σ error, as described for Figure 16.
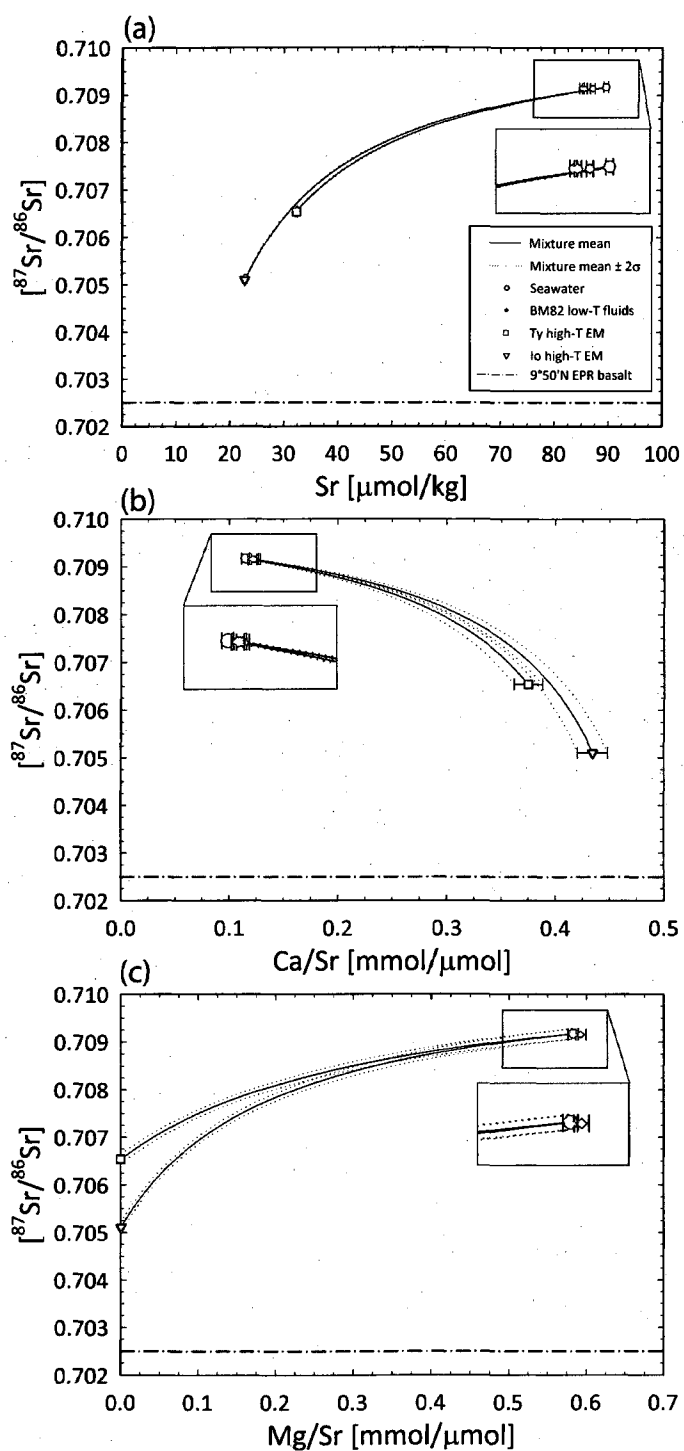
Figure 19: November 2006 high-temperature fluid-seawater binary mixture hyperbolae. Black lines are the mean [^{87}Sr/^{86}Sr], calculated as described in Methods, plotted versus (a) Sr, (b) Ca/Sr, and (c) Mg/Sr of the mixture. Dotted lines show the greatest 2σ error, as described for Figure 16.
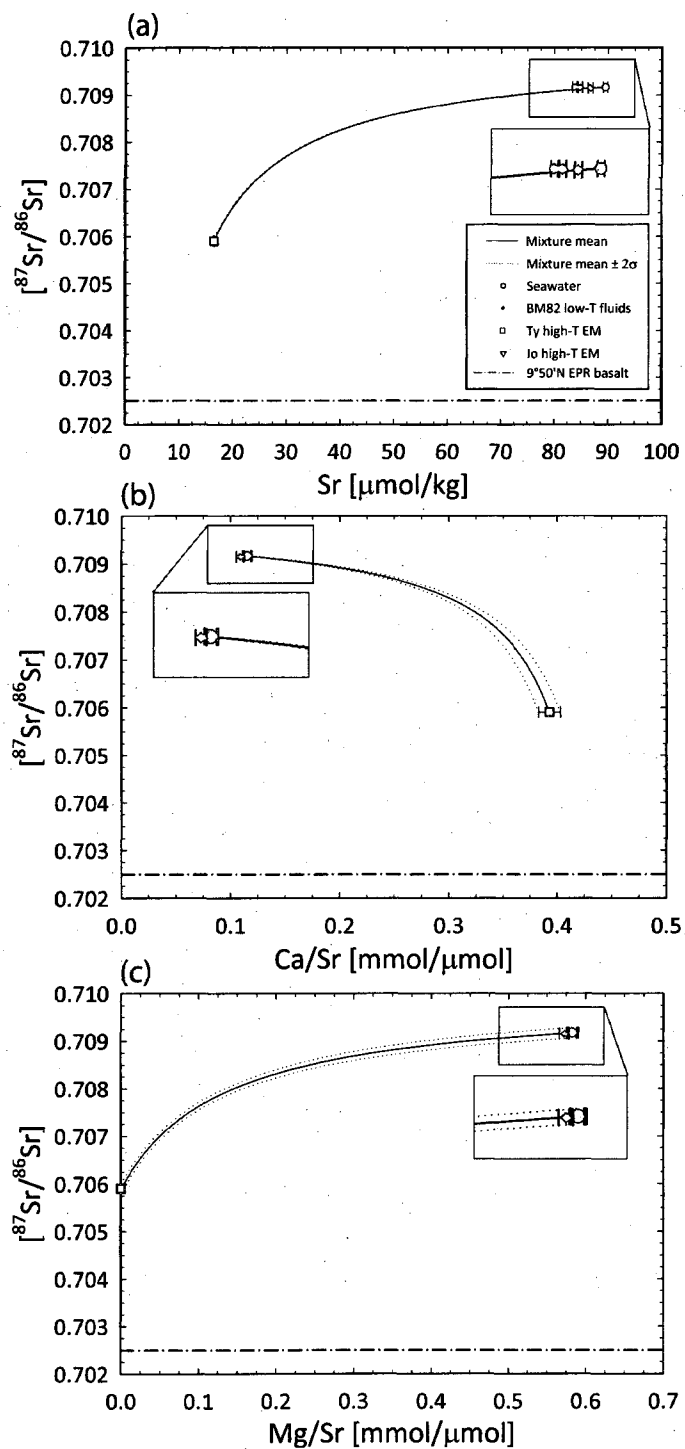
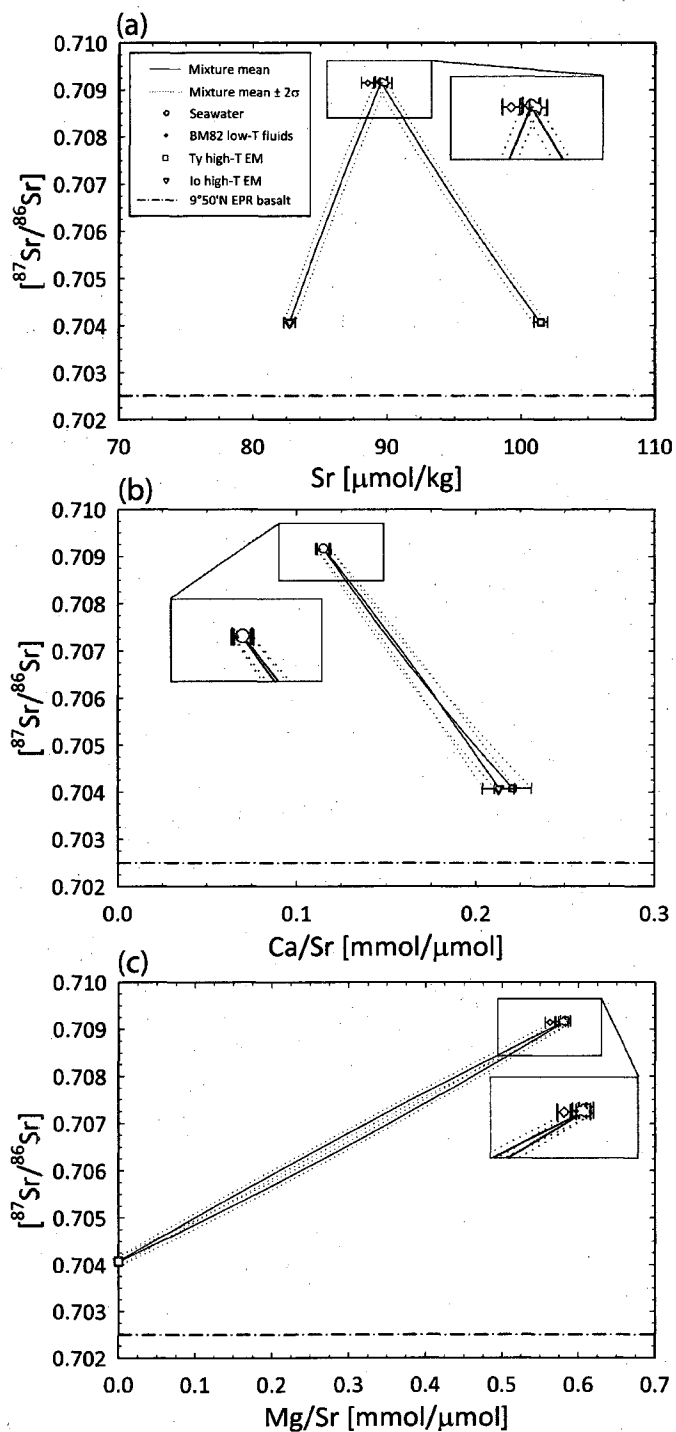**Figure 20:** December 2007 high-temperature fluid-seawater binary mixture hyperbolae. Black lines are the mean [^{87}Sr/^{86}Sr], calculated as described in Methods, plotted versus (a) Sr, (b) Ca/Sr, and (c) Mg/Sr of the mixture. Dotted lines show the greatest 2σ error, as described for Figure 16.
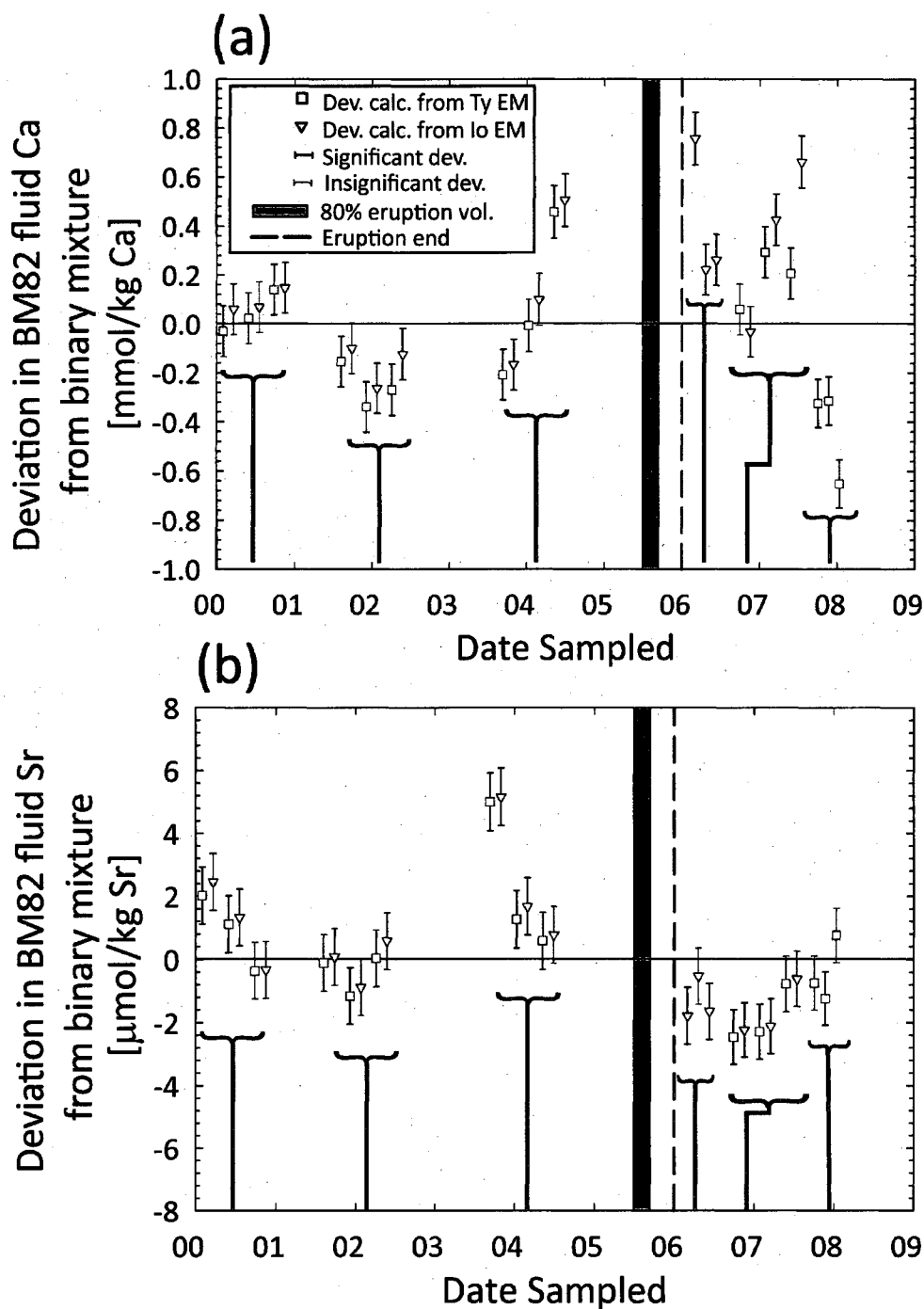
Figure 21: (a) Ca and (b) Sr molar deviations from the binary high-temperature fluid-seawater mixture throughout the time series, calculated for the 3 highest quality (lowest Mg) BM82 samples (of 3-4 samples total), using the Ca and Sr regression equations for Ty (open orange square) and Io (open red triangle) vents. Any BM82 sample in the (a) Ca deviation plot is plotted in the same relative position on the (b) Sr deviation plot. Reported errors are based on method precision. A significant deviation (marked with a black error bar) is one in which the total error does not overlap the 0.0 mmol/kg value (Ca) or the 0.0 μmol/kg value (Sr).
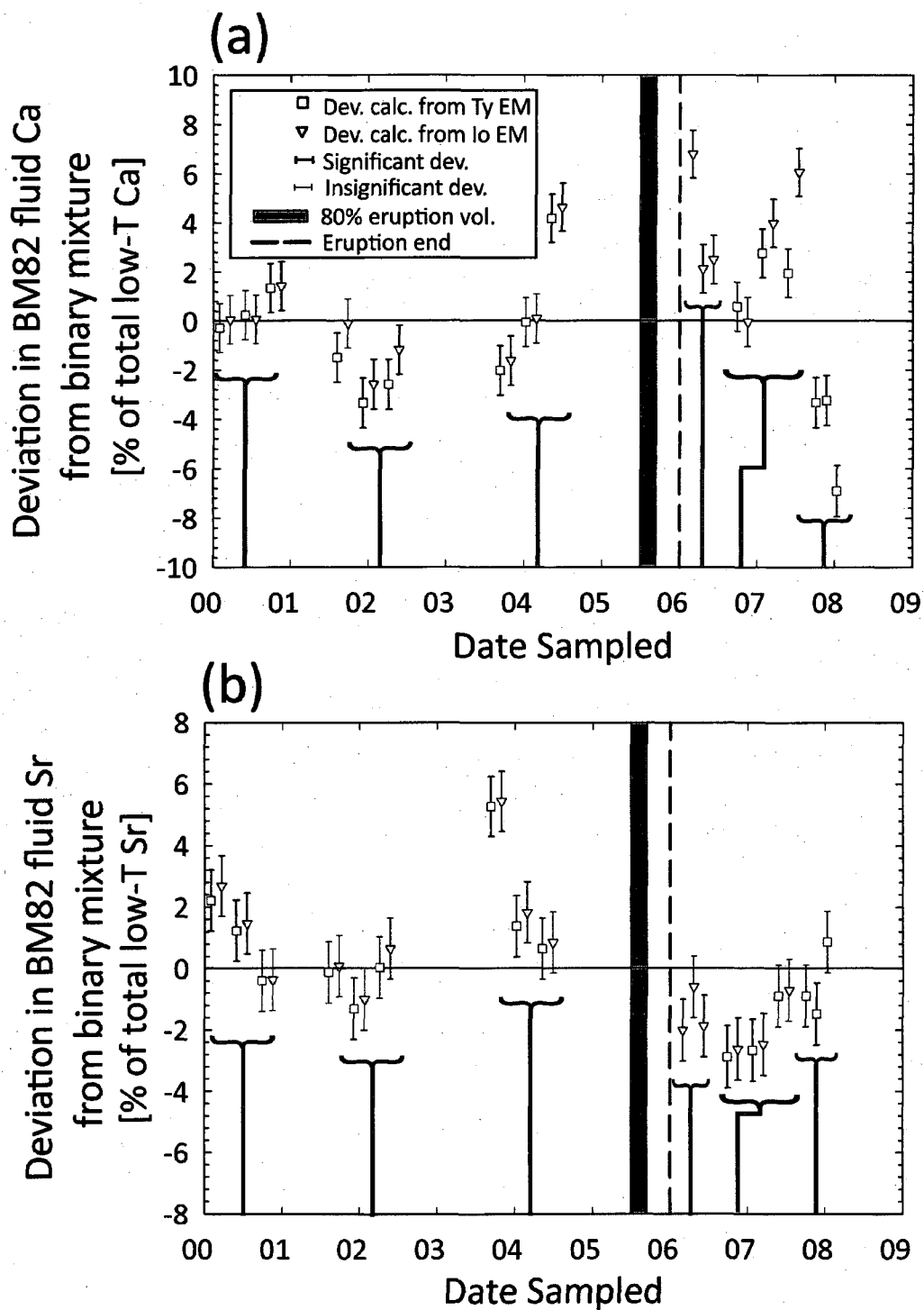
Figure 22: (a) Ca and (b) Sr deviations as in Figure 21, adjusted to represent the percent of total Ca or Sr in the individual BM82 sample that is due to the deviation from the binary high-temperature fluid-seawater mixture. Symbols are as described in Figure 21. Any BM82 sample in the (a) Ca deviation plot is plotted in the same relative position on the (b) Sr deviation plot. Reported errors are based on method precision.

Figure 23: (a) Ca and (b) Sr deviations as in Figure 22, adjusted to represent the percent of total Ca or Sr in the individual BM82 sample that is due to the deviation from the binary high-temperature fluid-seawater mixture. Average deviations across every sampling interval are shown. Any BM82 sample in the (a) Ca deviation plot is plotted in the same relative position on the (b) Sr deviation plot. Reported errors are based on method precision.

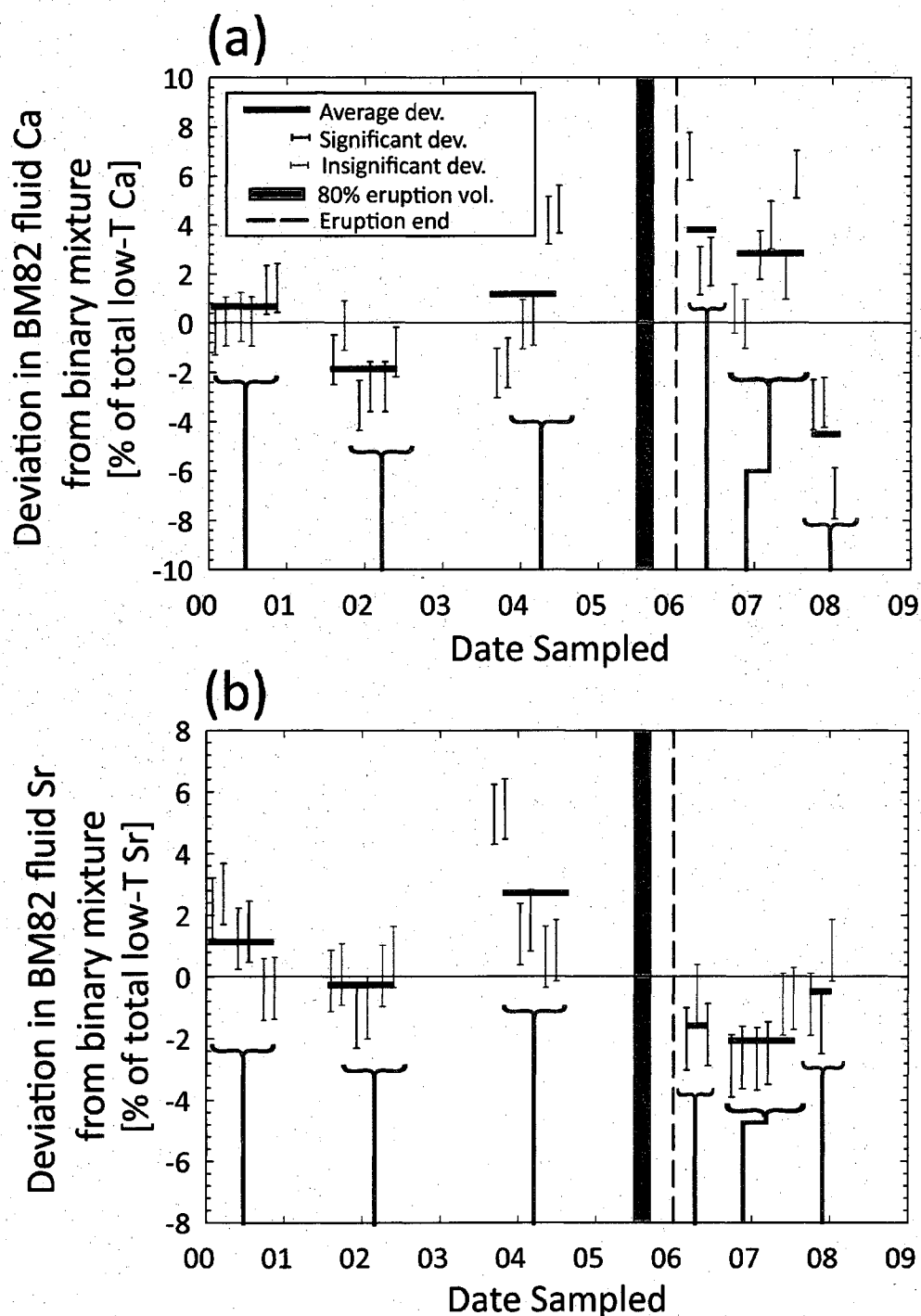A clear missing link, which will greatly enhance this study, is an examination of the Ca, Mg, elemental Sr and isotopic Sr composition and variability in anhydrite in altered basalts at 9°N EPR. All published work to date in exploring hydrothermal anhydrite deposits has been performed at slow spreading ridges, including the Juan de Fuca and Mid-Atlantic Ridge (e.g. Mills et al., 1998; Teagle et al., 1998; Amini et al., 2008). A fast-spreading ridge like the EPR represents a very different tectonic environment, with distinctive axis geometry and more frequent eruptive events. Anhydrite deposits in altered EPR basalts are fresh products of recent processes that are not overprinted by thousands to millions of years of low-temperature water-rock reactions, as at slow spreading ridges. Thus, comparable data from EPR anhydrite deposits are essential to understanding the fluid mixing.

Dr. Rachel Haymon at UCSB has a piece of altered basalt, or "stockwork," collected from the Tubeworm BBQ region (9°50.6'N) that contains anhydrite intergrown with pyrrhotite and chalcopyrite in the stockwork veins. Haymon has collected a small amount of preliminary Sr isotope data for this anhydrite, and the ratio is 0.7048. There have been two polished thin sections made from the BBQ stockwork sample, and one of these sections includes an anhydrite-bearing vein (Figure 24). Haymon and I plan to collaborate to re-run vein anhydrite from this stockwork sample to determine whether the TIMS at BU reports the same Sr isotope ratio. Additionally, Haymon describes the sample as very big, and containing many veins, and therefore it will be interesting to determine the mm-cm scale Sr isotope and elemental Sr, Ca, Mg variability within the veins. These data will be integral to
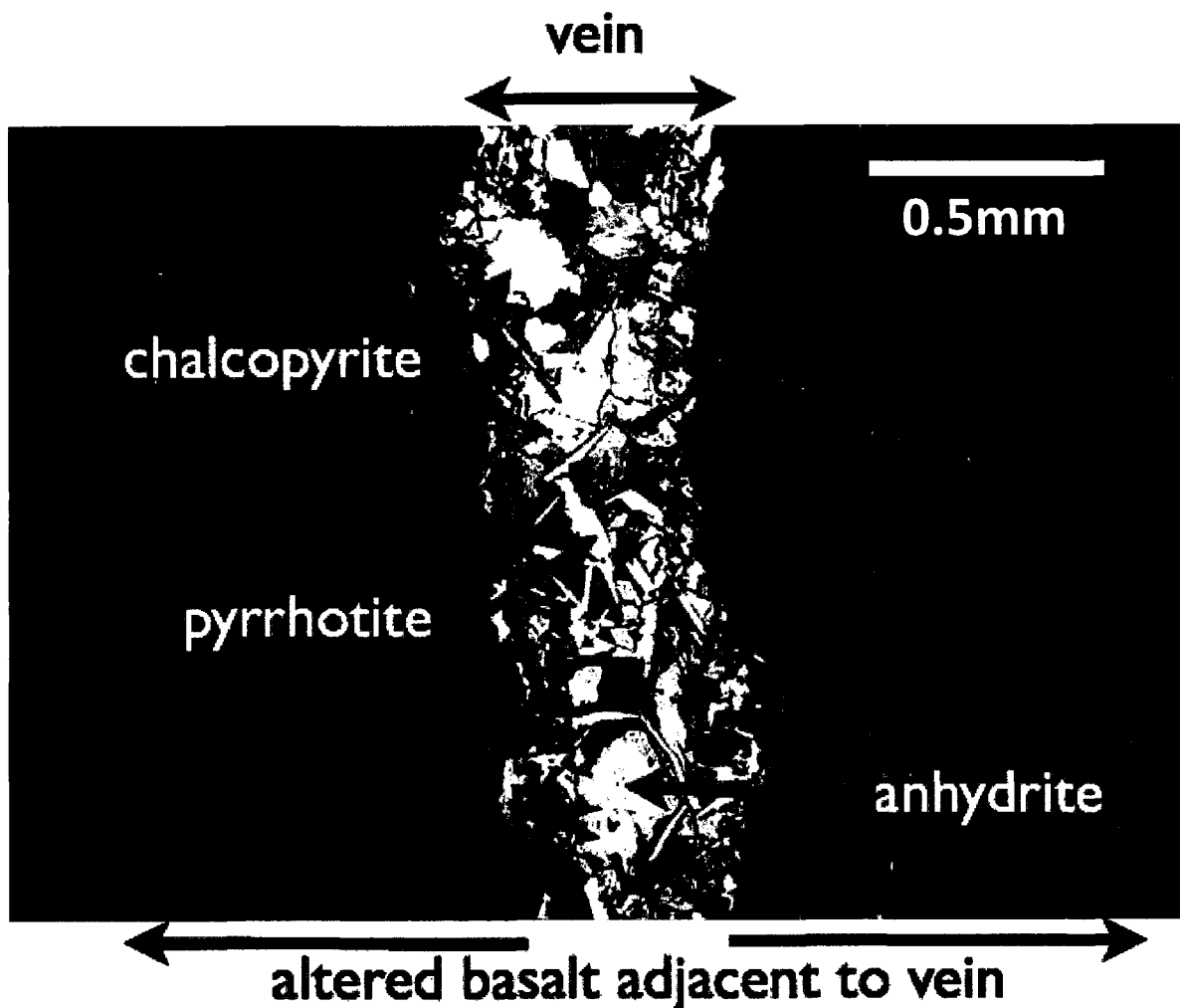
Figure 24: Photomicrograph of a thin section from the BBQ altered basalt stockwork sample, showing an anhydrite-bearing vein of about 0.5mm width. Part of the proposed work will involve re-running vein anhydrite from this stockwork sample to determine whether the TIMS at BU reports the same Sr isotope ratio. Image courtesy R.M. Haymon.

better understanding the potential chemical signature of anhydrite in the BM82 fluids, as

well as in other low- and high-temperature fluids sampled at 9°N EPR during the time series.

Additional insights to gain include the potential identification of caminite in the stockwork

sample mineralogy, as well as selecting sulfide minerals inter-grown with the anhydrite to

run for S isotopes. Sulfur isotopes will provide additional information about seawater

versus high-temperature fluid sources, and it will be interesting to determine whether S

isotopes from sulfides tell a fluid mixing story consistent with that provided by Sr isotopes

from anhydrite.

CHAPTER IV

CONCLUSIONS AND IMPLICATIONS

Pronounced elemental and isotopic variability of the low-temperature BM82 and high-temperature Ty and Io fluids at 9-10°N EPR in the pre- (1994-2004) and post-eruptive (2006-2007) time intervals emphasizes the short time scales on which these chemistries change, in addition to providing a mechanism by which we can elucidate subsurface chemical and heat transfer processes. The maximum sampled temperature, coupled with the Cl, and Si contents of Ty and Io describe a system in which the heat source was deepening prior to the 2005-2006 eruption, followed by a shallower heat source and vigorous convection immediately post-eruption, and most recently evidence for a deepening heat source. This observation is in good agreement with the trends observed in changes in hydrothermal vent chemistry at 9-10°N EPR following the 1991 eruption (Von Damm, 1995). That the heat source was deepening in 2007, and therefore driving convection less vigorously, may greatly impact the robustness of hydrothermal venting in the near future, and thus impact the micro and macro faunal ecosystems at the site. Indeed, Io was confirmed inactive in December 2007, and Ty is presently listed as inactive in the

vent database in the Ridge 2000 Data Portal (http://www.marine-geo.org/portals/ridge2000/).

Analysis of the variation in Ty and Io major and minor elements/species in the pre-(1994-2004) and post-eruptive (2006-2007) time intervals reveals several mineral-fluid reaction zone processes which have affected vent chemistry significantly, including albitization (depletion of Na with increase in Ca), halite precipitation (increased Br/Cl ratio, decreased Na/Cl ratio) and enhanced vigor of convection through the more porous subsurface rock in the post-eruptive time period, leading to the inability of fluids to achieve steady state chemistries due to kinetic constraints (higher maximum measured temperatures and depleted Li/Cl, K/Cl, and Sr/Cl ratios).

An analysis of the Sr isotopic composition of Ty and Io end member fluids, as well as BM82 fluids provides the first time series data set documenting Sr isotope variation in any hydrothermal system. Pre-eruption ^{87}Sr/^{86}Sr values for Ty and Io are approximately constant, and agree well with the Sr isotopic compositions of hydrothermal vents at 9-10°N EPR as well as at other fast- and slow-spreading ridges. Post-eruption ^{87}Sr/^{86}Sr values for Ty and Io are not constant, but rather are much closer to the seawater ratio than pre-eruption values or any previously published high-temperature end member values, thereby providing the first evidence that water-rock reactions are not at steady state with respect to basaltic Sr isotopes post-eruption. Sr isotopes may therefore offer an accurate new method of identifying the state of equilibration of a hydrothermal system, as well as a measure of fluid-seawater mixing in the subsurface. Although low-temperature BM82 fluid ^{87}Sr/^{86}Sr

values do not deviate greatly from the seawater value, most samples do show a deviation from seawater, and thus include some high-temperature fluid-derived Sr within the mixture. The Sr isotope ratios of low-temperature fluids do not provide conclusive evidence for or against the dissolution of anhydrite into low-temperature fluids. However, a careful analysis of deviations in low-temperature fluid elemental Ca and Sr from high-temperature fluid-seawater binary mixtures shows elevated Ca, interpreted as evidence for anhydrite dissolution, in the immediate post-eruptive system in both June-July and November 2006. These elevations in Ca composition make up 2-7% of the total low-temperature fluid Ca content, and thus the process of anhydrite dissolution may provide a greater hydrothermal source of Ca to the ocean at certain times in the eruptive cycle, and may be mostly likely to occur following an eruption, when the heat source is shallower.

In future work, I plan to collaborate with R. Haymon to perform isotopic Sr and Ca, elemental Sr, and Mg chemical analysis of mm-cm scale anhydrite veins in the TWP altered basalt sample. This future work will provide a better constraint on the chemical variability of EPR anhydrite deposits, as well as providing a comparison between the chemistry of subsurface anhydrite at the fast-spreading EPR and similar studies at slow spreading MORs.

APPENDICES

Appendix A

Elemental Sr by ICP-MS procedure

Light the plasma dry, with coolant set to 13 L/min, auxiliary Ar set to 0.90 L/min and nebulizer Ar set to 29.0 mL/min. After line of sight closes, introduce tuning solution and check for uptake and proper flow to waste. Allow to warm up for 1 hour minimum prior to data collection. During this time, tune on 1 ppb Y, starting first with torch alignment, followed by coolant, auxiliary, and nebulizer pressures, and lastly by adjusting source, quad 2, and high voltage settings. Adjust quad tables if necessary. A smooth, flat-topped peak of 750,000-1,000,000 cps on Y is acceptable to begin the run. Begin a run by checking the tuning solution Y, followed by the blanks, standards, and samples interspersed with the monitor, with a 30 second rinse in 2% Optima HNO_3 after every introduction. With samples containing ~22 nmol/kg Sr, ^{88}Sr should yield values of ~800,000 cps, and the 12 nmol/kg Y spike should yield values of ~800,000 cps. These values will decline over the run as the vacuum pressure will drop progressively. A drop of 100,000 cps over 3-4 hours is acceptable, and can be corrected for using the Y spike. When a run is complete, run the tuning solution for Y. Aspirate in 2% Optima HNO_3 for a few minutes, DI water for a few minutes, and lastly run dry for a few minutes, prior to turning off plasma.

HR-ICP-MS hardware and operating conditions

Plasma

Coolant	13 L/min
Auxiliary Ar	1.02 L/min
Nebulizer Ar	31.4 mL/min
Sample introduction	Manual, free aspiration solution mode

Mass Spectrometer

Sampler	Nickel, 1.2 mm orifice
Skimmer	Nickel, 0.6mm orifice
Magnet calibration	Optimized on 1 ppb 2% Optima HNO_3 tuning solution containing Li, Be, Mg, Sc, Co, Y, In, Cs, Tm, Tb, Pb, U
Lenses	Optimized on 1 ppb Y in tuning solution

Data Acquisition

Isotopes to scan	^{84}Sr, ^{86}Sr, ^{87}Sr, ^{88}Sr, ^{89}Y
Scanning mode	ESA scan, peak jumping
Number of cycles	5
Number of sweeps	500
Dwell time	3000 μsec
Switch delay	2
Threshold	10000
Reduction	None
Peak to center on	^{89}Y
Resolution	300
Number of steps	300

Appendix B

Strontium isotope extraction procedure

For all Sr work, clean gloves and acid-cleaned Teflon® supplies were used. All solution work was performed in a laminar flow bench in the Bryce lab. First, a blank check was performed. Von Damm lab and Bryce lab DI water blanks, as well as 2% solutions of Von Damm lab 3x quartz distilled HNO_3 and Bryce lab purchased 3x sub-boiling Teflon distilled "Optima" HNO_3 were checked for elemental Sr via ICP-MS. Additionally, 1 ppb (12nmol/kg) Sr standard and 1 ppb Y standard (12nmol/kg) in 2% HNO3 were run for Sr via the same method.

In preparation to run columns, 7 ml Teflon® Savillex vials (p/n# 0225R) were heated for one day partially filled with 50% HNO_3, heated for a second day filled with DI water, and dried in a laminar flow bench. Columns were made by cutting the top and bottom of transfer pipets and inserting a Teflon® frit into the end. Columns were soaked in 5N Optima HNO_3 for 2 days at room temperature to ensure clean columns but not weaken the frits.

Sample aliquots ranging between 0.2-2.0 mL were pipeted into cleaned Savillex vials from the acidified fluid fraction such that each sample would contain ~30 nmol of total Sr, based on FAAS results. Concentrated Optima HNO_3 was added such that the samples were in 3N HNO_3, and the samples were dried down on a hotplate under laminar flow to minimize their organic content. They were brought back up in 400 μL of 3N HNO_3, sonicated with DI water for 20 minutes, and allowed to sit for a few hours to equilibrate.

To prepare the columns, while working in a hood a small amount of Eichrom SrSpec resin was poured into a HNO_3 cleaned screw top large Teflon vial and DI water was added to rinse the resin. The mixture was shaken and allowed to settle. Fine particles were then skimmed off the top via pipet. The mixture was shaken and skimmed 4-5 times. To pack a column:

1. Fill column with water from the top and rinse (shake out), then rinse from bottom.
2. Fill from bottom with DI water, flip and fill from top. Continue running water through so that there are no air bubbles, then cap the bottom with thumb keeping the column full of water.
3. Load ~1 mL of resin slurry into column and allow to settle out. The resin should fill to the base of the reservoir of the column.

Packed columns can sit overnight in a laminar flow bench if placed in an HNO3 clean beaker covered with a watch glass. To run columns, work in a laminar flow bench and take care not to reach over samples:

1. Wash with DI water, filling the top reservoir portion of the column. Let drain to waste.
2. Wash with 1 N Ultrex HCl in the same way. Let drain to waste.
3. Wash again with DI water. Let drain to waste.
4. Repeat steps 2-3 twice.
5. Precondition the column by loading 1 ml of 3N Optima HNO3. Let drain to waste.
6. Load sample onto the column.
7. Wash with 400ul 3N Optima HNO_3. Let drain to waste. Use this to rinse the beaker that the loaded sample came out of, for quantitative transfer.
8. Wash with 400ul 3N Optima HNO_3 again. Let drain to waste.
9. Wash with 1600ul 3N Optima HNO_3. Let drain to waste.
10. Place new sample beaker under column for collection.
11. Elute with 2.3 mL DI water and collect in vial.
12. Repeat step 11 twice.
13. Cap sample collection vial.

To prepare columns for the next round, leave the columns to dry overnight under laminar flow. The next day, tap the dried resin out on weighing paper. The resin should not be discarded of down the drain, but ion chromatographic resin is not regulated and thus can be disposed of in the trash. Rinse the column well with DI water. Wash the empty column with ~0.5 mL of 2N Ultrex HCl, then DI water, and then repeat three times. Rinse several times with DIW, and place the columns in 5N Optima HNO_3 to clean for 2 days.

REFERENCES

Albarède, F. & A. Michard (1981), ^{87}Sr/^{86}Sr ratios in hydrothermal waters and deposits from the East Pacific Rise at 21°N, *Earth Planet. Sci. Lett., 55*, 229-236.

Alt, J. (1995), Subseafloor processes in mid-ocean ridge hydrothermal systems, in *Seafloor Hydrothermal Systems: Physical, Chemical, Biological, and Geological Interactions*, AGU Mono. 91, S. E. Humphris, R., A. Zierenberg, L.S. Mullineaux and R.E. Thomson, eds., pp. 85–114, American Geophysical Union, Washington, DC.

Amini, M., Eisenhauer, A., Böhm, F., Fietzke, J., Bach,W., Garbe-Schönberg, D., Rosner, M., Bock, B., Lackschewitz, K. S., and Hauff, F. (2008), Calcium isotope (δ^{44}/^{40}Ca) fractionation along hydrothermal pathways, Logatchev field (Mid-Atlantic Ridge, 14°45′N), *Geochim. et Cosmochim. Acta, 72*, 4107–4122.

Bevington, P. and D.K. Robinson (2003), *Data Reduction and Error Analysis for the Physical Sciences, 3rd edition,* pp. 328, McGraw-Hill, Boston, MA.

Bischoff, J.L. (1991), Densities of liquids and vapors in boiling NaCl-H$_2$O solutions: A PVTX summary from 300°-500°C, *Amer. J. Sci., 291*, 309-338.

Bischoff, J. L. and R. J. Rosenbauer (1985), An empirical equation of state for hydrothermal seawater (3.2 percent NaCl), *Amer. J. Sci., 285*, 725-763.

Bischoff, J.L. and and F. Dickson (1975), Seawater-basalt interaction at 200°C and 500 bars: Implications for origin of sea-floor heavy-metal deposits and regulation of seawater chemistry, *Earth Planet. Sci. Lett., 25*, 385-97.

Bryce., J.G., D.J. DePaolo, and J.C. Lassiter (2005), Geochemical structure of the Hawaiian plume: Sr, Nd, and Os isotopes in the 2.8 km HSDP-2 section of Mauna Kea volcano, *Geochem., Geophys. and Geosyst., 6*, Q09G18, doi:10.1029/2004GC000809.

Butterfield, D.A., I. R. Jonasson, G. J. Massoth, R. A. Feely, K. K. Roe, R. E. Embley, J. F. Holden, R. E. McDuff, M. D. Lilley, and J. R. Delaney (1997), Seafloor eruptions and evolution of hydrothermal fluid chemistry, *Phil. Trans. of the Royal Soc. London, 355*, 369-386.

Campbell, A.C., T.S. Bowers, C.I. Measures, K.K. Faulkner, M. Khadem, and J.M. Edmond (1988), A time series of vent fluid concentrations from 21°N, East Pacific Rise (1979, 1981, 1985), and the Guaymas Basin, Gulf of California (1982, 1985), *J. Geophys Res., 93*, 4537-4549.

Carbotte, S.M., and K.C. Macdonald (1992), East Pacific Rise 8°-10°30'N: Evolution of ridge segments and discontinuities from SeaMARC II and three-dimensional magnetic studies, *J. Geophys. Res. 97*, 6959-6982.

Cochran, J.R., D.J. Fornari, B.J. Coakley, R. Herr, and M.A. Tivey (1999), Continuous near-bottom gravity measurements made with a BGM-3 gravimeter in DSV Alvin on the East Pacific Rise crest near 9°31 'N and 9°50'N, *Journal of Geophys. Res., 104,* 10841-10862.

Corliss, J.B., J. Dymond, L.I. Gordon, J.M. Edmond, R.P. von Herzen, R.D. Ballard, K. Green, D. Williams, A. Bainbridge, K. Crane, and T.H. van Andel (1979), Submarine thermal springs on the Galapagos Rift, *Science, 203,*1073-1083.

Cowen, J.P., D.J. Fornari, T.M. Shank, B. Love, B. Glazer, A.H. Treusch, R.C. Holmes, S.A. Soule, E.T. Baker, M. Tolstoy, and K.R. Pomraning (2007), Volcanic Eruptions at East Pacific Rise Near 9°50'N, *EOS Trans. AGU*, 88, 81-82.

Detrick, R.S., P. Buhl, E. Vera, J. Mutter, J. Orcutt, J. Madsen and T. Brocher (1987), Multichannel seismic imaging of a crustal magma chamber along the East Pacific Rise between 9°N and 13°N, *Nature, 326,* 35-41.

DePaolo, D.J. and B.L. Ingram (1985), High resolution stratigraphy with Strontium isotopes, *Science, 227,* 938-941.

Edmond, J.M., C. Measures, B. Mangum, B. Grant, F.R. Sclater, R. Collier, and A. Hudson (1979b), On the formation of metal-rich deposits at ridge crests, *Earth Planet Sci. Lett.*, 46, 19-30.

Edmond, J.M., C. Measures, R. McDuff, L.H. Chan, R. Collier, B. Grant, L.I. Gordon, and J.B. Corliss (1979a), Ridge Crest Hydrothermal Activity and the balances of the major and minor elements in the ocean: The Galapagos data, *Earth Planet Sci. Lett.*, 46, 1-18.

Faure, G. (1977a), Geochemistry of Rubidium and Strontium, in *Principles of Isotope Geology,* pp. 75-76, John Wiley and Sons, New York.

Faure, G. (1977b), Strontium in Two-Component Mixtures, in *Principles of Isotope Geology,* pp. 97-100, John Wiley and Sons, New York.

Fietzke, J. and A. Eisenhauer (2006), Determination of temperature-dependent stable strontium isotope ($^{87}Sr/^{88}Sr$) fractionation via bracketing standard MC-ICP-MS, *Geochem. Geophys. Geosyst., 7,* Q08009.

Foustoukos D.I. and Seyfried W.E., Jr. (2007), Quartz solubility in the two-phase and critical region of the NaCl-KCl-H2O system: Implications for the submarine hydrothermal systems at 9o50N East Pacific Rise, *Geochim. et Cosmochim. Acta, 71,* 186-201.

German, C.R., and K.L. Von Damm (2004), Hydrothermal processes, in *Treatise On Geochemistry, Volume 6: The Oceans and Marine Geochemistry*. H.D. Holland and K.K. Turekian, eds., pp. 181–222, Elsevier, London.

Goldfarb, M.S., D.R. Converse, H.D. Holland, and J.M. Edmond (1983), The genesis of hot spring deposits on the East Pacific Rise, 21°N, *Econ. Geol. Mono., 5,* 184-197.

Halicz, L., Segal, I., Fruchter, N., Stein, M., Lazar, B., 2008, Sr stable isotopes fractionate in the soil environments?, *Earth Planet Sci. Lett., 272,* 406-411.

Haymon, R.M., and M. Cormier (2006), Ridge 2000 Proposal For an Integrated Study Site at a Fast-Spreading Ridge: The East Pacific Rise, 8°-11° N, 2002, accessed from http://www.ridge2000.org/science/downloads/epr/epr_SiteProposal.pdf on 8 December 2007.

Haymon, R.M., D.J. Fornari, K.L. Von Damm, M.D. Lilley, M.R. Perfit, J.M. Edmond, W.C. Shanks, III, R.A. Lutz, J.M. Grebmeier, S. Carbotte, D. Wright, E. McLaughlin, M. Smith, N. Beedle, and E. Olson (1993), Volcanic eruption of the mid-ocean ridge along the East Pacific Rise crest at 9°45-52'N: Direct submersible observations of seafloor phenomena associated with an eruption in April, 1991, *Earth Planet. Sci. Lett., 119,* 85-101.

Haymon, R.M., D.J. Fornari, M.H. Edwards, S. Carbotte, D. Wright, and K.C. Macdonald (1991), Hydrothermal vent distribution along the East Pacific Rise crest (9°09'-54'N) and its relationship to magmatic and tectonic processes on fast-spreading mid-ocean ridges, *Earth and Planet Sci. Lett., 104,* 513-534.

Haymon, R.M. and M. Kastner (1981), Hot spring deposits on the East Pacific Rise at 21°N - Preliminary description of mineralogy and genesis, *Earth Planet. Sci. Lett., 53,* 363-381.

Hodell, D.A., G.A. Mead, and P.A. Mueller (1990), Variation in the strontium isotopic composition of seawater (8 Ma to present): Implications for chemical weathering rates and dissolved fluxes to the oceans, *Chem. Geol (Isot. Geosci. Section), 80,* 291-307.

Kinsey, R. R., (1996), Sr isotope abundances. Accessed on "Table of the Nuclides" at atom.kaeri.re.kr/ on 5 April 2009.

Klitgord, K.D. and J. Mammerickx (1982), Northern East Pacific Rise: Magnetic anomaly and bathymetric framework, *Journal of Geophys. Res., 87,* 6725-6750.

Lilley, M.D., D.A. Butterfield, J.E. Lupton, and E.J. Olson (2003), Magmatic events can produce rapid changes in hydrothermal vent chemistry, *Nature, 422,* 878–881.

Mills, R.A., D.A.H. Teagle and M.K. Tivey (1998), Fluid mixing and anhydrite precipitation within the TAG mound, Proceedings of the Ocean Drilling Program, 158, P.M. Herzig et al., ed., 119-127.

Mottl, M.J. (2003), Partitioning of energy and mass fluxes between mid-ocean ridge axes and flanks at high and low temperature, in *Energy and Mass Transfer in Marine Hydrothermal Systems,* P.E. Halbach, V. Tunnicliffe, and J.R. Hein, eds., pp. 271-286, Dahlem University Press, Berlin.

Oosting, S.E. and K.L. Von Damm (1996), Bromide/chloride fractionation in seafloor hydrothermal fluids from 9–10°N East Pacific Rise, *Earth and Planet. Sci. Lett., 144,* 133-145.

Ravizza, G., J. Blusztajn, K.L. Von Damm, A.M. Bray, W. Bach, and S.R. Hart (2001), Sr isotope variations in vent fluids from 9°46'-9°54'N East Pacific Rise: Evidence of a non-zero Mg fluid component, *Geochim. et Cosmochim. Acta,* 65, 729-739.

Rosenberg, N. D., F. J. Spera, and R. M. Haymon (1993), The Relationship between Flow and Permeability Field in Seafloor Hydrothermal Systems, *Earth Planet Sci.* Lett., *116,* 135-153.

Rubin, K.H., M. Tolstoy, D.J. Fornari, R.P. Dziak, S.A. Soule, F. Waldhauser, K.L. Von Damm (2008), Integrating Radiometric, Geophysical and Thermal Signals of Volcanic Unrest and Eruption in 2005-06 at 9°50'N EPR, *AGU Fall Meet. Suppl., 89,* Abstract B23F-07.

Rubin, K.H., J.D. Macdougall and M.R. Perfit (1994), ^{210}Po–^{210}Pb dating of recent volcanic eruptions on the seafloor, *Nature,* 368, 841-844.

Ruggeberg, A., J. Fietzke, V. Liebetrau, A. Eisenhauer, W.C. Dullo, and A. Freiwald (2008), Stable strontium isotopes (d88/86Sr in cold-water corals – A new proxy for reconstruction of intermediate ocean water temperatures, *Earth and Planet Sci. Lett., 269,* 570-579.

Schultz, A. and H. Elderfield (1997), Controls on the physics and chemistry of seafloor hydrothermal circulation, *Phil. Trans. Roy. Soc.,* 355, 387-425.

Seyfried, W.E. and K. Ding (1995), Phase equilibria in subseafloor hydrothermal systems: A review of the role of redox, temperature, pH and dissolved Cl on the chemistry of hot spring fluids at mid-ocean ridges, in *Seafloor Hydrothermal Systems: Physical, Chemical, Biological, and Geological Interactions,* AGU Mono. 91, S. E. Humphris, R., A. Zierenberg, L.S. Mullineaux and R.E. Thomson, eds., pp.248-272, American Geophysical Union, Washington, DC.

Shank, T.M., D. J. Fornari, K.L. Von Damm, M.D. Lilley, R.M. Haymon, and R.A Lutz (1998), Temporal and spatial patterns of biological community development at nascent deep-sea hydrothermal vents along the East Pacific Rise, *Deep Sea Res. Part II, 45,* 465-515.

Shanks W.C., III (2001), Stable isotopes in seafloor hydrothermal systems: vent fluids, hydrothermal deposits, hydrothermal alteration, and microbial processes, in *Stable Isotope Geochemistry,* Rev. Mineral. Geochem. 43, J.W. Valley and D.R. Cole, eds., pp. 469-525, Mineralogical Society of American, pp. 469-525.

Sillén, L.G. (1961), The physical chemistry of seawater, in *Oceanography,* Amer. Assoc. Advancement Sci. Pub. No. 67, M. Sears, ed., pp. 549-581, Washington, DC.

Sims, K.W.W., S.J. Goldstein, J. Blichert-Toft, M.R. Perfit, P. Kelemen, D.J. Fornari, P. Michael, M.T. Murrell, S.R. Hart, D.J. DePaolo, G. Layne, L. Ball, M. Jull and J. Bender (2002), Chemical and isotopic constraints on the generation and transport of magma beneath the East Pacific Rise, *Geochim. et Cosmochim. Acta,* 66, 3481-3504.

Spiess, F.N., K.C. Macdonald, T. Atwater, R. Ballard, A. Carranza, D. Cordoba, C. Cox, V.M. Diazgarcia, J. Francheteau, J. Guerrero, J. Hawkins, R. Haymon, R. Hessler, T. Juteau, M. Kastner, R. Larson, B. Luyendyk, J.D. MacDougall, S. Miller, W. Normark, J. Orcutt, and C. Rangin (1980), East Pacific Rise: Black smokers and geophysical experiments, *Science, 207,* 1421-1433.

Staudigel, H. and S. R. Hart (1983), Alteration of basaltic glass: mechanisms and significance of the oceanic crust-seawater budget, *Geochim. Cosmochim. Acta, 47,* 337-350.

Teagle, D.A.H., J.C. Alt, H. Chiba and A.N. Halliday (1998), Dissecting an active hydrothermal deposit: The Strontium and Oxygen isotopic anatomy of the TAG hydrothermal mound - anhydrite, Proceedings of the Ocean Drilling Program, 158, P.M. Herzig et al., eds., 129-141.

Tolstoy, M., J.P. Cowen, E.T. Baker, D.J. Fornari, K.H. Rubin, T.M. Shank, F. Waldhauser, D.R. Bohnenstiehl, D.W. Forsyth, R.C. Holmes, B. Love, M.R. Perfit, R.T. Weekly, S.A. Soule, and B. Glazer (2006), A Seafloor Spreading Event Captured by Seismometers, *Science, 314,* 1920-1922.

Veirs, S.R., R.E. McDuff, and F.R. Stahr (2006), Magnitude and variance of near-bottom horizontal heat flux at the Main Endeavour hydrothermal vent field, *Geochem., Geophys. and Geosyst.,* 7, Q02004, doi:10.1029/ 2005GC000952.

Von Damm, K. L. (2004), Mid-Ocean Ridges: Hydrothermal Interactions Between the Lithosphere and Oceans. AGU Mono. 148, American Geophysical Union, 10.1029/148GM12.

Von Damm, K.L. (2000), Chemistry of hydrothermal vent fluids from 9-10°N, East Pacific Rise: "Time zero," the immediate posteruptive period, *J. Geophys Res, 105,* 11203-11222.

Von Damm, K.L. (1995), Controls on the chemistry and temporal variability of seafloor hydrothermal fluids, in *Seafloor Hydrothermal Systems: Physical, Chemical, Biological, and Geological Interactions, AGU Mono. 91,* S.E. Humphris, R.A. Zierenberg, L.S. Mullineaux and R.E. Thomson, eds., 222-247.

Von Damm, K. L., Bates, M., Carmichael, S., Meana-Prado, F., McDermott, J. and RESET06 Science Party (2006), Response of the 9-10N EPR Hydrothermal Systems to Recent Volcanic Eruptions, *Eos Trans. AGU 87,* Fall Meet. Suppl., Abstract V13C-02.

Von Damm, K.L. and M.D. Lilley (2004), Diffuse flow hydrothermal fluids from 9°50'N East Pacific Rise: Origin, evolution and biogeochemical controls, The Subsurface Biosphere at Mid-Ocean Ridges, AGU Mono. 144, W.S.D. Wilcock, E.F. et. al. eds., 243-266.

Von Damm, K.L., L.G. Buttermore, S.E. Oosting, A.M. Bray, D.J. Fornari, M.D. Lilley, and W.C. Shanks III (1997), Direct observation of the evolution of a seafloor "black smoker" from vapor to brine, *Earth and Planet Sci. Lett., 149,* 101-112.

Von Damm, K.L., S.E. Oosting, R. Kozlowski, L.G. Buttermore, D.C. Colodner, H.N. Edmonds, J.M. Edmond and J.M. Grebmeier (1995), Evolution of East Pacific Rise hydrothermal vent fluids following a volcanic eruption, *Nature,* 375, 45-50.

Von Damm, K. L., Bischoff, J. L. and R. J. Rosenbauer, R. J. (1991), Quartz solubility in hydrothermal seawater: An experimental study and equation describing quartz solubility for up to 0.5M NaCl solutions, *Am. J. Sci., 291,* 977–1007.

Von Damm, K.L., J.M. Edmond, B. Grant, C.I. Measures, B. Walden, and R.F. Weiss (1985), Chemistry of submarine hydrothermal solutions at 21°N, East Pacific Rise, *Geochim. Cosmochim. Acta, 49*, 2197-2220.

Wolery, T.J., EQ3/6 (1992), *A software package for geochemical modeling of aqueous systems: Package overview and installation guide,* Version 7.0, 70pp., Lawrence Livermore National Lab., California.